ABSTRACT

QASIMOV, HEYDAR R. O. Lacunae-based stabilization of PMLs. (Under the direction of Professor S. Tsynkov).

Perfectly matched layers (PML) enclose the computational domain for simulating electromagnetic phenomena defined over unbounded regions. While being overall very successful, this procedure has sometimes been reported to develop instabilities and exhibit a physically unaccountable growth of the solution inside the layer over long integration times. In the thesis, we conduct a numerical as well as analytical study of the PML's response after a long time of integration. The physical and mathematical PMLs are implemented with several well-known schemes: Yee, leap-frog, Lax-Wendroff, and Runge-Kutta in time with central differences in space. Then, the eigen-structure of each discretization at quiescent state is studied to gain an insight into the nature of instability, the sources of growth of the solution and the potential contamination of the domain of interest. The results of this investigation provide useful information regarding the better and worse performers among the specific combinations of schemes and PMLs, yet they do not precisely identify the mechanism behind the growth of the solution. Therefore, the main focus of the thesis is to build a methodology that would inhibit the instability of the PML regardless of its source. The approach is based on the concept of numerical integration that exploits the presence of lacunae in the solutions. It applies to hyperbolic partial differential equations and systems that satisfy the Huygens' principle, in particular, the Maxwell's system of equations that governs the propagation of electromagnetic waves. The methodology does not modify the equations inside the layer and hence, while eliminating the undesirable growth, it fully preserves all the advantageous properties of a given PML, such as matching at the interface and the degree of absorption. A practical algorithm is constructed in the thesis, and a theorem is proved that guarantees a temporally uniform error bound over the domain of interest. The theoretical findings are corroborated numerically, and the potential for extending the methodology is discussed.

Lacunae-Based Stabilization of PMLs

by
Heydar Qasimov

A dissertation submitted to the Graduate Faculty of
North Carolina State University
in partial fulfillment of the
requirements for the degree of
Doctor of Philosophy

Mathematics

Raleigh, NC
October 14, 2008

Approved By:

Dr. P. Gremaud	Dr. D. Zenkov
Dr. R. Smith	Dr. S. Rahman
Dr. S. Tsynkov Chair of Advisory Committee	

BIOGRAPHY

Biography withheld for personal reasons.

ACKNOWLEDGMENTS

First and foremost, I would like to express my deeply felt gratitude to Dr. Semyon Tsynkov. His pedagogical instinct, advice, guidance, and support have enriched my experiences and broadened my views on life within the academic environment and beyond. Dr. Tsynkov introduced me into the field of Numerical Analysis, and, as he patiently and enthusiastically led me, he generously shared his knowledge, motivating and at times gently nudging when I needed it most.

Thanks are due to Dr. Saul Abarbanel of Tel Aviv University for his vital role in the first part of the study, as well as for contributing his vast expertise in the field toward the success of the project.

I would also like to thank the faculty of the Department of Mathematics at NCSU — I am truly indebted to everyone who taught and helped me along the way.

I thankfully acknowledge the financial support provided by the US Air Force Office of Scientific Research (AFOSR) and the National Science Foundation (NSF).

TABLE OF CONTENTS

LIST OF FIGURES . . . . . **vi**

LIST OF TABLES . . . . . **viii**

1 Introduction **1**
1.1 Numerical Solution of Infinite Domain Problems: A Quick Overview 1
1.2 Local Methods 3
1.2.1 The Engquist and Majda Boundary Conditions 3
1.2.2 The Higdon Boundary Conditions 6
1.2.3 The Bayliss-Turkel Boundary Conditions 8
1.2.4 Other Local Methods 10
1.3 Global Methods 12
1.3.1 The Method by Engquist and Majda and Its Generalization by Gustafsson . 13
1.3.2 DtN Maps — the Method by J. Keller and Givoli 14
1.3.3 The Method by Ferm and Gustafsson 16
1.3.4 The Method by Hagstrom 18
1.3.5 The Method of Difference Potentials 19
1.4 High Order Local Methods 23
1.5 Perfectly Matched Layers 28
1.5.1 Background 28
1.5.2 Concerns about PMLs 30

2 Performance of Unsplit PMLs with Explicit Second Order Schemes **34**
2.1 Motivation and Background 34
2.2 Computational Setup 36
2.3 The Yee Scheme 37
2.4 The Leap Frog Scheme 39
2.5 The Lax-Wendroff Scheme 40
2.6 The Central Difference Scheme 43
2.7 Summary and Intermediate Conclusions 44

3 Lacunae-Based Stabilization of PMLs **46**
3.1 Introduction 46
3.2 Essentials of the Algorithm and the Main Theorem 47
3.3 Numerical Experiments 54
3.3.1 Computational Setup 54
3.3.2 Test Solution 61
3.3.3 Implementation Issues 64
3.3.4 Results of Computations 66
3.4 Extensions 74
3.5 Discussion 75

4 Conclusions **78**

List of References **81**

Appendices **92**
4.A Well-Posedness of the Cauchy Problem for Hyperbolic Systems 93
4.A.1 Introduction 93
4.A.2 Well-Posedness of the Cauchy Problem 93
4.A.3 Hyperbolicity of the Cauchy Problem 96

LIST OF FIGURES

Figure 1.1 Schematic for J. Keller and Givoli approach of [89]. 15

Figure 1.2 Typical problem configurations and grid geometries for the DPM-based ABCs as applied to external configuration analysis. 22

Figure 1.3 Setup for setting the ABCs for the semi-infinite strip, from [53] 26

Figure 1.4 The TE problem, [20] 28

Figure 1.5 Interface between 2 matched media normal to the x-axis, from [20]. 30

Figure 1.6 The PML technique schematic, from [20]. 31

Figure 2.1 E_x for the Yee scheme (2.3) at $t = 500T$; the contours are equally spaced between -0.475 and 0.475 with the increment 0.05. 38

Figure 2.2 E_x for the Law-Wendroff scheme (2.8) at $t = 500T$; the contours are equally spaced between -0.575 and 0.575 with the increment 0.05. 42

Figure 2.3 H for the central difference scheme (2.10a)–(2.10b) applied to the PML (2.1) at $t = 15T$; the contours are equally spaced between -0.4 and 0.4 with the increment 0.1 and with the exception of the zero contour. 44

Figure 3.1 Schematic. 48

Figure 3.2 Geometric setup in the space. 56

Figure 3.3 Smooth partition of unity. 65

Figure 3.4 Computation with the PML (3.24). Binary logarithm of the maximum norm error for H_θ vs. time. 67

Figure 3.5 Computation with the the characteristic boundary conditions (3.27) only. Binary logarithm of the maximum norm error for H_θ vs. time. 68

Figure 3.6 Comparison of the case with the PML against that with no PML on four grids. Binary logarithm of the maximum norm error for H_θ vs. time. 69

Figure 3.7 Computation with the PML (3.24) and lacunae-based correction. Binary logarithm of the maximum norm error for H_θ vs. time. 71

Figure 3.8 Comparison of the pure PML case against that with the PML and lacunae on four grids. Binary logarithm of the maximum norm error for H_θ vs. time. 72

Figure 3.9 Comparison of the pure lacunae case against that with the PML and lacunae on four grids. Binary logarithm of the maximum norm error for H_θ vs. time. 73

Figure 3.10 Decomposition of the problem. 74

LIST OF TABLES

Tabel 2.1 Long-time behavior of unsplit PMLs with second order schemes. 44

Chapter 1

Introduction

1.1 Numerical Solution of Infinite Domain Problems: A Quick Overview

In a wide variety of scientific applications there is a need to solve problems formulated on unbounded domains. To obtain numerical solutions of such problems it is necessary to truncate the domain of computation and set artificial boundary conditions (ABCs). The problems that require ABCs arise in computing wave phenomena (radiation and/or scattering of electromagnetic and acoustic waves), geophysics (computations with elastic waves), problems of fluid dynamics (e.g., modeling of internal flows), petroleum engineering, aerodynamics and many others. Their numerical solution essentially becomes a simulation of the corresponding phenomena over a finite domain; therefore, the role of artificial boundary conditions (ABCs) becomes particularly important.

Significant efforts have been expended by many researchers to construct ABCs for a wide variety of problems and, obviously, there are many different ways of doing it for each particular formulation. As one should expect, the ABCs will affect the accuracy of the numerical approximation and may also affect other important characteristics of the algorithm, e.g., the rate of convergence for an iterative solver. Therefore, a key question is that of the criteria the ABCs must meet. First and foremost, the ABCs should enable simulation that would approximate the physical reality. Mathematically, one requires that the treatment on the boundaries ensure solvability and lead to a well-posed mixed initial boundary value problem. In addition, one should also require that the approximation be "close" to the solution of the original problem; incidentally, this prompts the formulation of *exact* ABCs. The latter are such that by appending the numerically obtained solution to the solution of the original problem *outside* the truncated domain one obtains the solution of the original problem in the whole domain; this definition is useful for the purposes of analysis, [116]. Of course, even

before building the ABCs one must require of the original problem on the unbounded domain to be uniquely solvable and well-posed; otherwise, an approximation is meaningless.

The treatment of outer boundaries can be broadly categorized into 2 groups of ABCs - *local* and *global*. Global ABCs provide high accuracy and robustness but are often thought to be impractical as they couple the values of the solution along the entire boundary in space and, in the case of unsteady problems, in time as well. Global ABCs typically involve pseudodifferential operators and as such may be restricted geometrically to the artificial boundaries of a regular shape, such as linear, circular, etc. Local (in space and/or in time) ABCs, on the other hand, are cheaper to implement and geometrically universal but in most cases are also less accurate. Historically local methods were introduced first. Later, it was realized that for a number of problems they can be interpreted as approximations of global methods. There are also methods that can be thought of as occupying an intermediate position between the global and local ones (high order local methods, see below). In practice, one always pursues the best possible balance between the requirements of accuracy and efficiency. For a number of problems, new methods have also been developed that merge the advantages of the two existing types of ABCs and help overcome the difficulties of the global techniques while still providing high accuracy. Those approaches are based on the difference potentials method by Ryaben'kii [106], a summary can be found in the review article by Tsynkov, [116].

High order local ABCs are obtained as approximations of nonlocal boundary conditions that involve pseudodifferential operators. Using Fourier representation for the pseudodifferential operator, one can think of the order as the number of terms left in the truncated expansion. High order local methods are typically more accurate than the standard (low order) local ABCs. At the same time, they may be easier and cheaper to implement than the full-fledged nonlocal ABCs. However, they inherit the same geometric restrictions as those pertinent to the global ABCs, from which a given high order local method is derived.

As an alternative to the boundary conditions per se, an enclosure of the computational domain by a perfectly matched layer (PML) was proposed by J.-P. Bérenger in [20, 21]. Bérenger's approach consists of surrounding the computational domain with a special layer of artificial material designed to absorb impinging waves without generating reflections and then attenuate them in the layer. Most of the work described in the subsequent parts of the dissertation will revolve around this method of treating the outer boundaries.

The existing literature on the subject of ABCs is extensive. In the rest of the introduction we will present a brief and by no means comprehensive review of some of the more noteworthy examples for each of the aforementioned categories. We also describe a certain type of "annoying" numerical difficulties that "haunt" the PMLs which have otherwise proven very efficient. Those

are the instabilities that manifest themselves over long integration times, see, e.g., [3]. The core chapters of the dissertation are primarily devoted to the study of PMLs with the aim of suppressing the aforementioned instabilities. In Chapter 2 we present the results of a study of two popular types of PMLs implemented with some commonly employed explicit second order discretizations with the objective of gaining insight into the nature of the long-term instabilities that have been reported in the literature, e.g., [3]. In Chapter 3, a theorem and an algorithm providing a temporally uniform error bound (i.e., stabilizing the computation) for linear hyperbolic PDE/systems that satisfy the Huygens' principle are presented. This method successfully employs the existence of lacunae for the integration in time. In Section 3.3 the numerical experiments supporting the theoretical findings are presented. Chapter 4 provides general conclusions.

1.2 Local Methods

1.2.1 The Engquist and Majda Boundary Conditions

In [27] Engquist and Majda initially develop a theoretical *nonlocal* perfectly absorbing boundary conditions and then construct a sequence of highly absorbing local approximations (for general classes of wave equations). Essentially, they represent the solution as a superposition of waves; then, interpreting the incoming waves as reflections from the boundary they seek the solution in the exterior of the domain of interest only in the class of the outgoing waves (resembling the far-field behavior of the solution) using Fourier transforms. For example, in the Cartesian coordinates $(x,\, y)$ with the time t, consider the plane wave solution $u(x,\, y,\, t) = u(t\omega + x\xi + y\eta)$, $\omega > 0$, of the two-dimensional wave equation

$$\frac{\partial^2 u}{\partial t^2} = \frac{\partial^2 u}{\partial x^2} + \frac{\partial^2 u}{\partial y^2}. \tag{1.1}$$

The dispersion relation for the solution of this type is $\omega^2 = \xi^2 + \eta^2$. The constant phase surfaces for the plane wave are given by $t\omega + x\xi + y\eta = const$, therefore the two-dimensional vector $(-\xi,\, -\eta)$ determines the direction of the wave propagation. Let now the computational domain be the half-plane $x \leq 0$. Then, the incoming waves will be those that propagate in the negative x-direction, i.e., those that have $\xi > 0$, and the outgoing waves will be those that have $\xi < 0$. Assuming that $\omega^2 - \eta^2 > 0$, we can derive the one-way dispersion relation

$$\xi = -\sqrt{\omega^2 - \eta^2} \tag{1.2a}$$

for the waves traveling to the right (outgoing) and the one-way dispersion relation

$$\xi = \sqrt{\omega^2 - \eta^2} \tag{1.2b}$$

for the waves traveling to the left (incoming).

With

$$u(x,\eta,\omega) = \int \hat{u}(x,\eta,\omega) e^{-i(\eta,\omega)*(y,t)} d\eta d\omega \tag{1.3}$$

where $\hat{u}(x,\eta,\omega) \equiv \hat{u}_{\eta,\omega}(x)$ is the Fourier transform of $u(x,y,t)$ in the transversal coordinate y and t only equation (1.1) implies

$$\frac{d^2\hat{u}}{dx^2} + \xi^2 \hat{u} = 0. \tag{1.4}$$

Two linearly independent eigensolutions of equation (1.4) are $\hat{u}^{(1)}(x) = e^{-i|\xi|x}$ and $\hat{u}^{(2)}(x) = e^{i|\xi|x}$. For the waves traveling to the right $-|\xi| = \xi$ because of relation (1.2a) and therefore, the mode $\hat{u}^{(1)}(x)$ is outgoing; analogously, formula (1.2b) implies $|\xi| = \xi$ and consequently, the mode $\hat{u}^{(2)}(x)$ is incoming. The exact ABC's at $x = 0$ should explicitly prohibit all the incoming waves, therefore we require that the two-dimensional vector $\left[\hat{u}(x),\ \frac{d\hat{u}(x)}{dx}\right]^T$ be parallel to the vector $\left[\hat{u}^{(1)}(x),\ \frac{d\hat{u}^{(1)}(x)}{dx}\right]^T$ at $x = 0$, which can be written as the equality of the Wronskian to zero:

$$\det \left[\begin{array}{cc} \hat{u}(x) & \hat{u}^{(1)}(x) \\ \frac{d\hat{u}(x)}{dx} & \frac{d\hat{u}^{(1)}(x)}{dx} \end{array} \right] \Bigg|_{x=0} = 0, \tag{1.5a}$$

and then reduced to the following first-order homogeneous differential relation:

$$\left.\frac{d\hat{u}}{dx}\right|_{x=0} + i\sqrt{\omega^2 - \eta^2} \cdot \hat{u}\Big|_{x=0} = 0, \tag{1.5b}$$

Then, for a general wave, [27],

$$u(x,y,t) = \int e^{i(-(\omega^2-\eta^2)^{1/2}x + \omega t + \eta y)} \rho(\omega,\eta) \hat{u}(0,\eta,\omega) d\omega d\eta, \tag{1.6}$$

where $\rho(\omega,\eta)$ is a smooth function homogeneous of degree zero for $|\omega| + |\eta|$ large with support in $\omega^2 > \eta^2$ for (ω,η) large and unity on a neighborhood of the support of $\hat{u}\,(0,\omega,\eta)$, in analogy to (1.5b) the necessary boundary condition to cancel the incoming (left-traveling) waves is

$$\frac{du}{dx} + \int e^{i(\omega t + \eta y)} i(\omega^2 + \eta^2)^{1/2} \rho(\omega,\eta) \hat{u}(0,\eta,\omega) d\omega d\eta|_{x=0} = 0 \tag{1.7}$$

Next, we employ the following definition

$$b\left(y, t, \frac{\partial}{\partial y}, \frac{\partial}{\partial t}\right) u = \int e^{i(\omega t + \eta y)} i(\omega^2 - \eta^2) \rho(\omega,\eta) \hat{u}(0,\eta,\omega)$$

of the *pseudo-differential* operator, see [95], to express the boundary condition (1.7) in the form

$$\left(\frac{d}{dx} + \rho\left(\frac{\partial}{\partial t}, \frac{\partial}{\partial y}\right)\left(\frac{\partial^2}{\partial t^2} - \frac{\partial^2}{\partial y^2}\right)^{1/2}\right) \cdot u|_{x=0} = 0 \tag{1.8}$$

which is *nonlocal* in time and space. Hence, its efficacy is overshadowed by its implementability. Therefore, Engquist and Majda proceed to construct a sequence of highly absorbing approximations to the (1.8) that are *local* and, crucially, lead to a well-posed mixed boundary value problem for the wave equation. The first two are obtained under the assumption of normal incidence (i.e., $\eta = 0$) using first and second order Taylor approximations of $\sqrt{1 - \frac{\eta^2}{\omega^2}}$:

$$\left(\frac{\partial}{\partial t} + \frac{\partial}{\partial x}\right) u|_{x=0} = 0; \tag{1.9a}$$

and

$$\left(\frac{\partial^2}{\partial t^2} - \frac{1}{2}\frac{\partial^2}{\partial y^2} + \frac{\partial^2}{\partial x \partial t}\right) u|_{x=0} = 0 \tag{1.9b}$$

are well-posed. Subsequent approximations are obtained using, again, Taylor or Padé approximations to $\sqrt{1 - \frac{\eta^2}{\omega^2}}$; each approximation, however, has to be checked for well-posedness. For example, the boundary condition obtained from the second Taylor approximation of $\sqrt{1 + x}$ is proved in the paper to be *strongly ill posed* and therefore of no use. However, the corresponding Padé approximation yields a well posed boundary condition; i.e., the choice of a local approximation can be quite tricky.

The authors also show in [27] that these boundary conditions can be modified to address more complicated formulations, such as variable coefficient problems, systems, and so on.

A remark about the simplest Engquist-Majda boundary condition (1.9a) is in order. This boundary condition essentially renders the quasi-one-dimensional characteristic decomposition in the direction orthogonal to the boundary. Then, the boundary is made transparent for all the outgoing waves with normal incidence, whereas the incoming waves with normal incidence are disallowed. For systems, such as acoustics or Maxwell's, this can also be interpreted using the language of Riemann variables; the first order local characteristic boundary condition of type (1.9a) would basically mean that the incoming Riemann variable is zero. As a matter of fact, we use this approach in our numerical experiments (Section 3.3.1) to set the boundary conditions at the outer boundary of the PML for Maxwell's equations. A very similar approach can also be developed for nonlinear systems, such as Euler's equations. This was pioneered by Hedstrom in [81], we provide a brief account of this development in Section 1.2.4.

1.2.2 The Higdon Boundary Conditions

Another approach to constructing absorbing boundary conditions is taken by Higdon in [84]; here the boundary conditions are constructed for the difference approximation rather than for the analytical formulation. As it turns out, the derived boundary conditions in fact are discretizations of some perfectly absorbing analytical boundary conditions for waves traveling at certain angles. As in the previous case, Eq. (1.1) is considered, but now in the domain $\Omega = \{(x, y, t) : x > 0, y \in R, t > 0\}$. Higdon employs the centered second order difference approximation:

$$\frac{u_{j,m}^{n+1} - 2u_{j,m}^{n} + u_{j,m}^{n-1}}{(\Delta t)^2} = \frac{u_{j+1,m}^{n} - 2u_{j,m}^{n} + u_{j-1,m}^{n}}{(\Delta x)^2} + \frac{u_{j,m+1}^{n} - 2u_{j,m}^{n} + u_{j,m-1}^{n}}{(\Delta y)^2}$$

where n, j, m are the indices in time, x-direction and y-direction respectively. Consequently, the values on the boundary, i.e., for $x = 0$ correspond to the nodes $u_{0,m}^{n}$. In order to represent the values on the boundary in terms of the interior nodes and in terms of values at earlier times the following operators are defined:

$$Ku_{j,m}^{n} = u_{j+1,m}^{n}$$

is the shift operator with respect to the x coordinate and

$$Zu_{j,m}^{n} = u_{j,m}^{n+1}$$

is the shift operator with respect to t. The boundary condition has the form

$$B(K, Z^{-1})u_{0,m}^{n+1} = 0 \tag{1.11}$$

where B is a polynomial in two variables with a nonzero constant term. The solution of the wave equation can be written in the form

$$\kappa^j e^{i\eta y} z^n$$

where

$$\kappa = e^{i\xi \Delta x}$$

$$z = e^{i\omega \Delta t}$$

To minimize the reflection from the boundary the wave is written as a linear combination of the incoming and outgoing waves:

$$u_{j,m}^{n} = c_1 \kappa_{inc}^{j} (e^{i\eta \Delta y})^m z^n + c_2 \kappa_{out}^{j} (e^{i\eta \Delta y})^m z^n \tag{1.13}$$

with $\kappa_{inc} = e^{i\xi_{inc}\Delta x}$ and $\kappa_{out} = e^{i\xi_{out}\Delta x}$. Plugging (1.13) into (1.11) allows one to obtain the reflection coefficient

$$c_1 = -\frac{B(\kappa_{out}, z^{-1})}{B(\kappa_{inc}, z^{-1})} c_2 = Ref(\eta, z)$$

and to formulate the objectives so that $|Ref|$ is minimized and the subsequent discretization is stable. The first class of boundary conditions (the author calls it the *averaging method*) is defined by

$$\left(I + \left(\left(I + Z^{-1}\right)(I + K)\right) * (1/2)\right)^p u_{0,m}^{n+1} = 0$$

where p is a positive integer and K and Z the shift operators. For example, $p = 1$ gives $u_{0,m}^{n+1} = (u_{1,m}^{n+1} + u_{0,m}^{n} + u_{1,m}^{n})/3$. The second class — the *space-time extrapolation* boundary condition — is given by

$$\left(I - Z^{-1}K\right)^p u_{0,m}^{n+1} = 0$$

For example, $p = 2$ in this case gives $u_{0,m}^{n+1} = 2 \cdot u_{1,m}^{n} - u_{2,m}^{n-1}$.
The reflection coefficient for both methods satisfies

$$Ref(\eta, z) = -\left(\frac{\lambda - \cos(\theta)}{\lambda + \cos(\theta)}\right)^p + O(\omega\Delta t),$$

$\lambda = \frac{\Delta t}{\Delta x}$ where θ is the angle of incidence measured with respect to normal incidence. The author proceeds to show that both methods approximate the analytic boundary condition

$$\left(\lambda \frac{\partial}{\partial t} - \frac{\partial}{\partial x}\right)^p u|_{x=0} = 0$$

and λ is the cosine of the angle of best absorption which naturally suggests how that to cancel a wave traveling at an angle $\pm\alpha$ and more generally

$$\prod_j \left(\cos(\alpha_j)\frac{\partial}{\partial t} - \frac{\partial}{\partial x}\right) u|_{x=0} = 0 \tag{1.14}$$

which annihilates plane waves of the form $u(x, y, t) = u(t + \cos\alpha_j x \pm \sin\alpha_j y)$ traveling in the direction $(-\cos\alpha_j, \pm\sin\alpha_j)$ out of the region $x > 0$ at angles of incidence $\pm\alpha$.

In fact, Higdon's work is closely related to that of Engquist and Majda, [27]. Higdon proves a proposition stating that the p^{th}-order boundary condition of Engquist and Majda is, in fact, equivalent to

$$\left(\frac{\partial}{\partial t} - \frac{\partial}{\partial x}\right)^p u|_{x=0} = 0, \tag{1.15}$$

i.e., $\alpha_j = 0$ for all j and $\Omega = \{(x, y, t) : x > 0, y \in R, t > 0\}$. For example, consider $p = 2$; then

$$\left(\cos\alpha_j \frac{\partial u}{\partial t} - \frac{\partial u}{\partial x}\right)^2 = \left(\frac{\partial u}{\partial t} - \cos\alpha_j \frac{\partial u}{\partial x} + \sin\alpha_j \frac{\partial u}{\partial y}\right) + \left(\frac{\partial u}{\partial t} - \cos\alpha_j \frac{\partial u}{\partial x} - \sin\alpha_j \frac{\partial u}{\partial y}\right)$$

is identical to (1.9a) for α_j - normal incidence and once we remember the fact that the computational domain in the former case is at $x \leq 0$.

In his subsequent work, [88], Higdon developed similar boundary conditions for dispersive waves. Other papers by Higdon on the subject of artificial boundary conditions include [83, 85–87].

1.2.3 The Bayliss-Turkel Boundary Conditions

In [12] Bayliss, Gunzburger and Turkel develop boundary conditions for the Laplace equation (which describes e.g., the potential flow of incompressible fluid around a body and is also important in the study of electrostatic fields) in 3D

$$\Delta u = 0 \tag{1.16a}$$

subject to

$$u = O\left(\frac{1}{\rho}\right), \rho \to \infty \tag{1.16b}$$

and the Helmholtz equation, important to the study of time-harmonic waves exterior to given surfaces:

$$\Delta u + k^2 u = 0 \tag{1.17a}$$

with the Dirichlet or Neumann data specified on the surfaces of bodies and subject to

$$\left(\frac{\partial}{\partial \rho} - ik\right) u = o\left(\frac{1}{\rho}\right), \rho \to \infty \tag{1.17b}$$

The computational domain is given by the bounded region between the body and the sphere $\rho = r_1$. Therefore, to obtain a numerical approximation Eqs. (1.16) and (1.17) one has to incorporate into the discretization the radiation condition at infinity. One approach consists of reformulating the equations in the form of the Fredholm integral equations; this approach, however, yields only nonlocal boundary. The authors of [12] rather proceed to develop a sequence of operators that serve as local boundary conditions. These operators are applied at the *exterior* boundary at $\rho = r_1$.

The outgoing solution of Eq.(1.17a) exterior to the sphere of radius r_0 in the spherical coordinates (ρ, θ, ϕ) can be represented as a uniformly and absolutely convergent and therefore termwise differentiable sum, see [11]:

$$u(\rho, \theta, \phi) = \frac{e^{ik\rho}}{k\rho} \sum_{j=0}^{\infty} \frac{F_j(\theta, \phi)}{(k\rho)^j} \tag{1.18}$$

The expansion (1.18) means that the solution of problem (1.17) satisfy at

$$\left(\frac{\partial}{\partial\rho} - ik\right) u = O\left(\frac{1}{\rho^2}\right), \rho \to \infty$$

Bayliss, Gunzburger and Turkel define a sequence of linear differential operators B_m that annihilate the first m terms in the sum (1.18)

$$B_m = \prod_{j=1}^{m} \left(\frac{\partial}{\partial\rho} - ik + \frac{2j-1}{\rho}\right) \tag{1.19}$$

Clearly, $B_1\left[\frac{e^{ik\rho}}{k\rho}F(\theta,\phi)\right] = 0$ and $B_m\left[\frac{e^{kr}}{(kr)^l}F(\theta,\phi)\right] = 0$ for $l = 1,\ldots,m$. Moreover, for any function u in the form 1.18 the operator satisfies

$$B_m u|_{\rho=r_1} = O\left(\frac{1}{{r_1}^{2m+3}}\right)$$

In the same vein, the solution of the exterior Laplace equation has a multipole expansion

$$u(\rho,\theta,\phi) = \frac{1}{\rho}\sum_{j=0}^{\infty}\frac{F_j(\theta,\phi)}{\rho^j} \tag{1.20}$$

and the corresponding sequence of operators is defined simply by setting k in (1.19) to zero so that

$$B_m = \prod_{j=0}^{m} \left(\frac{\partial}{\partial\rho} + \frac{2j-1}{\rho}\right) \tag{1.21}$$

and similarly to the Helmholtz case, the operator B_m of the sequence (1.21) annihilates the first m terms of (1.20) and satisfies

$$B_m u|_{\rho=r_1} = O\left(\frac{1}{\rho^{2m+1}}\right) \tag{1.22}$$

Bayliss and Turkel also developed boundary conditions for time-dependent (wave-like) equations in [14]. For the 3D wave equation $u_{tt} = \Delta u$ in the spherical coordinates (ρ,θ,ϕ) the solution is given by

$$u(t,\rho,\theta,\phi) = \sum_{j=1}^{\infty}\frac{u_j(t-\rho,\theta,\phi)}{\rho^j}$$

and

$$B_m = \prod_{l=1}^{m} \left(\frac{\partial}{\partial t} + \frac{\partial}{\partial\rho} + \frac{2l-1}{\rho}\right) \tag{1.23}$$

satisfying equation (1.22). Other papers by Bayliss, Turkel and co-authors on the subject of artificial

boundary conditions include [13, 15, 16].

The Bayliss-Turkel methodology is employed in the present work to set boundary conditions in the radial direction for the cylindrically symmetric TE Maxwell's equations. As these boundary conditions are set for the components of a vector field rather than scalar quantities, a few wrinkles had to be smoothed out in their derivation; however, the resulting operators are, in fact, identical to the first operator of the sequence (1.23) modified for the 2D wave equation. The operator reads $B_1 = \left(\frac{\partial}{\partial t} + \frac{\partial}{\partial \rho} + \frac{1}{2\rho}\right)$, see [116]; full details can be found in Section 3.3.

1.2.4 Other Local Methods

To date, there exists a multitude of local methods. Many of these are derived for specific formulations and often, these derivations build upon and/or adapt existing methodologies to meet the present needs. We mention briefly some of these methods.

In [60] Guddati and Tassoulas consider the operator in the family of differential relations (1.5b) parameterized by ω and η. This family of relations allows to represent the solution as a superposition of waves by using the inverse Fourier transform; however, the inverse transform of the square root results in a non-local pseudo-differential operator. In an approach closely related to Engquist and Majda's of [28], Guddati and Tassoulas suggest more general rational approximations of the square root and write the boundary conditions as a *continued-fraction* expansion

$$i\xi + i\omega f_n = 0$$

where the proposed sequence of approximations of the radical is given by

$$f_1 = \cos\theta_1$$

$$f_{n+1} = \cos\theta_{n+1} - \frac{\cos^2(\theta_{n+1}) - (1-\sigma^2)}{\cos\theta_{n+1} + \cos\theta}$$

with θ_n chosen in advance based on the direction of the wave propagation.

The authors show that for $\sqrt{(1-\sigma^2)} = \cos\theta$ where $\sigma = \frac{\eta}{\omega}$ and θ is the angle of incidence of the impinging wave the reflection coefficient for the n^{th}-order approximation is

$$Ref_n = \prod_{k=1}^{n} \frac{\cos\theta_k - \cos\theta}{\cos\theta_k + \cos\theta}$$

which is the reflection coefficient for Higdon's boundary condition (1.14) with the exception that the outward normal here is in the positive x-direction.

In order to emphasize the variety of fields where it is necessary to construct ABCs, we note Hedstrom's contribution to solving the equations of gas dynamics with an outflow boundary, see [81]. Consider the nonlinear hyperbolic system

$$u_t + A(u)u_x = 0, (x,t) \in \Omega$$

$$u(x,0) = g(x)$$

where $\Omega = \{(x,t) : x > 0, t > 0\}$. Since the system is hyperbolic the eigenvalues are real and distinct and we assume

$$\delta(A(u)) = \{\overbrace{\underbrace{\lambda_1, \ldots, \lambda_m}_{negative}, \underbrace{\lambda_{m+1}, \ldots, \lambda_n}_{positive}}^{n \text{ eigenvalues}}\}$$

Denoting the set of the *left* eigenvalues by $\{l_j\}_{j=1}^m$ Hedstrom proves that the condition

$$l_j \cdot u_t = 0, j \in \{m+1, \ldots, n\}, x = 0, t > 0; \tag{1.26}$$

means that there are no waves coming into Ω from the boundary at $x = 0$ if there are only simple[1], otherwise known as rarefaction waves, going out. Hedstrom's approach is based on the Riemann invariants; for, the condition (1.26) essentially means $0 = l_j u_t = -l_j A(u) u_x = -\lambda_j l_j u_x$ for $j = m+1, \ldots, n$ on the boundary for $t > 0$ meaning that the positive velocities $\{\lambda_j\}_{j=m+1}^n$, corresponding to the incoming waves, are zero at the boundary. This machinery that basically separates the incoming waves from the outgoing ones, can be considered a generalization to the nonlinear case of the approach by Engquist and Majda (Section 1.9) and correctly reminds one of the first approximation of the pseudo-differential operator (1.9a).

Historically, as the field of scientific computation was reaching maturity (between the 1960s and 1980s), it was largely dominated by the problems of computational fluid dynamics. In that context, we note the extensive work of Rudy and Strikwerda, who were among the first to construct practical ABCs for fluid dynamics problems. They were interested in numerical treatment of outer boundaries for the computation of compressible viscous flows. In [101, 102], Rudy and Strikwerda have constructed inviscid inflow and outflow nonreflecting boundary conditions (NRBCs) and subsequently applied those to the solution of the 2D compressible Navier-Stokes equations over a flat plate. They also optimize the convergence of the transient process to a steady state and demonstrate the superiority of their NRBCs over the Dirichlet-type boundary conditions for the Navier-Stokes problems.

Even though the issue of ABCs has been discussed in the literature for at least thirty years, it

[1]For more information on simple waves see [24, 36].

still remains an active research area. The account of local methods that we have presented here is by no means comprehensive, we have just mentioned some of the most representative and well-known developments. For a more detailed review of the field, we refer the reader to the paper [39] and book [40] by Givoli, the paper by Tsynkov [116], and the paper by Hagstrom [67].

1.3 Global Methods

Global ABCs have also been obtained in the literature for a fairly broad range of problems, although altogether there are still far fewer publications than those that discuss local methods. Typically, global boundary conditions offer superior accuracy. As far as the approach to their construction is concerned, even though a variety of techniques are available that are attributed to different authors, many of them share the same basic principles of design. First, as the ABCs replace the truncated exterior part of the domain, it is the properties of the solution in this exterior region (i.e., the far field) that determine how the ABCs should look like. In most cases, the first assumption that one makes is that the governing equations in the far field are linear. This can be either a part of the original formulation or a result of linearization. The second key element of the design is the separation of variables, e.g., by means of the Fourier transform. To enable it, the artificial boundary must have a regular shape, say, a circle (sphere) or a straight line (plane), for which the variables will indeed separate. This is the source of geometric limitations that global ABCs often entail. Finally, once the variables have separated, the original multi-D problem is reduced to a collection uncoupled 1D problems (ODEs/systems) in the direction normal to the artificial boundary. Then, setting the ABCs basically reduces to selecting the proper modes among the solutions of each 1D system, for example, those that decay at infinity, or satisfy the 1D radiation boundary condition, or otherwise "behave appropriately" in the context of a particular formulation. The reason these ABCs become nonlocal is that the mode selection operation, an example of which is given by formulae (1.4), (1.5), is done naturally in the transformed space, but typically does not have a convenient local prototype in the original physical space.

In subsequent sections (Sections 1.3.1, 1.3.2, 1.3.3, and 1.3.4), we briefly discuss several well-known global ABCs methodologies. They all share similar principles of design, offer high accuracy, and require regular artificial boundaries. We also note that even though the aforementioned geometric limitations are prevalent, there are still nonlocal ABCs in the literature that can be set at the boundaries of a more general shape. One example is given by the perturbation based approach by Nicholls, Nigam, and co-authors [23,93,94]. Another example, which is perhaps the most notable methodology of this kind, is the ABCs based on Calderon's projections and the method of difference potentials. They were proposed by Ryaben'kii and Tsynkov, and we describe this approach in

Section 1.3.5.

1.3.1 The Method by Engquist and Majda and Its Generalization by Gustafsson

In Section 1.2.1, we have mentioned work [27] by Engquist and Majda on the development of boundary conditions for the wave equation. Even though the authors were ultimately interested in obtaining local methods, they have first built a full-fledged nonlocal NRBC with a pseudodifferential operator. Subsequently, Engquist and Majda have generalized their approach to acoustic waves [28] and transonic flows [29], with the analysis following the same path — first the nonlocal boundary condition and then its local approximations.

When deriving their boundary conditions, Engquist and Majda have always assumed that while all the outgoing waves should be able to leave the computational domain freely with no reflections from the artificial boundary, nothing should come into the computational domain from outside. In other words, no incoming waves were allowed. A generalization of this approach to the formulation that does include some incoming waves was given by Gustafsson in [62]. Gustafsson considers a hyperbolic system in two spatial dimensions with an additional complication that the support of the initial condition is not compact:

$$U_t + AU_x + BU_y = 0, \mathrm{x} \in [0, \infty), \mathrm{y} \in (-\infty, \infty), t \geq 0 \tag{1.27a}$$

$$B_0 U(0, y, t) = g(y, t) \tag{1.27b}$$

$$\sup_{x,y} |U(x, y, t)| < \infty, \ t \geq 0 \tag{1.27c}$$

$$U(x, y, 0) = f(x, y) \tag{1.27d}$$

where A and B are functions of x, y, t, and U, and the artificial boundary is at $x = L$.

To construct the exact artificial boundary conditions, Gustafsson assumes that outside the domain of interest, i.e., for $x \geq L$, the problem reduces to constant coefficients:

$$U_t + \tilde{A}U_x + \tilde{B}U_y = C, \ x \in [L, \infty), \ y \in (-\infty, \infty), \ t \geq 0 \tag{1.28a}$$

$$\sup_{x,y} |U(x, y, t)| < \infty, \ t \geq 0 \tag{1.28b}$$

$$U(x, y, 0) = f(x, y), \ x \in [L, \infty), \ y \in (-\infty, \infty) \tag{1.28c}$$

where $\tilde{A}$ and $\tilde{B}$ are constant matrices, and $\tilde{A}$ is diagonal:

$$\delta(\tilde{A}) = \{\overbrace{\underbrace{\lambda_1, \ldots, \lambda_l}_{negative}, \underbrace{\lambda_{l+1}, \ldots, \lambda_{l+m}}_{positive}}^{l+m \text{ eigenvalues}}\} \tag{1.29}$$

The exact boundary condition is obtained by Laplace-transforming system (1.28a) in time and Fourier-transforming it in y, which results in a system of ODEs for $\hat{U}(x, \omega, s)$ — the transformed vector function, where (ω, s) are the duals of (y, t):

$$\hat{U}(x, \omega, s) = -s\tilde{A}^{-1}\left(I + \frac{i\omega}{s}\tilde{B}\right)\hat{U}(x, \omega, s) + \tilde{A}^{-1}\hat{f}(x, \omega), \tag{1.30}$$

and $\hat{f}(x, \omega)$ denotes the Fourier transform of the initial function with respect to y. The exact artificial boundary condition in the Fourier-Laplace space is obtained on the basis of the general solution to (1.30). The latter is built under the assumption of block-diagonalizability of $\tilde{A}^{-1}(I + \frac{i\omega}{s}\tilde{B})$, which is true for hyperbolic systems; moreover, the eigenvalues of this matrix have the same signs as those of $\tilde{A}$. If the initial data happen to be zero outside the computational domain, then the boundary conditions by Gustafsson [62] become identical to those by Engquist and Majda [27], as expected.

In Section 1.3.3, we describe the work by Ferm and Gustafsson in relation to fluid flow problems.

1.3.2 DtN Maps — the Method by J. Keller and Givoli

In work [89], J. Keller and Givoli present global NRBCs for solving the inhomogeneous Helmholtz equation in an infinite domain $\Omega \subset \mathbb{R}^d$, $d \in \{2, 3\}$, bounded internally by the surface $\Gamma = \Gamma_g \cup \Gamma_h$, on which a combination of the Dirichlet and Neumann boundary conditions can be set:

$$\Delta u + k^2 u + f = 0, \text{ in } \Omega \tag{1.31a}$$

$$u = g, \text{ on } \Gamma_g \tag{1.31b}$$

$$u_\nu = h, \text{ on } \Gamma_h \tag{1.31c}$$

$$\lim_{r\to\infty} r^{(d-1)/2}\,(u_r - iku) = 0 \tag{1.31d}$$

The source term f in (1.31a) is assumed compactly supported, and the functions g and h in (1.31b) and (1.31c) are assumed known; the subscript ν denotes normal differentiation. Boundary condition (1.31d) is the Sommerfeld radiation condition at infinity. To solve problem (1.31) numerically, a computational domain Ξ is defined by the truncation of Ω so that Ξ is bounded internally by Γ and externally by the artificial boundary β. It is required that $\operatorname{supp} f \subseteq \Xi$. The domain outside the

exterior boundary β is denoted by Υ, i.e., $\Upsilon = \Omega \setminus \Xi$, see Figure 1.1. Over the truncated domain the problem (1.31) is written as

$$\Delta u + k^2 u + f = 0, \text{ in } \Xi \tag{1.32a}$$

$$u = g, \text{ on } \Gamma_g \tag{1.32b}$$

$$u_\nu = h, \text{ on } \Gamma_h \tag{1.32c}$$

while on β an exact boundary condition is defined by the Dirichlet to Neumann map (DtN) relating the Dirichlet data u to the Neumann data u_ν:

$$u_\nu = -Mu, \text{ on } \beta \tag{1.32d}$$

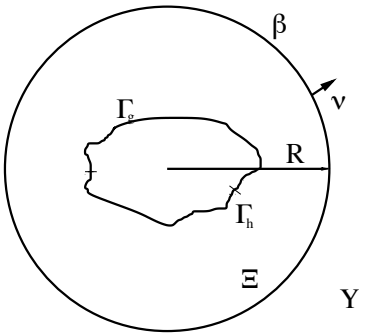

Figure 1.1: Schematic for J. Keller and Givoli approach of [89].

The map M is obtained by solving the Dirichlet problem in Υ (recall, $f \equiv 0$ on Υ) under the assumption that the artificial boundary β is a sphere of radius R:

$$\Delta u + k^2 u = 0, \text{ in } \Upsilon \tag{1.33a}$$

$$u = u(R, \theta), \text{ on } \beta \tag{1.33b}$$

$$\lim_{r \to \infty} r^{(d-1)/2} (u_r - iku) = 0 \tag{1.33c}$$

In 3D, the solution of problem (1.33) is obtained in terms of the Hankel functions of the first kind, the Legendre functions of the first kind, and the values of the solution u on the sphere of radius R. Then, the (global) DtN boundary condition (1.32d) can be explicitly written as

$$u_\nu(R, \theta, \phi) = -\sum_{n=0}^{\infty} \int_\beta m_n(\theta, \phi, \theta', \phi') u(R, \theta', \phi\prime) R^2 \sin\phi' d\theta' d\phi' \tag{1.34}$$

where the DtN kernel is given by

$$m_n(\theta, \phi, \theta', \phi') = \sum_{j=0}^{\infty} \alpha_{jn} P_n^j(\cos\phi) P_n^j(\cos\phi') \cos j(\theta - \theta')$$

with

$$\alpha_{jn} = -\frac{(2n+1)(n-j)!\gamma_n}{2\pi R^2 (n+j)!} \quad \text{and} \quad \gamma_n = \frac{(\frac{\partial}{\partial R})[R^{-1/2} H^{(1)}_{n+1/2}(kR)]}{R^{-1/2} H^{(1)}_{n+1/2}(kR)}$$

Problem (1.32) is discretized and solved in [89] using Galerkin finite elements. In the same article, Keller and Givoli extend their method to a variety of problems such as those over a finite, but large domain, the Laplace equation, the Poisson equation, and others. Further extensions of the DtN approach can be found in [41, 46, 47, 54], as well as in the work by a number of other authors. In particular, an essentially equivalent approach is also referred to as Poincaré-Steklov operators, see [6].

1.3.3 The Method by Ferm and Gustafsson

In [30], Ferm and Gustafsson solve the steady state Euler's equations that describe a flow of inviscid compressible fluid in an unbounded plane parallel duct $\Omega_\infty = \{(x, y) : x \in (0, \infty), y \in [0, 1]\}$:

$$A(w)w_x + B(w)w_y = 0 \tag{1.35}$$

where

$$w = \begin{bmatrix} \rho \\ u \\ v \end{bmatrix}$$

$$A(w) = \begin{bmatrix} u & \rho & 0 \\ c^2/\rho & u & 0 \\ 0 & 0 & u \end{bmatrix}$$

and

$$B(w) = \begin{bmatrix} v & 0 & \rho \\ 0/ & v & 0 \\ c^2/\rho & 0 & v \end{bmatrix}$$

The computational domain is obtained by truncating Ω_∞ in the x-direction at $x = L$; the boundary procedure is constructed downstream at $x = L$. A subsonic flow at the left (incoming) boundary is assumed, i.e., $u \in (0, c)$ at $x = 0$, where c is the local speed of sound defined through the presumed relationship between the pressure p and the density ρ expressed in the form $p = A\rho^\gamma$ and $c = \sqrt{(A\gamma\rho^{\gamma-1})}$.

The boundary procedure is naturally determined by the physical considerations. It is required that the solution be bounded further downstream: $\|w\|_2 < \infty$ for $x > L$, and that the mass flux

$$m = \int_0^1 \rho u dy \tag{1.37}$$

be independent of x. The exact ABCs at $x = L$ are derived by first linearizing the Euler's equations

(1.35) around a constant flow $\bar{w}$ parallel to the walls of the duct, $\bar{v} = 0$:

$$\bar{A}w_x + \bar{B}w_y = 0$$

$$\bar{A} = \begin{bmatrix} \bar{u} & \bar{\rho} & 0 \\ \bar{c}^2/\bar{\rho} & \bar{u} & 0 \\ 0 & 0 & \bar{u} \end{bmatrix}$$

and

$$\bar{B} = \begin{bmatrix} 0 & 0 & \bar{\rho} \\ 0 & 0 & 0 \\ \bar{c}^2/\bar{\rho} & 0 & 0 \end{bmatrix}$$

Then, the perturbations u & ρ are expanded in cosine Fourier series in the cross-stream direction y, and v is expanded in the sine series (to satisfy the impenetrability condition):

$$\rho(x,y) = \sum_{\omega=0}^{\infty} \hat{\rho}_\omega(x) \cos \pi\omega y$$

$$u(x,y) = \sum_{\omega=0}^{\infty} \hat{u}_\omega(x) \cos \pi\omega y$$

$$v(x,y) = \sum_{\omega=1}^{\infty} \hat{v}_\omega(x) \sin \pi\omega y$$

This yields:

$$\bar{A}\frac{\partial \hat{w}_\omega}{\partial x} + \pi\omega\tilde{B}\hat{w} = 0 \tag{1.40a}$$

where

$$\tilde{B} = \begin{bmatrix} 0 & 0 & \bar{\rho} \\ 0 & 0 & 0 \\ -\bar{c}^2/\bar{\rho} & 0 & 0 \end{bmatrix}$$

The general solution of problem (1.40a) has the form $\hat{w}_\omega = \sum_{j=1}^{3} \alpha_j q_j e^{\omega\pi\lambda_j(x-L)}$, where $\{\lambda_j, q_j\}_{j=1}^{3}$ are the eigenpairs of the generalized eigenvalue problem

$$(\bar{A}\lambda + \tilde{B})q = 0$$

The eigenvalues are $\lambda_1 = 0$ and $\lambda_{2,3} = \pm\bar{c}(\bar{c} - \bar{u})^{-1/2}$. To satisfy the condition of boundedness of the solution as $x \to \infty$, we must have $\alpha_2 = 0$; the condition (1.37) is satisfied by setting $\hat{\rho}_0 = \int_0^1 \rho(L,y)dy$.

Both authors of [30] have been active in the development of artificial boundaries for a variety of problems. To find out more, we refer the interested reader to [63] for the discussion of far-field ABCs for hyperbolic systems, [32] for the discussion of external flow problems, [31] for the discussion of inviscid flow problems, and to other papers [33–35].

1.3.4 The Method by Hagstrom

In this section we are discussing Hagstrom's construction of outflow boundary conditions in a model of transport and diffusion, [79]. The author considers the following formulation:

$$u_t + a(y)u_x = D(u_{xx} + u_{yy}),\ x \in\ [0,\infty),\ y \in [-1,1],\ t \geq 0, \tag{1.41a}$$

$$u(0,y,t) = u_0(y,t) \tag{1.41b}$$

$$\lim_{x\to\infty} u\,(x,y,t) = 0 \tag{1.41c}$$

$$u(x,y,0) = 0 \tag{1.41d}$$

$$a(y) \geq 0 \tag{1.41e}$$

where $a(y)$ is a smooth function. The computational domain Ω is obtained by truncating the unbounded domain at $x = L$.

The solution of problem (1.41) is represented in the form of the expansion:

$$u(x,y,t) = \sum_l \int_0^t c_l(p) Q_l(x,y,t-p)dp \tag{1.42a}$$

where

$$Q_l(x,y,t) = \frac{1}{2i\pi} \int_{-i\infty}^{i\infty} e^{st-\lambda_l(s)x} \cdot Y_l(y,s)ds \tag{1.42b}$$

The full extent of the corresponding derivation is beyond the scope of this review and we refer the reader to pages 70–73 of [79]. Here we only mention that $Y_l(y,s)$ is the solution of the eigenvalue problem:

$$sY_l(y,s) + \lambda_l a(y) Y_l(y,s) = D(Y_l''(y,s) + \lambda_l^2 Y_l(y,s)),\ y\ \in (-1,1) \tag{1.43a}$$

$$Y_l'(\pm 1,s) = 0 \tag{1.43b}$$

that arises once expansion (1.42a) is substituted into (1.41a). In the transformed space, expansion (1.42) naturally leads to the boundary condition at $x = L$, which is similar to the one by Engquist

and Majda (cf. boundary condition (1.4) in Section 1.2.1):

$$\frac{\partial \hat{Q}_l}{\partial x} = \lambda_l(s)\hat{Q}_l$$

For more on Hagstrom's work (with collaborators) in the area of nonlocal ABCs we refer the reader to [73] where downstream boundary conditions for the simulation of incompressible viscous flows are discussed, [72] where a general theory of boundary conditions for dissipative waves is presented, as well as to [68, 70, 71, 74, 76, 78, 80].

1.3.5 The Method of Difference Potentials

We have seen that what nonlocal ABCs essentially do is select a proper subspace in the entire space of solutions. For example, DtN maps or Poincaré-Steklov operators achieve that by imposing a certain linear relation between the function and its normal derivative at the boundary. More precisely, a DtN map expresses normal derivative through the function. In doing so, one implicitly assumes that this can be done, i.e., that there is no degeneration of any kind and the problem is well posed. While for simple equations, such as Laplace, this is fairly obvious, there may be more complicated situations as well. Hence, it is natural to try and search for a technique that would be capable of selecting a proper linear subspace without using the resolved forms of the operators, i.e., without having to explicitly express some components as a function of the others.

Along these lines, an ultimate generalization of all the methods such as DtN maps or Poincaré-Steklov operators is offered by the apparatus of Calderon's potentials and boundary projections, see [22]. The original constructs by Calderon were further developed by Seeley [112], and also obtained independently in an even more general form and then put into a discrete context by Ryaben'kii [103, 104, 106]. The method of building and computing the discrete counterparts of Calderon's operators is called the difference potentials method (DPM). The use of Calderon's operators and the DPM for setting the ABCs was proposed by Ryaben'kii in [105] and subsequently applied to a variety of problems. As it turns out, the proposed methodology meets the ambitious goal of applicability in geometrically universal settings, provides a high degree of accuracy for numerical approximations, and also appears quite usable in practice, i.e., not too cumbersome in implementation.

In this section, we first illustrate the concept of Calderon's operators and the corresponding ABCs using a very simple setting of the Helmholtz equation:

$$\mathbf{L}u \equiv \Delta u + k^2 u = 0 \tag{1.44}$$

subject to the Sommerfeld radiation boundary condition at infinity:

$$\frac{\partial u(\mathbf{x})}{\partial |\mathbf{x}|} + ik_0 u(\mathbf{x}) = o\left(|\mathbf{x}|^{\frac{1-n}{2}}\right) \tag{1.45}$$

We then discuss a number of generalizations and show the results of application of the DPM based ABCs to solving the problems of external aerodynamic configuration analysis. Those problems, solved by Ryaben'kii and Tsynkov, see [107, 117] and the bibliography thereon, involve three-dimensional flows of compressible viscous fluid and obviously present a far more sophisticated formulation than the simple settings for second order elliptic operators.

Following the agenda we have just identified, let us first denote by Ω the entire exterior domain (unbounded) that has to be truncated and replaced with ABCs. By Green's theorem, the solution of equation (1.44) on Ω subject to boundary condition (1.45) is a sum of the double-layer potential with density $u|_{\partial\Omega}$ and the single-layer potential with density $\partial_\nu u|_{\partial\Omega}$:

$$u(\boldsymbol{x}) = \int_{\partial\Omega} \left(u(\boldsymbol{y})\partial_\nu G(\boldsymbol{x}-y) - \partial_\nu u(\boldsymbol{y}) G(\boldsymbol{x}-y)\right) d\boldsymbol{y} \tag{1.46}$$

where ν denotes differentiation in the direction normal to the boundary $\partial\Omega$, and $G = -e^{ik|\boldsymbol{x}|}/4\pi|\boldsymbol{x}|$ is the fundamental solution of $\mathbf{L}$. This representation is valid if $\mathbf{L}u = 0$ on Ω. If, however, we substitute an arbitrary pair of functions as densities into the Green's formula (1.46), the resulting function u on Ω will still solve the Helmholtz equation (1.44) and satisfy the radiation condition (1.45), but the values of $u|_{\partial\Omega}$ and $\partial_\nu u|_{\partial\Omega}$ will not necessarily match the densities taken. This leads to the definition the *generalized Calderon's potential* with the vector density $\boldsymbol{\xi}_{\partial\Omega} = (\xi_0, \xi_1)|_{\partial\Omega}$:

$$\mathbf{P}_\Omega \boldsymbol{\xi}_{\partial\Omega} = \int_{\partial\Omega} (\xi_0 \partial_\nu G - \xi_1 G) d\boldsymbol{y}$$

Observe, the definition of Calderon's potential is not conditional upon the requirement that $\boldsymbol{\xi}_{\partial\Omega}$ coincide the values of a solution of $\mathbf{L}u = 0$ on $\partial\Omega$; if, however, the vector $\boldsymbol{\xi}_{\partial\Omega}$ happens to match the densities $u|_{\partial\Omega}$ *and* $\partial_\nu u|_{\partial\Omega}$ of some solution to $\mathbf{L}u = 0$, then this solution can be reconstructed in the form:

$$u(\boldsymbol{x}) = \mathbf{P}_\Omega (u, \partial_\nu u)|_{\partial\Omega}, \ \boldsymbol{x} \in \Omega$$

which is merely a way to re-write the Green's formula (1.46). Next we introduce the notion of the boundary trace of a (sufficiently smooth) function on $\partial\Omega$:

$$\mathbf{Tr} u = (u, \partial_\nu u)|_{\partial\Omega}$$

and define *Calderon's (pseudodifferential) boundary projection* as the composition

$$\mathbf{P}_{\partial\Omega} = \mathbf{Tr}\mathbf{P}_{\mathbf{\Omega}}$$

$\mathbf{P}_{\partial\Omega}$ is indeed a projection; for, let $w = \mathbf{P}_\Omega \boldsymbol{\xi}_{\partial\Omega} = \int_{\partial\Omega}(\xi_0 \partial_\nu G - \xi_1 G)d\boldsymbol{y}$. Then, by definition $\mathbf{P}_{\partial\Omega}\boldsymbol{\xi}_{\partial\Omega} = \mathbf{Tr}\mathbf{P}_\Omega\boldsymbol{\xi}_{\partial\Omega} = (w, \partial_\nu w)|_{\partial\Omega}$, while $\mathbf{P}_\Omega\mathbf{Tr}(\mathbf{P}_\Omega\boldsymbol{\xi}_{\partial\Omega}) = \mathbf{P}_\Omega\mathbf{Tr}(w) = w$ because $\mathbf{L}w = 0$ on Ω and w satisfies (1.45). Hence, $\mathbf{P}_{\partial\Omega} = \mathbf{P}^2_{\partial\Omega}$.

The crucial property of Calderon's boundary projection is that $\mathbf{P}_{\partial\Omega}\boldsymbol{\xi}_{\partial\Omega} = \boldsymbol{\xi}_{\partial\Omega}$ if and only if $\boldsymbol{\xi}_{\partial\Omega} = \mathbf{Tr}u$, where $\mathbf{L}u = 0$ on Ω and u satisfies (1.45). For, assume $\mathbf{P}_{\partial\Omega}\boldsymbol{\xi}_{\partial\Omega} = \boldsymbol{\xi}_{\partial\Omega}$. Then, the desired u on Ω can be taken as $u = \mathbf{P}_\Omega\boldsymbol{\xi}_{\partial\Omega}$. The opposite implication follows immediately from the foregoing analysis based on the Green's formula. The relationship

$$\mathbf{P}_{\partial\Omega}\boldsymbol{\xi}_{\partial\Omega} = \boldsymbol{\xi}_{\partial\Omega} \tag{1.47}$$

is called the *boundary equation with projection (BEP)*. It facilitates an equivalent reduction of the differential equation (1.44) subject to boundary condition (1.45) from the entire unbounded domain Ω to its boundary $\partial\Omega$. Therefore, the BEP (1.47) provides an ideal exact ABC for any combined interior/exterior problem such that the exterior portion reduces to (1.44), (1.45). The only requirement here is that the overall formulation must be uniquely solvable and well posed. Note also that a DtN map or a Poincaré-Steklov operator can be obtained as a resolved form of the Calderon projection $\mathbf{P}_{\partial\Omega}$, i.e., by solving equation (1.47) for ξ_1 assuming that ξ_0 is given.

The model naturally affords further generalizations. One can, for example, assume the existence of sources f on Ω; furthermore, there may be an impinging wave u^{imp} coming from infinity. Then, instead of (1.47), one arrives at the inhomogeneous BEP:

$$\mathbf{P}_{\partial\Omega}\boldsymbol{\xi}_{\partial\Omega} + \boldsymbol{\xi}^{\text{imp}}_{\partial\Omega} + \mathbf{Tr}\int_\Omega G_\Omega f d\boldsymbol{y} = \boldsymbol{\xi}_{\partial\Omega}$$

A very important consideration is that even though the foregoing example was analyzed with the help of convolution integrals that appear in the classical potential theory, in fact, the computation of Calderon's operators requires no fundamental solutions and no evaluation of singular integrals. Instead, one needs to solve a special auxiliary problem (AP) that can typically be chosen so that to enable an easy and efficient solution, e.g., by separation of variables or by multigrid [106]. Not only does it generally simplify the implementation of the method, but also facilitates its application to those cases when the fundamental solution does not exist (variable coefficients) or not easily available (e.g., the linearized Navier-Stokes equations in [107, 117]).

The second, equally important, consideration is that the method of difference potentials allows one to construct discrete counterparts of Calderon's potentials and projections directly for the scheme, bypassing the "dubious" stage of approximating the pseudodifferential operators on the grid. In fact, the DPM builds a full-fledged discrete theory completely parallel to the continuous theory of Calderon, and the approximation properties between the discrete and continuous potentials are later established independently, using certain relations between the continuous and discrete densities [106]. In the context of ABCs, this allows to set those directly on the grid, which is, again, a very natural thing to do, especially given that we only need the ABCs in the discrete context, when an infinite domain problem is to be solved on the computer.

The DPM was successfully employed for solving a variety of applied problems, not only those related to ABCs, and we refer the reader to the monograph [106] by Ryaben'kii and the references there for further detail. As far as the ABCs are concerned, perhaps the most well-known application of the DPM is that to solving external flow problems. Ryaben'kii and Tsynkov in [107] and Tsynkov in [115] have built the boundary projections for the linearized Navier-Stokes equations and thus set the ABCs for the computations of compressible viscous flows in two space dimensions. Later, Tsynkov and Vatsa in [121] and Tsynkov in [117] have extended this approach to the case of three space dimensions, and subsequently, Tsynkov, et al. have further generalized it and applied to computing the flows around slender bodies with jet exhaust [120].

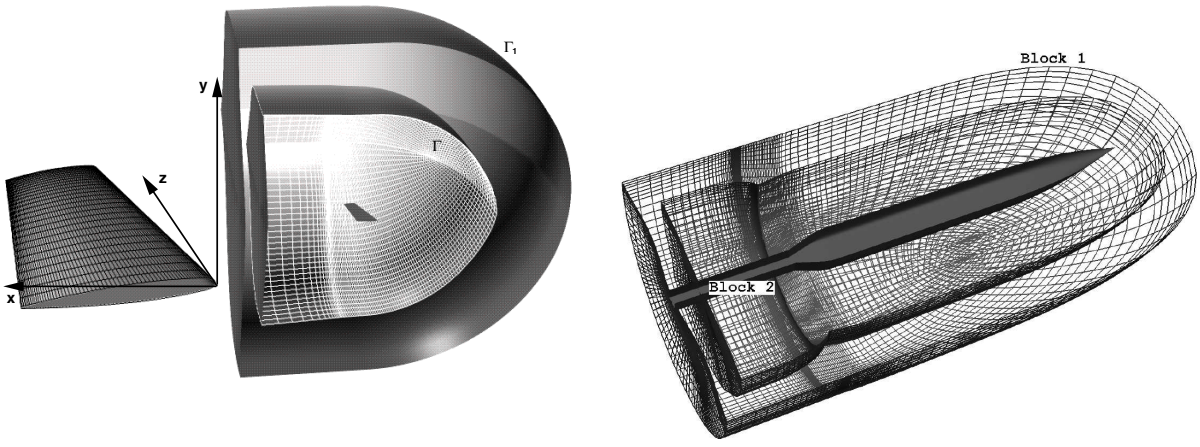

(a) External flow around a wing, from [117]

(b) Flow with jet exhaust, from [120]

Figure 1.2: Typical problem configurations and grid geometries for the DPM-based ABCs as applied to external configuration analysis.

In Figure 1.2, we are showing some typical configurations for setting the DPM-based ABCs. We emphasize that the artificial boundary does not have to have a regular shape. In all the cases analyzed in [107,115,117,120,121], the DPM-based ABCs have enabled major gains in performance by greatly improving the accuracy compared to that of the standard local methods used previously, and also by substantially speeding up the convergence of iterative solvers to steady state. At the same time, these boundary conditions have proven relatively inexpensive to implement and easy to combine with the existing NASA-developed production flow solvers.

1.4 High Order Local Methods

Since the mid 90s the so called high order local NRBCs have gained prominence. These methods can essentially be viewed as sequential *localizations* of global NRBCs; recall, in Section 1.2.3 we encountered a somewhat similar example in the case of the Bayliss-Turkel boundary conditions. However, high order local methods, along with being increasingly accurate, are *practically* implementable for arbitrary high order. As such, the expression *high order* is overloaded with meaning; the first of these naturally captures the accuracy that the methodology provides and the origin of the others will be clarified as we go on.

High order local methods are often obtained by truncating and *localizing* the DtN maps, such as boundary condition (1.34) in Section 1.3.2. For an example of the truncation of a global DtN map we turn to Grote and Keller, [55]. Consider a bounded domain Ξ in $\mathbb{R}^d$ where $d \in \{2,3\}$ with Γ being its piecewise boundary and

$$\Delta U + k^2 U = f, \text{ outside } \Xi \tag{1.48a}$$

$$\alpha U + \beta \partial_\nu U = g \text{ on } \Gamma \tag{1.48b}$$

subject to

$$\lim_{r\to\infty} r^{(d-1)/2}(\partial_r - ik)U = 0, \text{ where } k \text{ is the wavenumber} \tag{1.48c}$$

with α, β and g defined on Γ and f compactly supported. The computational domain is defined by enclosing the domain Ξ and $suppf$ by a circular or spherical artificial boundary Ω of radius $r = a$. Note, the artificial boundary must necessarily be smooth to enable the separation variables. The global artificial boundary condition on Ω is

$$\partial_r U = MU \text{ on } \Omega \tag{1.49}$$

In the 2-dimensional case the boundary condition has the form

$$\partial_r U(a,\theta) = \frac{1}{\pi}\sum_{n=0}^{\infty} \frac{kH_n^{(1)'}(ka)}{H_n^{(1)}(ka)} \int_0^{2\pi} \cos n(\theta-\theta')U(a,\theta')d\theta',$$

where $H_n^{(1)}$ is the Hankel function of the first kind of order n and the primed term with $n = 0$ is multiplied by $\frac{1}{2}$. The solution of (1.48a), (1.48b) subject to the condition (1.49) on Ω coincides with the restriction of the solution of (1.48) to the interior of Ω, see [55]. The map is approximated by truncating the infinite series at some finite mode N; the approximation is exact for modes $0 \le n \le N$ but it will be incorrect for all higher modes and may require retaining more nodes to achieve the desired accuracy. In [55] Grote and Keller supplant the truncation with an additional condition for the higher modes $N+1, N+2, \ldots$ in a way that does not affect the lower modes. The general idea for achieving this is the following: let B be a linear operator such that (1.48a) and (1.48b) subject to $\partial_r U = BU$ on Ω is well-posed. The modified DtN boundary condition then is given by

$$\partial_r U = (M^N - B^N)U + BU \text{ on } \Omega \tag{1.50}$$

where B^N is the truncation of the operator B at mode N. In $\mathbb{R}^2$, i.e., Ω-circular, the Bayliss-Turkel boundary condition (1.19) in Section (1.2.3) can serve in the capacity of the operator B. For example, in the 2-dimensional case for $N = 1$ the artificial boundary condition is

$$\partial_r U(a,\theta) = \left(ik - \frac{1}{2a}\right)U(a,\theta) + \frac{1}{\pi}\sum_{n=0}^{N}\left(\frac{kH_n^{(1)'}(ka)}{H_n^{(1)}(ka)} - ik + \frac{1}{2a}\right)\int_0^{2\pi}\cos n(\theta-\theta')U(a,\theta')d\theta'$$

where the primed term $n = 0$ is multiplied by $\frac{1}{2}$. The authors verified the intuitive assumption that the the artificial boundary condition (1.50) is more accurate for $N = 2$. Similar artificial boundary conditions are derived for the spherical and elliptic cases. This fundamental example sheds light upon another reason for using the term *high order* in the context of this methodology; as such, it reflects the fact that the infinite series (1.49) can be truncated at an arbitrarily high mode.

Even once the DtN map has been truncated, boundary condition (1.50) still remains nonlocal. For the solutions U composed of a finite number of harmonics (that does not exceed N) this boundary condition is exact. In [56], Grote and Keller propose an approach to localizing boundary conditions that are exact for a finite number of harmonics; they conduct their analysis for the spherical geometry and in a more general time-dependent setting (the d'Alembert equation). Localization is achieved by recasting the coefficients of the expansion that yields the ABCs in the particular form that allows to interpret its individual terms as the results of application of one and the same operator (more precisely, powers of the Beltrami operator on the sphere) that does not depend on the summation

index. The localized form of the ABCs contains high order derivatives in the radial direction, and to avoid the potential adverse effects on the numerical algorithm, the authors of [56] propose an alternative form of the boundary condition that does not contain high order derivatives but requires the computation of a number of auxiliary quantities at the boundary. Subsequent paper [57] by Grote and Keller addresses a number of delicate issues related to the numerical implementation of the localized ABCs.

In [53] Givoli, Patlashenko and Keller also address the crucial question of localizing a DtN map. Consider an elliptic second-order boundary value problem in 2 dimensions:

$$(\bar{\kappa}^{-1})\nabla \cdot \kappa(x)\nabla u + \beta(x)u + f(x) = 0 \text{ in } \Omega \tag{1.51a}$$

$$\nabla^2 u + \beta u = 0 \text{ in } \mathcal{D} \tag{1.51b}$$

$$u = g \text{ on } \Gamma_g \tag{1.51c}$$

$$\partial_\nu u = h \text{ on } \Gamma_h \tag{1.51d}$$

$$u \equiv 0 \text{ on } \gamma_u \text{ and } \gamma_l \tag{1.51e}$$

$$\text{An additional condition at infinity} \tag{1.51f}$$

where the computational domain Ω is bounded in by $\mathcal{B}$ and Γ; in turn, $\Gamma = \Gamma_g \cup \Gamma_h$. D is the exterior of the computational domain and is itself bounded by the parallel rays γ_u and γ_l, see Figure 1.3. The functions $f,\ g,\ h,\ \kappa,\ \beta$ are known and in $\mathcal{D}$, $\beta(x) \equiv \beta$, $\kappa(x) \equiv \bar{\kappa} \neq 0$. . Incidentally, depending on the sign of β the equation (1.51b) is Laplace ($\beta = 0$), Helmholtz ($\beta \geq 0$), or Yukawa, i.e., modified Helmholtz ($\beta \leq 0$). To obtain a numerical approximation of the problem (1.51), it is reformulated over a finite domain by truncating the domain at $x = x_0$; $y \in [0, b]$. The reformulated problem consists of (1.51a), (1.51c), (1.51d) and a condition on $\mathcal{B}$ — the DtN map. The general form of the DtN map is given by (1.49); its adaptation to the present geometry reads as

$$\partial_x u(x) = -Mu(x) \equiv \sum_{n=0}^{\infty} \int_B m_n(x, x')u(x')dx',\ x\ \in \mathcal{B}$$

To obtain the exact form of the map on $\mathcal{B}$ the problem is analyzed in $\mathcal{D}$; the general form of the solution for the prescribed values on γ_l and γ_u is obtained by separating the variables and it reads

$$u(x, y) = \sum_{n=1}^{\infty} A_n e^{im_n x} \sin \frac{n\pi y}{b} \tag{1.52}$$

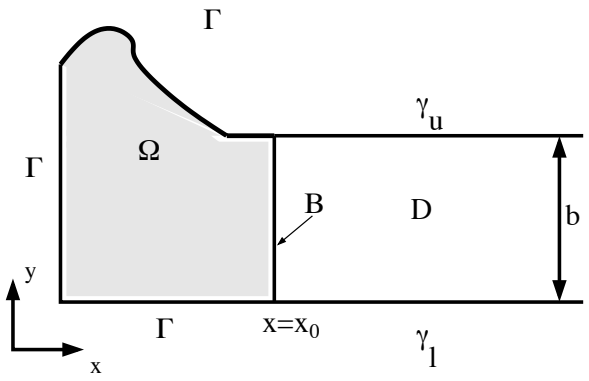

Figure 1.3: Setup for setting the ABCs for the semi-infinite strip, from [53]

.

with

$$m_n = \sqrt{\beta - \left(\frac{n\pi}{b}\right)^2}$$

The DtN map on $\mathcal{B}$ is obtained by Fourier expanding the solution at x_0 in order to obtain the constant coefficients A_n in terms of the Fourier coefficients of $u(x_0, y)$; the expression (1.52) then reads

$$u(x,y) = \frac{2}{b}\sum_{n=1}^{\infty} e^{im_n(x-x_0)} \int_0^b \sin\frac{ny\pi}{b} \sin\frac{n\pi y'}{b} u(x_0, y')dy'$$

immediately yielding the *exact* DtN map at x_0

$$\partial_x u(x_0, y) = -Mu(x_0, y) \equiv -\frac{2\pi}{b^2}\sum_{n=1}^{\infty} Z_n \int_0^b \sin\frac{ny\pi}{b} \sin\frac{n\pi y'}{b} u(x_0, y')dy' \tag{1.53}$$

where the values of Z_n are determined by the sign of β and the geometric setup; some of these are tabulated in [53]. Let us now assume that the solution of the problem (1.51) on $\mathcal{B}$ is a sum of the first N harmonics (i.e., the localization in this case will be exact; for an infinite series solution the localization with the first N harmonics will be inexact, of course)

$$u(x_0, y) = \sum_{n=1}^{N} u_n \sin\frac{ny\pi}{b} \tag{1.54}$$

where u_n are the Fourier coefficients. Substituting the general form (1.54) into the DtN condition

(1.53) and recalling the orthogonality of the sine series one obtains

$$\frac{\partial u}{\partial x}(x_0, y) = -\frac{\pi}{b} \sum_{n=1}^{N} Z_n u_n \sin \frac{ny\pi}{b} \tag{1.55}$$

The form of the boundary condition (1.53) necessitates the expression

$$Z_n \sin \frac{ny\pi}{b} = L_N \left[\sin \frac{ny\pi}{b} \right], \ n = 1, \ldots, N \tag{1.56}$$

where L_N is a linear differential operator *independent of n.* The operator in (1.56) allows to rewrite the boundary condition (1.55) in the form:

$$\frac{\partial u}{\partial x}(x_0, y) = -\frac{\pi}{b} L_N \left[\sum_{n=1}^{N} u_n \sin \frac{ny\pi}{b} \right] = -\frac{\pi}{b} L_N [u(x_0, y)]$$

Then, the operator L_N itself is found by re-expressing Z_n as a solution of a system of N linear equations:

$$Z_n = \sum_{m=0}^{N} \alpha_m^{(N)} n^{2m}, \ n = 1, \ldots, N$$

where $\left\{ \alpha_j^{(N)} \right\}_{j=0}^{N-1}$ is a constant unknown vector, and using the relationship

$$n^{2m} \sin \frac{ny\pi}{b} = \left(- \left(\frac{b}{\pi} \right)^2 \frac{\partial^2}{\partial y^2} \right)^m \sin \frac{ny\pi}{b}$$

which yields:

$$L_N = \sum_{m=0}^{N-1} \alpha_m^{(N)} \left(- \left(\frac{b}{\pi} \right)^2 \frac{\partial^2}{\partial y^2} \right)^m \tag{1.57}$$

The definition (1.57) leads to the *localized* truncated DtN map:

$$\partial_x u = - \sum_{m=0}^{N-1} (-1)^m \alpha_m^{(N)} \left(\frac{b}{\pi} \right)^{2m-1} \partial_y^{2m} u, \quad x = x_0, \ y \ \in [0, b] \tag{1.58}$$

Certain benefits as well as some disadvantages of such methodologies are evident. The most obvious benefit is the arbitrarily high accuracy, robustness and reliability of the procedure stemming from the global nature of the DtN maps; also beneficial is the the subsequent localization achieved through the truncation of the global map. On the other hand, since the methodology is obtained from a global method, one has to face inflexible geometric restrictions that allow the separation of variables; note, all examples are constructed for "manageable" domains. Secondly, DtN maps are

often written in terms of special functions; as the approximation (1.58) attests to it, derivatives of high order are required in localizing such a map thus presenting additional computational costs. Furthermore, presence of high order derivatives in a low order problem is usually undesirable while high order temporal derivatives in time dependent problems exacerbate the matters from the perspective of numerical time-integration.

Some practical problems that arise with the truncation of the DtN maps have been addressed. In [52], within the C^∞ framework for the class of functions that admit separation of variables, Givoli and Patlashenko find the best approximation of the DtN map that will guarantee the predetermined order of accuracy. Givoli and Patlashenko achieve this by approximating the RHS of (1.34) with a K^{th} order local operator L_K (K here is referring to the order of the NRBCs) whose coefficients are as of yet unknown. The objective is to find L_K with K-low such, that it can essentially replicate a high order NRBCs up to the desired order N; that is, the approach increases accuracy without increasing the order of the approximating operator. Minimizing the Euclidean norm of the difference of the RHS and its local approximation yields the necessary coefficients. In [42] Givoli reduces the differential order of the NRBC by introducing new *auxiliary* variables to avoid approximating the high order derivatives. This allows the use of a more compact computational stencil (albeit, at the cost of having to evaluate more unknowns) as well as provides a NRBC of arbitrarily high order with a symmetric structure. Further references on local high order methods include [7, 8, 43–45, 48–51, 53, 58, 59, 69, 75, 77, 96, 122–124].

1.5 Perfectly Matched Layers

1.5.1 Background

In his seminal work [20], J.P. Berenger has introduced an efficient technique based on an absorbing layer for computing the propagation of electromagnetic waves over unbounded domains. The methodology came to be known as the perfectly matched layer (PML). Initially developed for the 2-dimensional case, [20], the technique was subsequently expanded to encompass the 3-dimensional case as well, see [21]. Berenger proposed truncating the domain of computation and then surrounding it by an artificial medium with a built-in ability to absorb incident electromagnetic radiation with no reflection. The PML capabilities are attained by splitting the field components, i.e., introducing additional unknowns and equations into the layer, and then using the resulting added degrees of freedom to

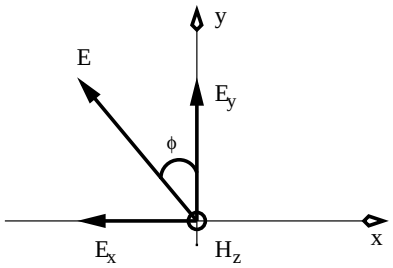

Figure 1.4: The TE problem, [20]

attenuate the waves. For simplicity and without any loss of generality, we present the split field PML by Berenger for the two-dimensional Maxwell's equations in the Cartesian coordinates with $\frac{\partial}{\partial z}(\cdot) \equiv 0$. In this case, the equations uncouple into two independent sets known as the transverse electric (TE) and the transverse magnetic (TM) cases. We will consider the TE case, see Figure 1.4, that involves the components E_x, E_y, and H_z:

$$\epsilon_0 \partial_t E_x + \sigma E_x = \partial_y H_z \tag{1.59a}$$

$$\epsilon_0 \partial_t E_y + \sigma E_y = -\partial_x H_z \tag{1.59b}$$

$$\mu_0 \partial_t H_z + \sigma^\star H_z = \partial_y E_x - \partial_x E_y \tag{1.59c}$$

The quantities σ and $\sigma^\star$ in system (1.59) denote the electric and magnetic conductivities, respectively, which are responsible for dissipation (damping). The TM case is analogous. If the condition

$$\frac{\sigma}{\epsilon_0} = \frac{\sigma^\star}{\mu_0}, \tag{1.60}$$

holds, the impedance of the material (1.59) is equal to that of vacuum, and no reflection occurs at the interface for normal incidence. In the Berenger's split field system that corresponds to (1.59), the vector component H_z is split into H_{zx} and H_{zy} that "live" in the planes zx and zy, respectively. Accordingly, the new conductivity variables $\sigma_x^\star$ and $\sigma_y^\star$ are introduced so that

$$\epsilon_0 \partial_t E_x + \sigma_y E_x = \partial_y (H_{zx} + H_{zy}) \tag{1.61a}$$

$$\epsilon_0 \partial_t E_y + \sigma_x E_y = -\partial_x (H_{zx} + H_{zy}) \tag{1.61b}$$

$$\mu_0 \partial_t H_{zx} + \sigma_x^\star H_{zx} = -\partial_x E_y \tag{1.61c}$$

$$\mu_0 \partial_t H_{zy} + \sigma_y^\star H_{zy} = \partial_y E_x \tag{1.61d}$$

Observe, if $\sigma_x = \sigma_y = \sigma_x^\star = \sigma_y^\star = 0$, then equations (1.61) reduce the Maxwell's equations in vacuum; if $\sigma_x^\star = \sigma_y^\star$, then equations (1.61) reduce to the set (1.59). Note that the formulation does not alter the propagation speed in the medium since this would immediately create a scattering mechanism for the waves; instead, only the amplitudes of the waves are reduced by appropriately choosing the conductivities. Typically, the conductivity is equal to zero at the interface and then smoothly increases into the layer. Special attention is given to vacuum–layer interfaces; in particular, it has been shown that the *theoretical* reflection factor of a plane wave striking the interface is null at *any* frequency and at *any* incidence angle, see [20], unlike in the earlier absorption layers proposed in the literature.

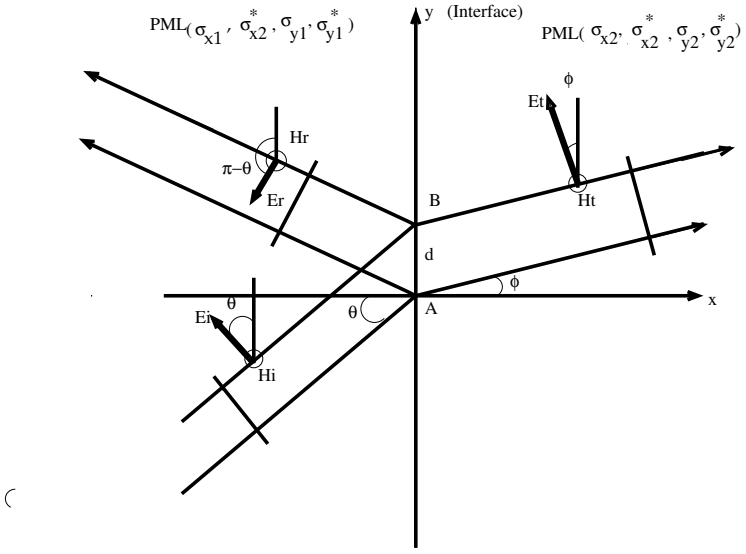

Figure 1.5: Interface between 2 matched media normal to the x-axis, from [20].

As an example, consider an infinite interface normal to the x-axis and an incident plane wave, see Figure 1.5. Here the indices i, r, and t correspond to the incident, reflected and transmitted fields. The angles of the incidence and refraction are θ and ϕ, respectively. It is proven in [20] that if the half-plane $x < 0$ is vacuum, then the media are perfectly matched if the PML, i.e., the half-plane $x \geq 0$, is defined by $(\sigma_x, \sigma_x^\star, 0, 0)$. Analogously, in the case of an interface normal to the y-axis the media would be matched if the PML $y \geq 0$ is defined by $(0, 0, \sigma_y, \sigma_y^\star)$. Figure 1.6 provides a visualization of the general application of the PML methodology. The computational domain (vacuum) is surrounded by the PML; observe how the corners match the adjacent regions rather than the domain of computation. In Chapter 3, we will encounter an analogous setup for the alternative *unsplit* formulation formulation of the PML. The reasons for its development are discussed in the next section.

1.5.2 Concerns about PMLs

Bérenger's split field formulation has been extensively studied and exploited in the literature. Overall, it has demonstrated excellent performance for numerous applications. At the same time, it has been noticed [1] that the Bérenger's split transforms the strongly hyperbolic (symmetric) Maxwell's

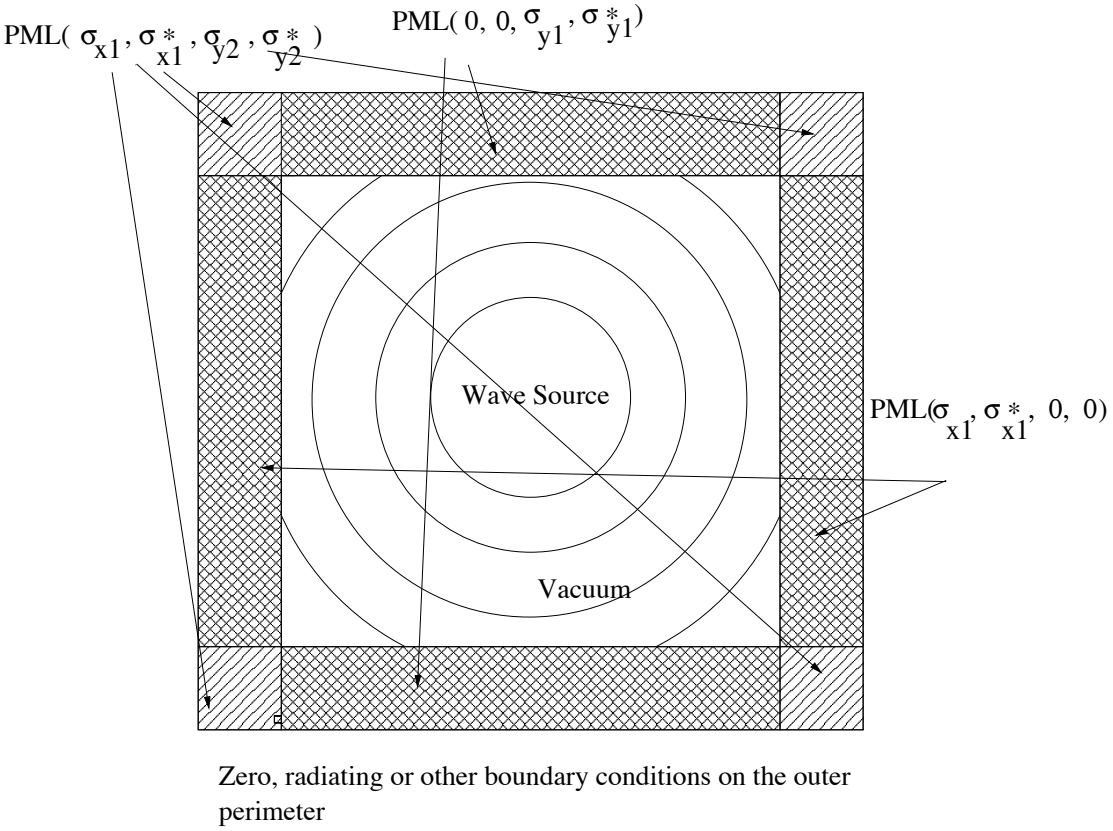

Figure 1.6: The PML technique schematic, from [20].

equations into a weakly hyperbolic system, which, in turn, implies transition from strong well-posedness to weak well-posedness of the Cauchy problem [90].[2] A weakly well-posed system can become ill-posed under a low order perturbation[3], and an example of such a perturbation for the Bérenger's equations was given in [1]. Even though it has later been shown [17] that the actual form of the Bérenger's system does not lead to ill-posedness, the system still remains only weakly well-posed, *and a linear growth of the split field components inside the PML is possible.* This behavior may also lead to a purely numerical instability of the discretization. In particular, it has been proved in [1] that the very popular Yee scheme [125] becomes unconditionally unstable in the PML [20, 21], with the powers of the amplification matrices growing linearly as the number of time steps increases.

Concerns about well-posedness and stability of the PMLs have prompted the development of other types of absorbing layers for computational electromagnetism [2, 37, 126] and other areas (e.g.,

[2] In fact, weak well-posedness characterizes all split field PMLs, see, e.g., [26].
[3] For the general discussion on well-posedness of the Cauchy problem for hyperbolic systems see Appendix 4.A.

acoustics [82]). These alternative strategies do not require splitting the field components in the PML, although they still introduce additional unknowns inside the layer. Accordingly, they came to be known as unsplit PMLs. Later, however, *the unsplit PMLs have also been found susceptible to gradually developing instabilities [3].* They have first been predicted theoretically and then *corroborated by actual computations,* e.g., for the two-dimensional TE polarized Maxwell's equations [3]. Two of the more popular unsplit PMLs, the mathematically derived formulation (2.1) and the physically derived formulation (2.2), appear in Chapter 2 which is wholly devoted to a systematic study of the long-time performance of unsplit PMLs with several commonly used explicit second order schemes.

Note that if some components of the solution begin to grow inside the PML, the resulting numerical artifacts from the layer may or may not contaminate the computational domain, depending on the particular application and the design of the scheme. As mentioned, e.g., in [18], the Yee scheme can keep the instability inside the layer, whereas a higher order scheme of [3] propagates it back into the domain. As, however, has been noticed in [114], for the reason of improving the numerical performance on parallel platforms, a code that includes a split field PML is often designed in such a way that the equations solved inside the domain (not in the layer) are also split, although with no damping factors. In this case, even the Yee scheme appears capable of allowing the contamination from the layer into the domain.

An approach has been proposed in [3] to cure the long-time instability of unsplit PMLs. This approach is based on changing the governing equations in the layer. It has been experimentally shown to work well, but theoretically it is unclear whether the modified layer remains perfectly matched and absorbing.

Other remedies can also be found in the literature. For example, the nonlinear PML of [4] guarantees boundedness of the energy integrals and strong well-posedness of the governing equations in the layer. However, its practical implementation requires a certain regularization to keep the denominators away from zero. Again, computationally it has been shown to perform well, but the analysis does not extend to this case. The complex frequency-shifted PML introduced in [38, 100] and analyzed in detail in [18] also guarantees boundedness of the energy integrals and strong well-posedness.[4] However, the frequency shift in the PML leads to the loss of frequency independent absorption [18].

Altogether, the aforementioned stabilizing changes inside the PML often show no detrimental effect of any kind in the experiments, even when the supporting analysis is lacking. Moreover, according to a number of authors (see, e.g., [26]), the long-time instability of the PMLs may only have a limited negative effect in practical computations, in particular, because often by the time

[4]For the analysis of well-posedness see also [97].

it manifests itself the phase errors would have already killed the solution [114]. We tend to believe, however, that the deterioration of solution due to the phase errors is not always that rapid (Section 3.3), and as any potentially adverse phenomenon, the long-term instability of the PMLs needs to be carefully addressed. Therefore, *the objective of this dissertation is to introduce a cure for the long-time instability of the PMLs while keeping all the advantageous properties of a given layer unaffected (such as matching, absorption, etc.). It is equally important that the proposed cure be fully and rigorously justified.* The first step towards this goal is understanding the long-time behavior of the solution inside the PML. In Chapter 2, we report the findings of the analytical and experimental investigation of the phenomenon of long-time growth inside the layer.

Chapter 2

Performance of Unsplit PMLs with Explicit Second Order Schemes

2.1 Motivation and Background

As has been previously mentioned, the undesirable phenomenon of gradual long-time growth of the solution in PMLs may hamper the performance of the layer. For unsplit PMLs, prior studies [1–3] have attributed the growth to the presence of multiple eigenvalues in the amplification matrix of the governing system of differential equations. In the current chapter, we analyze the temporal behavior of unsplit PMLs for some commonly used second order explicit finite-difference schemes that approximate the Maxwell's equations. Our conclusion is that on top of having the PML as a potential source of long-time growth, the type of the layer and the choice of the scheme play a major role in how rapidly this growth may manifest itself and whether or not it manifests itself at all.

The analysis in this chapter follows that of our recent paper [5]. In turn, the computational setup of [5] "borrows" certain components from [3] for the sake of enabling an easier comparison. Two unsplit PMLs were investigated in [3] for the 2D Cartesian transverse electric (TE) Maxwell's equations. For the layer that truncates the domain in the x-direction, the so-called mathematically

derived PML of [2] is given by:

$$\begin{aligned}
\frac{\partial E_x}{\partial t} &= \frac{\partial H_z}{\partial y} \\
\frac{\partial E_y}{\partial t} &= -\frac{\partial H_z}{\partial x} - 2\sigma E_y - \sigma P \\
\frac{\partial H_z}{\partial t} &= \frac{\partial E_x}{\partial y} - \frac{\partial E_y}{\partial x} + \sigma' Q \\
\frac{\partial P}{\partial t} &= \sigma E_y \\
\frac{\partial Q}{\partial t} &= -\sigma Q - E_y
\end{aligned} \tag{2.1}$$

The additional quantities P and Q are non-zero only in the layer, and the damping of waves is controlled by the parameter $\sigma(x) = \frac{(x-a)^3}{d^3}$, where d is the PML thickness and $x = a$ is the interface between the domain and the layer.

An alternative to (2.1) is the physically motivated unsplit PML of [37] or [126], which can be written in the following form [2]:

$$\begin{aligned}
\frac{\partial E_x}{\partial t} &= \frac{\partial H_z}{\partial y} + \sigma(E_x - P) \\
\frac{\partial E_y}{\partial t} &= -\frac{\partial H_z}{\partial x} - \sigma E_y \\
\frac{\partial H_z}{\partial t} &= \frac{\partial E_x}{\partial y} - \frac{\partial E_y}{\partial x} - \sigma H_z \\
\frac{\partial P}{\partial t} &= \sigma(E_x - P)
\end{aligned} \tag{2.2}$$

Unlike in (2.1), there is only one additional quantity, P, inside the PML (2.2).

The analysis of [3] focuses on the quiescent solutions inside the PML, long after the initial perturbation has been absorbed. It is shown that if the spatial derivatives are neglected, then the system of ODEs that results from either (2.1) or (2.2) would be characterized by multiple eigenvalues and the degeneracy of eigenvectors. This indicates the possibility of a polynomial growth. Experimentally, a slow growth originating in the PML was indeed observed in [3] for one specific choice of the discrete approximation, namely when equations (2.1) or (2.2) were approximated using fourth order central differences in space accompanied by a fourth order Runge-Kutta method in time.

On the other hand, there have been reports in the literature that for a given computational setup the growth may or may not be observable, and that the artifacts generated in the PML, if any, may or may not propagate back into the computational domain [18]. Hence, in the current paper we set our goal as to systematically study the long-time behavior of the PMLs (2.1) and (2.2) with a number of

commonly used explicit second order finite-difference schemes. Specifically, we consider the staggered Yee scheme [125], the leap-frog scheme, the Lax-Wendroff scheme, and the central difference scheme supplemented by the Runge-Kutta time integration. Compared to [3], we complement our analysis by looking at the eigenvalues (amplification factors) of the actual discretizations, as opposed to only those of the differential problem. Besides, we conduct extensive numerical tests for each of the aforementioned schemes.

It turns out that the growth can, in fact, be effectively removed by just the discretization itself. The Yee scheme, the Lax-Wendroff scheme, and the central scheme applied to the PML (2.2) exhibit no growth at all in our experiments, whereas the Yee scheme and the Lax-Wendroff scheme applied to the PML (2.1) exhibit a growth which is so slow that can be deemed non-existent for any practical purpose. On the other hand, the discretization may also greatly exacerbate the growth and make the computations impossible, which is what happens to the leap-frog scheme with both PMLs. Finally, the popular family of central schemes with Runge-Kutta smoothers[1] remains susceptible to a moderately slow growth of the solution in the PML (2.1), which indicates that the appropriate remedies need to be sought for. Altogether, we conclude that the phenomenon of growth of the numerical solution in the PML proves to depend strongly on both the choice of the PML and the choice of the scheme.

2.2 Computational Setup

To enable an easier comparison, we take the same setup as in [3]. Our computational domain is a Cartesian square: $\{(x,y)\,|\,-a\le x\le a,\ -a\le y\le a\}$ with $a=50$; it is terminated in the x-direction by two symmetrically located PMLs: $-a-d\le x\le -a$ and $a\le x\le a+d$, where $d=10$. The Cartesian discretization grid has square cells: $h_x=h_y=1$. At the top and bottom boundaries, $y=a$ and $y=-a$, as well as at the outer boundaries of the PML, $x=a+d$ and $x=-a-d$, we use classical locally one-dimensional characteristic artificial boundary conditions (ABCs, see [116]) obtained by setting to zero the Riemann invariant that corresponds to the incoming characteristic.

In all forthcoming simulations, we investigate numerically the evolution on the grid of a smooth initial perturbation of the magnetic field:

$$H(x,y,0)=\begin{cases}\cos^8\left(\frac{\pi\sqrt{x^2+y^2}}{2r_0}\right), & \text{if } \sqrt{x^2+y^2}\le r_0\\ 0, & \text{if } \sqrt{x^2+y^2}>r_0\end{cases}$$

where $r_0=10$. The initial values of the electric field E_x and E_y are zero.

[1] It is apparently the most straightforward venue to high order approximations.

We also emphasize that as we terminate the PML by characteristic ABCs, we can determine conclusively whether or not the long-term growth, in case it is observed, shall actually be attributed to the PML. Indeed, we can first run the computation with the PML. Then, we can merely turn off the PML (by setting $\sigma(x) \equiv 0$) while leaving all other components of the algorithm intact and while still keeping all the boundaries nonreflecting (to the degree permitted by the locally one-dimensional treatment). If no growth is detected in the second case (no PML), then the previously observed growth is clearly due to the PML and nothing else. Hereafter, if the growth is reported, it shall be assumed that it has been verified this way.

Finally, let us quantify the notion of a long time. Introduce the unit of time as the domain size over the propagation speed: $T = 2a/c$, where $c = 1$. We will be investigating the phenomena that start manifesting themselves no earlier than $10T$ to $15T$ and all the way up to hundreds and thousands of T's.

2.3 The Yee Scheme

The staggered Yee scheme [125] as applied to the mathematical PML (2.1) reads

$$\begin{aligned}
\frac{E_{x}{}^{p+1/2}_{m,n+1/2} - E_{x}{}^{p-1/2}_{m,n+1/2}}{\tau} &= \frac{H^{p}_{m,n+1} - H^{p}_{m,n}}{h_y} \\
\frac{E_{y}{}^{p+1/2}_{m+1/2,n} - E_{y}{}^{p-1/2}_{m+1/2,n}}{\tau} &= -\frac{H^{p}_{m+1,n} - H^{p}_{m,n}}{h_x} - 2\sigma_{m+1/2}\frac{E_{y}{}^{p+1/2}_{m+1/2,n} + E_{y}{}^{p-1/2}_{m+1/2,n}}{2} - \sigma_{m+1/2}P^{p}_{m+1/2,n} \\
\frac{H^{p+1}_{m,n} - H^{p}_{m,n}}{\tau} &= \frac{E_{x}{}^{p+1/2}_{m,n+1/2} - E_{x}{}^{p+1/2}_{m,n-1/2}}{h_y} - \frac{E_{y}{}^{p+1/2}_{m+1/2,n} - E_{y}{}^{p+1/2}_{m-1/2,n}}{h_x} + \sigma'_m\frac{Q^{p+1}_{m,n} + Q^{p}_{m,n}}{2} \\
\frac{P^{p+1}_{m+1/2,n} - P^{p}_{m+1/2,n}}{\tau} &= \sigma_{m+1/2}E_{y}{}^{p+1/2}_{m+1/2,n} \\
\frac{Q^{p+1}_{m,n} - Q^{p}_{m,n}}{\tau} &= -\sigma_m\frac{Q^{p+1}_{m,n} + Q^{p}_{m,n}}{2} - \frac{E_{y}{}^{p+1/2}_{m+1/2,n} + E_{y}{}^{p+1/2}_{m-1/2,n}}{2}
\end{aligned} \tag{2.3}$$

and for the physical PML (2.2) it is

$$\begin{aligned}
\frac{E_x{}_{m,n+1/2}^{p+1/2} - E_x{}_{m,n+1/2}^{p-1/2}}{\tau} &= \frac{H_{m,n+1}^p - H_{m,n}^p}{h_y} + \frac{\sigma_m}{2}(E_x{}_{m,n+1/2}^{p+1/2} + E_x{}_{m,n+1/2}^{p-1/2}) - \sigma_m P_{m,n+1/2}^p \\
\frac{E_y{}_{m+1/2,n}^{p+1/2} - E_y{}_{m+1/2,n}^{p-1/2}}{\tau} &= -\frac{H_{m+1,n}^p - H_{m,n}^p}{h_x} - \sigma_{m+1/2}\frac{E_y{}_{m+1/2,n}^{p+1/2} + E_y{}_{m+1/2,n}^{p-1/2}}{2} \\
\frac{H_{m,n}^{p+1} - H_{m,n}^p}{\tau} &= \frac{E_x{}_{m,n+1/2}^{p+1/2} - E_x{}_{m,n-1/2}^{p+1/2}}{h_y} - \frac{E_y{}_{m+1/2,n}^{p+1/2} - E_y{}_{m-1/2,n}^{p+1/2}}{h_x} - \sigma_m\frac{H_{m,n}^{p+1} + H_{m,n}^p}{2} \\
\frac{P_{m,n+1/2}^{p+1} - P_{m,n+1/2}^p}{\tau} &= \sigma_m E_x{}_{m,n+1/2}^{p+1/2} - \sigma_m\frac{P_{m,n+1/2}^{p+1} + P_{m,n+1/2}^p}{2}
\end{aligned} \tag{2.4}$$

where $H_z \equiv H$, and the indices m, n, and p correspond to x, y, and t, respectively. In the discretization (2.3) the equations for E_y and Q are approximated semi-implicitly. In the case of the discretization (2.4), all variables are updated semi-implicitly. In actual numerical runs, the Yee scheme exhibits no growth with the physical PML (2.2). More specifically, the magnitude of the solution decays gradually and does not exceed 10^{-6} at $t = 2500T$. From the standpoint of practice, this value is extremely large, and hence we can say that the growth does not manifest itself at all. For the mathematical PML (2.1), scheme (2.3) still displays some growth but it is very slow; no artifacts can be seen until several hundred T.

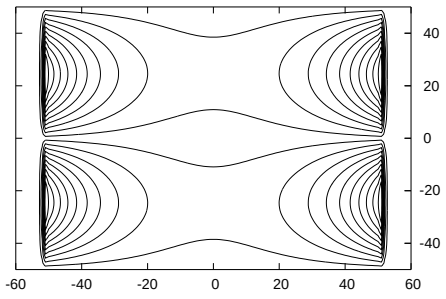

Figure 2.1: E_x for the Yee scheme (2.3) at $t = 500T$; the contours are equally spaced between -0.475 and 0.475 with the increment 0.05.

In Figure 2.1, we are showing a typical snapshot of the solution obtained using scheme (2.3) — the level lines of $E_x(x, y, t)$ at $t = 500T$. Other quantities look similar, their magnitude across the domain does not exceed 0.5. In practice, the time $t = 500T$ is also very large and we therefore believe that the growth shown in Figure 2.1 can be disregarded in most cases. Moreover, one can see from Figure 2.1 that the artifacts originate in the PML near its interface with the domain, i.e., in the region where $\sigma(x)$ is small. This observation is generally in agreement with the analysis of [3].

It is also interesting to see what happens to the eigenvalues. We adopt an approach similar to that of [3] and analyze quiescent solutions in the PML, i.e., assume that there is no spatial variation and neglect all spatial differences. Then, the difference equations for E_y and P decouple from the

rest of system (2.3), and dropping m and n for convenience, we have (at a given location):

$$\begin{aligned} \frac{{E_y}^{p+1/2} - {E_y}^{p-1/2}}{\tau} &= -\sigma({E_y}^{p+1/2} + {E_y}^{p-1/2}) - \sigma P^p \\ \frac{P^{p+1} - P^p}{\tau} &= \sigma {E_y}^{p+1/2} \end{aligned} \tag{2.5}$$

System (2.5) is a second order system of ordinary difference equations. Its eigenvalues can be easily computed: $\lambda_1 = 1/(1+\sigma\tau)$ and $\lambda_2 = 1-\sigma\tau$. Compared to the continuous case [3], we observe a split of the eigenvalue, because the differential counterpart of system (2.5) has a degenerate eigenvalue $\lambda = -\sigma$. The differential physical PML (2.2) in the quiescent state is characterized by a double eigenvalue $\lambda = 0$ with only one eigenvector. For the Yee scheme, however, it translates into a degenerate double eigenvalue as well, $\lambda = 1$, i.e., there is no split. We note that in [3], the growth of the solution in the PML (2.1) was attributed precisely to the degenerate eigenvalue $\lambda = -\sigma$. Yet our numerical experiments with the Yee scheme show that this growth, no matter how slow it is, is present for the PML (2.1), for which the double eigenvalue gets split, and is not present for the PML (2.2), for which it stays unsplit.

2.4 The Leap Frog Scheme

For the mathematical PML(2.1) the leap-frog scheme reads:

$$\begin{aligned} \frac{{E_x}_{m,n}^{p+1} - {E_x}_{m,n}^{p-1}}{2\tau} &= \frac{H_{m,n+1}^p - H_{m,n-1}^p}{2h_y} \\ \frac{{E_y}_{m,n}^{p+1} - {E_y}_{m,n}^{p-1}}{2\tau} &= -\frac{H_{m+1,n}^p - H_{m-1,n}^p}{2h_x} - \sigma_m \left(2{E_y}_{m,n}^p + P_{m,n}^p\right) \\ \frac{H_{m,n}^{p+1} - H_{m,n}^{p-1}}{2\tau} &= \frac{{E_x}_{m,n+1}^p - {E_x}_{m,n-1}^p}{2h_y} - \frac{{E_y}_{m+1,n}^p - {E_y}_{m-1,n}^p}{2h_x} - {\sigma'}_m Q_{m,n}^p \\ \frac{P_{m,n}^{p+1} - P_{m,n}^{p-1}}{2\tau} &= \sigma_m {E_y}_{m,n}^p \\ \frac{Q_{m,n}^{p+1} - Q_{m,n}^{p-1}}{2\tau} &= -\sigma_m Q_{m,n}^p - {E_y}_{m,n}^p \end{aligned} \tag{2.6}$$

Let us also write down the leap-frog scheme as it applies to system (2.2):

$$\begin{aligned}
\frac{{E_x}_{m,n}^{p+1} - {E_x}_{m,n}^{p-1}}{2\tau} &= \frac{H_{m,n+1}^{p} - H_{m,n-1}^{p}}{2h_y} + \sigma_m({E_x}_{m,n}^{p} - P_{m,n}^{p}) \\
\frac{{E_y}_{m,n}^{p+1} - {E_y}_{m,n}^{p-1}}{2\tau} &= -\frac{H_{m+1,n}^{p} - H_{m-1,n}^{p}}{2h_x} - \sigma_m {E_y}_{m,n}^{p} \\
\frac{H_{m,n}^{p+1} - H_{m,n}^{p-1}}{2\tau} &= \frac{{E_x}_{m,n+1}^{p} - {E_x}_{m,n-1}^{p}}{2h_y} - \frac{{E_y}_{m+1,n}^{p} - {E_y}_{m-1,n}^{p}}{2h_x} - \sigma_m H_{m,n}^{p} \\
\frac{P_{m,n}^{p+1} - P_{m,n}^{p-1}}{2\tau} &= \sigma_m({E_x}_{m,n}^{p} - P_{m,n}^{p})
\end{aligned} \tag{2.7}$$

We will use the principle of frozen coefficients and investigate the von Neumann stability of scheme (2.7) for a fixed value of $\sigma \neq 0$. Substituting the solution $\boldsymbol{q}\lambda^p e^{i(\alpha m + \beta n)}$ into (2.7), where $\boldsymbol{q}$ is a 4-dimensional vector and α and β are the frequencies that correspond to x and y, we require that the corresponding determinant be zero and obtain ($h_x = h_y = h$):

$$4\lambda^2(\lambda^2-1)^2\tau^2\sin^2\alpha + (-1+\lambda^2+2\lambda\sigma\tau)^2(h^2(\lambda^2-1)^2 + 4\lambda^2\tau^2\sin^2\beta) = 0$$

An algebraic equation of degree 8 is impossible to solve in the general case. However, for the simplest case of a quiescent solution, $\alpha = \beta = 0$, we have:

$$\lambda_{1,2} = -\sigma\tau - \sqrt{1+\sigma^2\tau^2}, \quad \lambda_{3,4} = -\sigma\tau + \sqrt{1+\sigma^2\tau^2}, \quad \text{and} \quad \lambda_{5,6,7,8} = 1$$

We see that the eigenvalues $\lambda_{1,2}$ get out of the unit disk. Speaking formally it is not fatal, because for sufficiently small time steps we can always claim that $|\lambda_{1,2}| \leq 1 + \text{const}\,\tau$. Hence, the necessary von Neumann condition of stability may still hold for scheme (2.7), provided that its other eigenvalues will not "misbehave" for non-zero frequencies. However, the stability constant becomes exponentially large and obviously cannot be made grow slower than an exponential (in time) even if all $\alpha \neq 0$ and $\beta \neq 0$ are taken into account. In practice, the computation is completely ruined already at short times $t \sim T$. The results for the mathematical PML (2.1) and scheme (2.6) are virtually identical.

2.5 The Lax-Wendroff Scheme

The Lax-Wendroff scheme for either type of the PML is obtained in the usual way, by re-expressing the second time derivative of each unknown quantity through the corresponding equation(s) and subsequently canceling the $\mathcal{O}(\tau)$ term in the truncation error by subtraction. For PML (2.1), this

yields:

$$
\begin{aligned}
\frac{{E_x}_{m,n}^{p+1} - {E_x}_{m,n}^{p}}{\tau} &= \frac{H_{m,n+1}^{p} - H_{m,n-1}^{p}}{2h_y} + \frac{\tau}{2}\Bigg[\underbrace{\frac{\partial^2 E_x}{\partial y^2} - \frac{\partial^2 E_y}{\partial x \partial y} + \sigma' \frac{\partial Q}{\partial y}}_{\mathcal{O}(h^2) \text{ by central differences}}\Bigg]_{m,n}^{p} \\
\frac{{E_y}_{m,n}^{p+1} - {E_y}_{m,n}^{p}}{\tau} &= -\frac{H_{m+1,n}^{p} - H_{m-1,n}^{p}}{2h_x} - 2\sigma_m {E_y}_{m,n}^{p} - \sigma_m P_{m,n}^{p} \\
&\quad + \frac{\tau}{2}\Bigg[\underbrace{\frac{\partial^2 E_y}{\partial x^2} - \frac{\partial^2 E_x}{\partial y \partial x} - \sigma' \frac{\partial Q}{\partial x}}_{\mathcal{O}(h^2) \text{ by central differences}} - \sigma'' Q - \underbrace{2\sigma \frac{\partial E_y}{\partial t} - \sigma \frac{\partial P}{\partial t}}_{\substack{\text{via the equations} \\ \text{then also } \mathcal{O}(h^2)}}\Bigg]_{m,n}^{p} \\
\frac{H_{m,n}^{p+1} - H_{m,n}^{p}}{\tau} &= \frac{{E_x}_{m,n+1}^{p} - {E_x}_{m,n-1}^{p}}{2h_y} - \frac{{E_y}_{m+1,n}^{p} - {E_y}_{m-1,n}^{p}}{2h_x} + \sigma'_m Q_{m,n}^{p} \\
&\quad + \frac{\tau}{2}\Bigg[\underbrace{\frac{\partial^2 H}{\partial x^2} - \frac{\partial^2 H}{\partial y^2} + 2\sigma \frac{\partial E_y}{\partial x} + \sigma \frac{\partial P}{\partial x}}_{\mathcal{O}(h^2) \text{ by central differences}} + 2\sigma' E_y + \sigma' P - \sigma'(\sigma Q + E_y)\Bigg]_{m,n}^{p} \\
\frac{P_{m,n}^{p+1} - P_{m,n}^{p}}{\tau} &= \sigma_m {E_y}_{m,n}^{p} + \frac{\tau}{2}\sigma\Bigg[-\frac{\partial H}{\partial x} - 2\sigma E_y - \sigma P\Bigg]_{m,n}^{p} \\
\frac{Q_{m,n}^{p+1} - Q_{m,n}^{p}}{\tau} &= -\sigma_m Q_{m,n}^{p} - {E_y}_{m,n}^{p} + \frac{\tau}{2}\Bigg[\sigma^2 Q + 3\sigma E_y + \sigma P + \frac{\partial H}{\partial x}\Bigg]_{m,n}^{p}
\end{aligned}
\tag{2.8}
$$

In the quiescent state, equations for E_y and P decouple from system (2.8), cf. equations (2.5). Then, analysis of the eigenvalues similar to the one conducted in Section 2.3 yields: $\lambda_{1,2} = 1 - \sigma\tau + \frac{\sigma^2\tau^2}{2}$. We see that the multiple eigenvalue from the differential system does not get split by the discretization.

There is, however, an alternative way of discretizing the ODEs from system (2.1). Namely, one can use a semi-implicit (Crank-Nicolson type) scheme for these two equations and still maintain the overall second order accuracy. In this case, the continuous multiple eigenvalue gets split by the discretization:

$$\lambda_{1,2} = 1 - \sigma\tau + \frac{\sigma^2\tau^2}{2} + \frac{\sigma^3\tau^3}{4} \pm \frac{\sigma^2\tau^2}{4}\sqrt{-4 + 4\sigma\tau + \sigma^2\tau^2}$$

Yet in our numerical experiments no difference in the long-time behavior has been observed between scheme (2.8) and the Lax-Wendroff scheme with the ODEs approximated semi-implicitly. Both schemes develop a very slow growth, with the artifacts becoming noticeable at about $500T$, see Figure 2.2. In accordance with the observations of [3], they originate near the interface between the domain and the layer.

The Lax-Wendroff scheme for the physical PML (2.2) is built in much the same way as scheme

(2.8):

$$\begin{aligned}
\frac{E_x{}^{p+1}_{m,n} - E_x{}^{p}_{m,n}}{\tau} &= \frac{H^p_{m,n+1} - H^p_{m,n-1}}{2h_y} + \frac{\tau}{2}\Bigg[\underbrace{\frac{\partial^2 E_x}{\partial x^2} - \frac{\partial^2 E_y}{\partial x \partial y}}_{\substack{O(h^2)\text{ by}\\ \text{central differences}}} - \sigma' H\Bigg]^p_{m,n} \\
\frac{E_y{}^{p+1}_{m,n} - E_y{}^{p}_{m,n}}{\tau} &= -\frac{H^p_{m+1,n} - H^p_{m-1,n}}{2h_y} + \frac{\tau}{2}\Bigg[\underbrace{\frac{\partial^2 E_x}{\partial x \partial y} + \frac{\partial^2 E_y}{\partial x^2}}_{\substack{O(h^2)\text{ by}\\ \text{central differences}}} - \sigma' H - \sigma^2 \boldsymbol{E}_y\Bigg]^p_{m,n} \qquad (2.9) \\
\frac{H^{p+1}_{m,n} - H^p_{m,n}}{\tau} &= \frac{E_x{}^{p}_{m,n+1} - E_x{}^{p}_{m,n-1}}{2h_y} - \frac{E_y{}^{p}_{m+1,n} - E_y{}^{p}_{m-1,n}}{2h_x} + \frac{\tau}{2}\frac{\partial^2 H}{\partial t^2} - \sigma H \\
\frac{P^{p+1}_{m,n} - P^p_{m,n}}{\tau} &= \sigma_m (E_x{}^{p}_{m,n}) + \frac{\tau}{2}\sigma \cdot \frac{\partial H}{\partial y}
\end{aligned}$$

where the second time derivative is expressed via the equation:

$$\frac{\partial^2 H}{\partial t^2} = \Bigg[\underbrace{\frac{\partial^2 H}{\partial y^2} + \sigma\frac{\partial P}{\partial y} + \frac{\partial^2 H}{\partial x^2} + 2\sigma\frac{\partial E_y}{\partial x}}_{O(h^2)\text{ by central differences}} + \sigma'(E_x - P + E_y) + \sigma^2 H\Bigg]^p_{m,n}$$

In the experiments, PML (2.2) with scheme (2.9) exhibits no artificial growth at least until $t = 2500T$. Altogether, this behavior is very similar to what we have seen for the Yee scheme in Section 2.3.

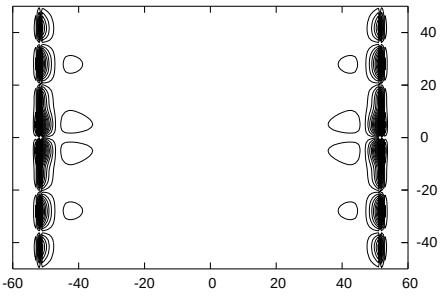

Figure 2.2: E_x for the Law-Wendroff scheme (2.8) at $t = 500T$; the contours are equally spaced between -0.575 and 0.575 with the increment 0.05.

It should also be pointed out that the implementation of scheme (2.8) requires one special consideration. Originally, it was noticed that the artifacts in the solution could develop much more rapidly than shown in Figure 2.2, and starting predominantly at the intersections of the interfaces between the domain and the PML $x = \pm a$ with the lateral boundaries $y = \pm a$. This was attributed to the presence of the term $\sigma'' Q$ in the equation for E_y in system (2.8). For the cubic profile of $\sigma(x)$, this term has relatively low regularity at the interfaces $x = \pm a$, it is continuous with discontinuous first derivative. If, however, this term is merely removed, the growth displayed by scheme (2.8) slows down very considerably and does not noticeably manifest itself until several hundred T. In doing so, inside the computational domain the scheme still remains a complete second order Lax-Wendroff.

2.6 The Central Difference Scheme

Let $\boldsymbol{q}^p_{m,n}$ denote the complete vector of unknowns at the spatial location (m,n) and time level p. This vector has five components for the PML (2.1) and four components for the PML (2.2). Let $\boldsymbol{G}(\boldsymbol{q})$ denote the operator of spatial discretization. It replaces the x and y partial derivatives on the right-hand side of either (2.1) or (2.2) by the corresponding second order central differences. It also replaces the non-differentiated terms by the appropriate nodal values. Then, the central difference second order scheme for either system (2.1) or system (2.2) with the standard fourth order Runge-Kutta evolution in time is given by:

$$\frac{\boldsymbol{q}^{p+1}_{m,n} - \boldsymbol{q}^p_{m,n}}{\tau} = \frac{1}{6}(\boldsymbol{k}_1 + 2\boldsymbol{k}_2 + 2\boldsymbol{k}_3 + \boldsymbol{k}_4) \tag{2.10a}$$

where

$$\begin{aligned} &\boldsymbol{k}_1 = \boldsymbol{G}(\boldsymbol{q}^p_{m,n}), && \boldsymbol{k}_2 = \boldsymbol{G}(\boldsymbol{q}^p_{m,n} + \tau\boldsymbol{k}_1/2) \\ &\boldsymbol{k}_3 = \boldsymbol{G}(\boldsymbol{q}^p_{m,n} + \tau\boldsymbol{k}_2/2), && \boldsymbol{k}_4 = \boldsymbol{G}(\boldsymbol{q}^p_{m,n} + \tau\boldsymbol{k}_3) \end{aligned} \tag{2.10b}$$

Alternatively, one can use a third order Runge-Kutta evolution in time, which yields:

$$\frac{\boldsymbol{q}^{p+1}_{m,n} - \boldsymbol{q}^p_{m,n}}{\tau} = \frac{1}{4}(\boldsymbol{k}_1 + 3\boldsymbol{k}_3) \tag{2.11a}$$

where

$$\boldsymbol{k}_1 = \boldsymbol{G}(\boldsymbol{q}^p_{m,n}), \quad \boldsymbol{k}_2 = \boldsymbol{G}(\boldsymbol{q}^p_{m,n} + \tau\boldsymbol{k}_1/3), \quad \boldsymbol{k}_3 = \boldsymbol{G}(\boldsymbol{q}^p_{m,n} + 2\tau\boldsymbol{k}_2/3) \tag{2.11b}$$

Note that second order Runge-Kutta methods cannot be applied to the central difference spatial discretization $\boldsymbol{G}(\boldsymbol{q})$ because the resulting scheme will be unstable. In doing so, the instability will not be due to the PML, it will rather be a genuine von Neumann instability. On the other hand, both schemes (2.10a)–(2.10b) and (2.11a)–(2.11b) are stable, provided that the Courant number does not exceed 2.8 for scheme (2.10a)–(2.10b) and about 1.7 for scheme (2.11a)–(2.11b).

Analysis of the eigenvalues in the quiescent state (similar to the analysis conducted in Sections 2.3 and 2.5) shows that either scheme, (2.10a)–(2.10b) or (2.11a)–(2.11b), applied to either system, (2.1) or (2.2), preserves multiple eigenvalues that characterize the differential formulation.

As far as the numerical results, both schemes (2.10a)–(2.10b) and (2.11a)–(2.11b) applied to the mathematical PML (2.1) produce a moderate growth, with the artifacts clearly observable already for the times t ranging between $10T$ and $15T$, see Figure 2.3. Furthermore, unlike in the previous settings (Sections 2.3 and 2.5), we could not see here the artifacts developing in the layer and then propagating toward the domain. We rather saw them gradually picking up throughout the entire computational region, as Figure 2.3 shows. We are completely sure though that these artifacts are

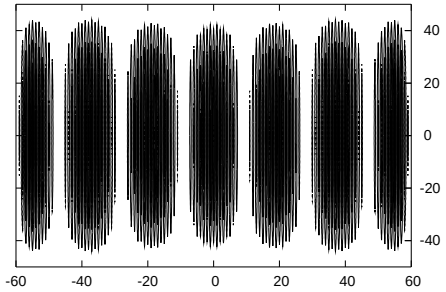

Figure 2.3: H for the central difference scheme (2.10a)–(2.10b) applied to the PML (2.1) at $t = 15T$; the contours are equally spaced between -0.4 and 0.4 with the increment 0.1 and with the exception of the zero contour.

still due to the layer and nothing else, because it has been verified by switching off the PML while keeping all other parameters intact, as explained in Section 3.3.1. Moreover, it has also been verified that these artifacts are not due to any von Neumann type instability. They develop with the same rate (with respect to the actual time rather than the number of steps) for the Courant number taken on the borderline of stability region, as well as for the three times smaller Courant number.

For the physical PML (2.2), no growth of the Runge-Kutta solution could be observed at least until $t = 2500T$. This is in contrast with the findings of [3], although in [3] the differences in space were fourth order, and the code was multi-block with characteristics-based treatment of the interfaces.

2.7 Summary and Intermediate Conclusions

We summarize our observations and results of the analysis in Table 2.1.

Table 2.1: Long-time behavior of unsplit PMLs with second order schemes.

		Schemes					
		Yee	leap-frog	Lax-Wendroff		central difference	
				expl. ODEs	impl. ODEs	4-th RK	3-rd RK
mathemat.	growth	$\sim 500T$	rapid	$\sim 500T$	$\sim 500T$	$\sim 15T$	$\sim 15T$
PML (2.1)	eigenvalues	split	$\|\lambda\| > 1$	multiple	split	multiple	multiple
physical	growth	no	rapid	no		no	
PML (2.2)	eigenvalues	multiple	$\|\lambda\| > 1$	multiple		multiple	multiple

Altogether, the physical unsplit PML (2.2) seems somewhat less susceptible to developing the long-time growth. For the mathematical PML (2.1), when it is used with the Yee scheme or Lax-Wendroff scheme, the growth can still be disregarded for all practical purposes. This growth, however, is more rapid for the central difference scheme with Runge-Kutta evolution in time.

We realize, of course, that the analysis in this chapter is somewhat limited in its scope. For example, we cannot say ahead of time what's going to happen to the reader's favorite high order scheme if applied to one of the PMLs we have considered. On the other hand, we have analyzed the performance of all commonly used second order explicit finite-difference schemes, and within this class of methods reliable predictions can be made based on the data from Table 2.1. Otherwise, analysis of the eigenvalues for a discretization not covered in this chapter can be performed similarly.

To summarize, the growth of the numerical solution inside the PML seems to be strongly affected by both the type of the layer and the type of discretization. In addition, we think that our observations may justify the development of special methodologies for stabilizing the PMLs over long propagation times. Chapter 3 of the dissertation addresses precisely this objective.

Chapter 3

Lacunae-Based Stabilization of PMLs

3.1 Introduction

In this chapter, we propose a fully rigorous cure for the long-time instability of the PMLs that will preserve all the design properties of a given layer. Our methodology employs the lacunae-based integration, and the analysis in the chapter follows that of the recent paper [99]. We should additionally note that even though the lacunae-based integration is presented hereafter as an approach to mitigating the long-time instability of the PMLs, the analysis of Section 3.2 clearly indicates that *it can also be used for alleviating any other undesirable long-time phenomenon in computation,* e.g., the deterioration of accuracy of low order local ABCs.

Lacunae-based methods for the numerical integration of hyperbolic equations and systems have been developed during the past several years [108–110, 118, 119]. They apply to the equations that satisfy the Huygens' principle [25, 36][1] and hence have lacunae [98] in their solutions. We briefly illustrate the phenomenon of lacunae using the example of a three-dimensional wave (d'Alembert) equation:

$$\frac{1}{c^2}\varphi_{tt} - (\varphi_{xx} + \varphi_{yy} + \varphi_{zz}) = f(\boldsymbol{x}, t),\ t \geq\ 0 \tag{3.1a}$$

subject to

$$\varphi|_{t=0} = \varphi_t|_{t=0} = 0 \tag{3.1b}$$

Let us assume that the RHS of (3.1a) is *compactly supported in space-time*, that is $\mathrm{supp} f \in Q \subset \mathbb{R}^3 \times [0, \infty)$, and note that while the homogeneity of the initial conditions (3.1b) is convenient it is not required. Solution of problem (3.1) at $(\boldsymbol{x}, t)$ is given by the Kirchhoff integral, see [36]:

$$\varphi(\boldsymbol{x}, t) = \frac{1}{4\pi} \iiint_{\varrho \leq ct} \frac{f(\boldsymbol{\xi}, t - \varrho/c)}{\varrho} d\boldsymbol{\xi} \tag{3.2}$$

[1] For more detail on the Huygens' principle, including history of the related developments, see [19, 25, 61, 64–66].

where $\boldsymbol{x} = (x, y, z)$, $\boldsymbol{\xi} = (\xi_1, \xi_2, \xi_3)$, $\varrho = |\boldsymbol{x} - \boldsymbol{\xi}| = \sqrt{(x-\xi_1)^2 + (y-\xi_2)^2 + (z-\xi_3)^2}$ and $d\boldsymbol{\xi} = d\xi_1 d\xi_2 d\xi_3$. Since the RHS of (3.1a) is compactly supported

$$\varphi(\boldsymbol{\xi}, t) \equiv 0 \ \forall (\boldsymbol{x}, t) \in \bigcap_{(\boldsymbol{\xi}, t)} \{(\boldsymbol{x}, t) : |\boldsymbol{x} - \boldsymbol{\xi}| < c(t - \tau), t > \tau\} \tag{3.3}$$

The region of space-time defined by the formula (3.3) is called *lacuna of the solution* $\varphi(\boldsymbol{x}, t)$. It can be interpreted as the intersection of the characteristic cones of equation (3.1a) once the vertex of the cone sweeps the support of $f(\boldsymbol{x}, t)$. Physically, lacunae correspond to the part of space-time which the waves generated by the compactly supported RHS have passed and the solution is zero *again*. The surfaces of lacunae are trajectories of the aft (trailing) fronts of the waves. The notion of lacunae was first introduced in [98] and subsequently studied in [9, 10].

The basic idea of lacunae-based methods is that once the domain of interest falls completely into the lacuna of the solution [98], the integration does not need to be continued any further. The presence of lacunae can also be efficiently exploited for the construction of exact ABCs[2] for various wave propagation problems [108, 118, 119]. These ABCs have only fixed and limited extent of temporal nonlocality. For the problem of radiation of waves by a known source, lacunae-based methods guarantee a temporally uniform grid convergence for any consistent and stable scheme [109].

Hereafter, we apply the concepts of lacunae-based integration to the task of stabilization of PMLs. Our main result is formulated in Section 3.2, see Theorem 3.1. It says that given a computational domain of finite size, lacunae-based integration guarantees that the PML-generated errors will remain uniformly bounded for all times. This results holds for any linear PML, and the governing equations in the layer do not have to be modified. In Section 3.3, we present the results of our numerical experiments for Maxwell's equations that corroborate the theoretical design properties of the algorithm. In Section 3.4, we describe the decomposition of the original problem into the interior and auxiliary subproblems, which is the key element of lacunae-based ABCs [108, 118, 119]. As for the PMLs, this decomposition will also allow us to address a much broader class of formulations than only the radiation of waves by known sources (e.g., scatterers in the domain). Finally, Section 3.5 contains the conclusions and some general discussion.

3.2 Essentials of the Algorithm and the Main Theorem

A typical problem setup is schematically represented in Figure 3.1, and it is only for the convenience of plotting that $\boldsymbol{x}$ is shown one-dimensional. In fact, we will always assume that $\boldsymbol{x} \in \mathbb{R}^3$, because lacunae exist only if the number of space dimensions is odd [25]. Accordingly, the computational

[2] ABCs that introduce no error due to the domain truncation.

domain Ω is assumed to have diameter d in $\mathbb{R}^3$. As far as its shape is concerned, from the standpoint of lacunae-based algorithms it is not important. However, the application of PMLs typically requires simple computational domains, most often Cartesian rectangles (parallelepipeds) or, sometimes, cylinders or spheres [97, 113, 114].

The PML surrounds the computational domain, see Figure 3.1, and for simplicity we first assume that it has infinite thickness. This means that all the waves entering the PML completely die off in the layer. In practice, a PML always has finite thickness, such as in our numerical experiments of Section 3.3.

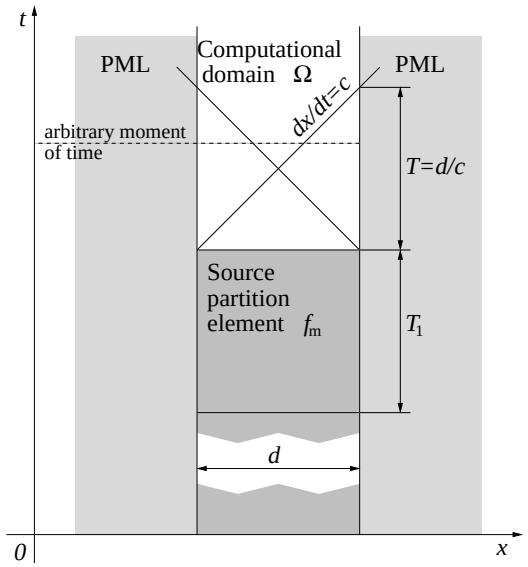

Figure 3.1: Schematic.

Let $\boldsymbol{w} = \boldsymbol{w}(\boldsymbol{x}, t)$ denote the vector of unknowns (e.g., components of the electromagnetic field or parameters of the fluid), and let it be governed by:

$$\begin{aligned} \frac{\partial \boldsymbol{w}}{\partial t} + \boldsymbol{L}\boldsymbol{w} = \boldsymbol{f}(\boldsymbol{x}, t), \quad \boldsymbol{x} \in \mathbb{R}^3, \quad t > 0, \\ \boldsymbol{w}(\boldsymbol{x}, 0) = \boldsymbol{\varphi}, \quad \boldsymbol{x} \in \mathbb{R}^3, \end{aligned} \tag{3.4}$$

where the operator $\boldsymbol{L}$ is supposed to be linear and contain all the appropriate spatial derivatives of $\boldsymbol{w}$ as well as, maybe, non-differentiated terms. We require that the differential operator $\partial/\partial t + \boldsymbol{L}$ of (3.4) satisfies the Huygens' principle [19, 25, 61, 64–66]. Mathematically, this means that the waves due to a compactly supported source (in space-time) have sharp aft fronts. In other words, at any fixed location of the observer these waves come and go, and the solution becomes identically zero

after a finite interval of time, see Section 3.1. This interval is no greater than the maximum distance between the observer and the source divided by the propagation speed c (e.g., the speed of light or speed of sound).

According to [92], a scalar differential equation in the conventional $3+1$ dimensional Minkowski space-time is Huygens' if and only if it is equivalent to the d'Alembert equation.This is a convenient criterion for practice; in particular, both Maxwell's equations [119] and linearized Euler's equations (once the entropy waves have been decoupled [118]) reduce to d'Alembert equations for individual electromagnetic or acoustic variables, and as such are Huygens'.

The right-hand side (RHS) $\boldsymbol{f}(\boldsymbol{x},t)$ in (3.4) represents the sources of the field; it is supposed to be compactly supported in space and may operate continuously in time: $\mathrm{supp}\boldsymbol{f} \subseteq \Omega \times [0,+\infty)$. The initial data for problem (3.4) are also assumed compactly supported: $\mathrm{supp}\boldsymbol{\varphi} \subseteq \Omega$. For Maxwell's equations, $\boldsymbol{f}(\boldsymbol{x},t)$ contains the extraneous electric currents, and for the acoustics equations it contains volume velocities and forces that are assumed to be given explicitly.

Let us denote by $T = d/c$ the characteristic time, which is required for the waves to cross the domain Ω, and let $T_1 > 0$, see Figure 3.1. We can represent the RHS $\boldsymbol{f}(\boldsymbol{x},t)$ of (3.4), $\boldsymbol{x} \in \Omega$, using the partition:

$$\boldsymbol{f}(\boldsymbol{x},t) = \sum_{m=0}^{\infty} \boldsymbol{f}_m(\boldsymbol{x},t), \qquad \boldsymbol{f}_m(\boldsymbol{x},t) = \begin{cases} \boldsymbol{f}(\boldsymbol{x},t), & t_m \le t < t_{m+1}, \\ \boldsymbol{0}, & \text{otherwise}, \end{cases} \tag{3.5}$$

where $t_m = mT_1$, $m = 0,1,2,\ldots$. Next, consider the Cauchy problems:

$$\begin{gathered} \frac{\partial \boldsymbol{w}_m}{\partial t} + \boldsymbol{L}\boldsymbol{w}_m = \boldsymbol{f}_m(\boldsymbol{x},t), \quad \boldsymbol{x} \in \mathbb{R}^3, \quad t > t_m, \\ \boldsymbol{w}_m(\boldsymbol{x},t_m) = \begin{cases} \boldsymbol{\varphi}, & m = 0, \\ \boldsymbol{0}, & m > 0, \end{cases} \quad \boldsymbol{x} \in \mathbb{R}^3. \end{gathered} \tag{3.6}$$

Solution of problem number m from the set (3.6) is defined for $t \ge t_m \equiv mT_1$, but we can think that it is defined for all $t \ge 0$ and is equal to zero for $0 \le t < t_m$. Then, because of the linear superposition and causality we have:

$$\boldsymbol{w}(\boldsymbol{x},t) = \sum_{m=0}^{M} \boldsymbol{w}_m(\boldsymbol{x},t), \quad \boldsymbol{x} \in \mathbb{R}^3, \quad t \ge 0, \tag{3.7}$$

where $M \stackrel{\text{def}}{=} \lceil t/T_1 \rceil - 1$, and $\lceil \alpha \rceil$ is the smallest integer $\ge \alpha$ (ceiling function).

Moreover, as the operator $\partial/\partial t + \boldsymbol{L}$ is Huygens', the solution of each problem (3.6) has a lacuna [98]. For the constant propagation speed c, the shape of the lacuna is determined by the Kirchhoff

integral [25] as explained, e.g., in [109]. It is basically the common interior of all the light cones generated by a particular source. For a given $m \geq 0$, the domain Ω falls into this lacuna at the moment of time $t_m + T_1 + T \equiv t_{m+1} + T$. In other words, once the source $\boldsymbol{f}_m(\boldsymbol{x}, t)$ ceases to operate (at $t = t_{m+1}$), it takes another T seconds for the waves it has generated to completely leave the domain Ω, see Figure 3.1. Consequently,

$$\boldsymbol{w}_m(\boldsymbol{x}, t) = \boldsymbol{0}, \quad \boldsymbol{x} \in \Omega, \quad t \geq t_{m+1} + T \equiv t_{m+1} + d/c, \tag{3.8}$$

and using (3.8), we can write instead of (3.7):

$$\boldsymbol{w}(\boldsymbol{x}, t) = \sum_{m=M_0}^{M} \boldsymbol{w}_m(\boldsymbol{x}, t), \quad \boldsymbol{x} \in \Omega, \quad t \geq 0, \tag{3.9}$$

where $M_0 \stackrel{\text{def}}{=} [(t-T)/T_1]$, and $[\,\cdot\,]$ denotes the integer part. Hence, we conclude that for any moment of time t, see Figure 3.1, only so many components $\boldsymbol{w}_m$ of (3.6) contribute to the solution $\boldsymbol{w}(\boldsymbol{x}, t)$ of problem (3.4) on the domain Ω. These components are the $M - M_0 + 1$ terms in the sum (3.9), and their maximum number does not depend on t. Moreover, each term may only differ from zero on Ω during the interval $T_1 + T$, see (3.8), which does not depend on t either.

Representation of the solution $\boldsymbol{w}(\boldsymbol{x}, t)$ as *the sum of a finite non-increasing number of components $\boldsymbol{w}_m(\boldsymbol{x}, t)$ that each has a finite non-increasing "lifespan" on Ω is the key advantage provided by lacunae-based integration;* it will be of fundamental importance for our subsequent analysis. As an example, consider $T_1 = T = d/c$, see Figure 3.1. Then, clearly, $M_0 = M - 1$ unless t happens to be an integer multiple of T, in which case $M_0 = M$. Consequently, the number of terms in the sum (3.9) in the case $T_1 = T$ is normally equal to 2 and sometimes reduces to 1. In practice, however, it will be both feasible and beneficial to take the value of T_1 several times larger than T, see Sections 3.3.3 and 3.3.4.

In reality we are not solving problem (3.4) directly. Instead, we are solving a combined formulation that involves the PML outside Ω (see Figure 3.1):

$$\begin{gathered} \frac{\partial \boldsymbol{w}^{(\Omega)}}{\partial t} + \boldsymbol{L}\boldsymbol{w}^{(\Omega)} = \boldsymbol{f}(\boldsymbol{x}, t), \quad \boldsymbol{x} \in \Omega, \quad t > 0, \\ \boldsymbol{w}^{(\Omega)}(\boldsymbol{x}, 0) = \boldsymbol{\varphi}, \quad \boldsymbol{x} \in \Omega, \end{gathered} \tag{3.10a}$$

$$\begin{gathered} \frac{\partial \boldsymbol{w}^{(\mathrm{PML})}}{\partial t} + \boldsymbol{L}^{(\mathrm{PML})}\boldsymbol{w}^{(\mathrm{PML})} = \boldsymbol{0}, \quad \boldsymbol{x} \in \mathbb{R}^3 \setminus \Omega, \quad t > 0, \\ \boldsymbol{w}^{(\mathrm{PML})}(\boldsymbol{x}, 0) = \boldsymbol{0}, \quad \boldsymbol{x} \in \mathbb{R}^3 \setminus \Omega. \end{gathered} \tag{3.10b}$$

In doing so, problem (3.10a) is identical to (3.4) except that it is formulated on the bounded region

Ω rather than on $\mathbb{R}^3$. For the second problem, (3.10b), the vector of unknowns $\boldsymbol{w}^{(\mathrm{PML})}$ typically has more components than $\boldsymbol{w}^{(\Omega)}$, and the operator $\boldsymbol{L}^{(\mathrm{PML})}$ has additional terms that render the damping of waves. It is also required that *the continuity* be enforced across the interface $\partial\Omega$:

$$\boldsymbol{w}^{(\Omega)}(\boldsymbol{x},t) = \boldsymbol{M}\boldsymbol{w}^{(\mathrm{PML})}(\boldsymbol{x},t), \quad \boldsymbol{x} \in \partial\Omega. \tag{3.10c}$$

For unsplit PMLs, the matrix $\boldsymbol{M}$ should simply match the respective components. For split PMLs, the sum of the split components in $\boldsymbol{w}^{(\mathrm{PML})}$ should be equal to the corresponding component of $\boldsymbol{w}^{(\Omega)}$. Altogether, *the ideal PML* of infinite thickness (3.10b)-(3.10c) applied to the interior problem (3.10a) will guarantee:

$$\boldsymbol{w}^{(\Omega)}(\boldsymbol{x},t) \equiv \boldsymbol{w}(\boldsymbol{x},t), \quad \boldsymbol{x} \in \Omega, \quad t \geq 0. \tag{3.11}$$

The PML, however, is not ideal, and a convenient way to account for that is to introduce small perturbations $\boldsymbol{\xi}$ of the initial data. In the continuous setting these perturbations are artificial, but in reality they originate from the small residual terms of the approximation, i.e., from the truncation error [3]:

$$\begin{aligned} \frac{\partial \tilde{\boldsymbol{w}}^{(\Omega)}}{\partial t} + \boldsymbol{L}\tilde{\boldsymbol{w}}^{(\Omega)} &= \boldsymbol{f}(\boldsymbol{x},t), \quad \boldsymbol{x} \in \Omega, \quad t > 0, \\ \tilde{\boldsymbol{w}}^{(\Omega)}(\boldsymbol{x},0) &= \boldsymbol{\varphi} + \boldsymbol{\xi}, \quad \boldsymbol{x} \in \Omega, \end{aligned} \tag{3.12a}$$

$$\begin{aligned} \frac{\partial \tilde{\boldsymbol{w}}^{(\mathrm{PML})}}{\partial t} + \boldsymbol{L}^{(\mathrm{PML})}\tilde{\boldsymbol{w}}^{(\mathrm{PML})} &= \boldsymbol{0}, \quad \boldsymbol{x} \in \mathbb{R}^3 \setminus \Omega, \quad t > 0, \\ \tilde{\boldsymbol{w}}^{(\mathrm{PML})}(\boldsymbol{x},0) &= \boldsymbol{\xi}, \quad \boldsymbol{x} \in \mathbb{R}^3 \setminus \Omega. \end{aligned} \tag{3.12b}$$

System (3.12) is to be supplemented by the same continuity condition (3.10c). It has been shown [1,3] that for both split and unsplit PMLs the difference between the perturbed and unperturbed solution can grow as the time elapses:

$$\|\tilde{\boldsymbol{w}}^{(\Omega)}(\,\cdot\,,t) - \boldsymbol{w}^{(\Omega)}(\,\cdot\,,t)\| \leq \mu(t)\|\boldsymbol{\xi}\|', \tag{3.13a}$$

$$\|\tilde{\boldsymbol{w}}^{(\mathrm{PML})}(\,\cdot\,,t) - \boldsymbol{w}^{(\mathrm{PML})}(\,\cdot\,,t)\| \leq \mu(t)\|\boldsymbol{\xi}\|'. \tag{3.13b}$$

The rate of growth $\mu(t)$ is determined by the particular PML; for standard PMLs it is either linear or quadratic [1,3,17]. The appropriate choice of the norms $\|\,\cdot\,\|$ and $\|\,\cdot\,\|'$ for some specific cases is discussed in [1,3,17]. Note that estimate (3.13b) is always sharp, because the growth of certain components of the solution inside the PML has actually been demonstrated in [3,17]. As far as the first estimate, (3.13a), according to [18] numerical artifacts from the PML may or may not propagate back into the domain Ω. If they don't, then $\mu(t)$ can be replaced by a true constant in (3.13a). We, however, will still be assuming the worst case scenario (3.13), for it was experimentally shown

in Chapter 2, see also [3, 5], that the artifacts from the layer can contaminate the computational domain. Moreover, the implementation strategies that emphasize parallel efficiency may make the propagation of artifacts from the layer to the domain more likely [114].

Our goal is to show that if the plain integration of system (3.10) is replaced by the lacunae-based integration, then estimates (3.13) can be improved and made *uniform in time.* First of all, we need to see that lacunae-based integration applies to (3.10). In the unperturbed case, formula (3.11) means that if $\boldsymbol{f}(\boldsymbol{x}, t)$ is partitioned according to (3.5), then the solutions of individual problems with the PML will still have lacunae on the domain Ω. The only difference is that the waves that leave Ω after the time T elapses will no longer travel freely but will rather be absorbed by the PML. Hence, we can write similarly to (3.9):

$$\boldsymbol{w}^{(\Omega)}(\boldsymbol{x}, t) = \sum_{m=M_0}^{M} \boldsymbol{w}_m^{(\Omega)}(\boldsymbol{x}, t), \quad \boldsymbol{x} \in \Omega, \quad t \geq 0, \tag{3.14}$$

where the individual terms $\boldsymbol{w}_m^{(\Omega)}(\boldsymbol{x}, t)$, $m = 0, 1, 2, \ldots$, satisfy [cf. (3.6), (3.10)]:

$$\begin{aligned} &\frac{\partial \boldsymbol{w}_m^{(\Omega)}}{\partial t} + \boldsymbol{L}\boldsymbol{w}_m^{(\Omega)} = \boldsymbol{f}_m(\boldsymbol{x}, t), \quad \boldsymbol{x} \in \Omega, \quad t > t_m, \\ &\boldsymbol{w}_m^{(\Omega)}(\boldsymbol{x}, t_m) = \begin{cases} \boldsymbol{\varphi}, & m = 0 \\ \boldsymbol{0}, & m > 0, \end{cases} \quad \boldsymbol{x} \in \Omega, \end{aligned} \tag{3.15a}$$

$$\begin{aligned} \frac{\partial \boldsymbol{w}_m^{(\mathrm{PML})}}{\partial t} + \boldsymbol{L}^{(\mathrm{PML})}\boldsymbol{w}_m^{(\mathrm{PML})} = \boldsymbol{0}, \quad \boldsymbol{x} \in \mathbb{R}^3 \setminus \Omega, \quad t > t_m, \\ \boldsymbol{w}_m^{(\mathrm{PML})}(\boldsymbol{x}, t_m) = \boldsymbol{0}, \quad \boldsymbol{x} \in \mathbb{R}^3 \setminus \Omega, \end{aligned} \tag{3.15b}$$

$$\boldsymbol{w}_m^{(\Omega)}(\boldsymbol{x}, t) = \boldsymbol{M}\boldsymbol{w}_m^{(\mathrm{PML})}(\boldsymbol{x}, t), \quad \boldsymbol{x} \in \partial\Omega. \tag{3.15c}$$

To account for the "misbehavior" of the PML, equations (3.15a), (3.15b) need to be perturbed the same way as we have perturbed (3.10a), (3.10b) to obtain (3.12):

$$\begin{aligned} &\frac{\partial \tilde{\boldsymbol{w}}_m^{(\Omega)}}{\partial t} + \boldsymbol{L}\tilde{\boldsymbol{w}}_m^{(\Omega)} = \boldsymbol{f}_m(\boldsymbol{x}, t), \quad \boldsymbol{x} \in \Omega, \quad t > t_m, \\ &\tilde{\boldsymbol{w}}_m^{(\Omega)}(\boldsymbol{x}, t_m) = \begin{cases} \boldsymbol{\varphi} + \boldsymbol{\xi}_0, & m = 0 \\ \boldsymbol{\xi}_m, & m > 0, \end{cases} \quad \boldsymbol{x} \in \Omega, \end{aligned} \tag{3.16a}$$

$$\begin{aligned} \frac{\partial \tilde{\boldsymbol{w}}_m^{(\mathrm{PML})}}{\partial t} + \boldsymbol{L}^{(\mathrm{PML})} \tilde{\boldsymbol{w}}_m^{(\mathrm{PML})} = \boldsymbol{0}, \quad \boldsymbol{x} \in \mathbb{R}^3 \setminus \Omega, \quad t > t_m, \\ \tilde{\boldsymbol{w}}_m^{(\mathrm{PML})}(\boldsymbol{x}, t_m) = \boldsymbol{\xi}_m, \quad \boldsymbol{x} \in \mathbb{R}^3 \setminus \Omega. \end{aligned} \tag{3.16b}$$

Solutions of the respective problems (3.15) and (3.16)-(3.15c) will satisfy the same estimates (3.13) as satisfied by the solutions of (3.10) and (3.12). However, the key advantage of exploiting the lacunae is that for every $m = 0, 1, 2, \ldots$, the corresponding system only needs to be integrated over the interval $T_1 + T$. Hence,

$$\|\tilde{\boldsymbol{w}}_m^{(\Omega)}(\,\cdot\,, t) - \boldsymbol{w}_m^{(\Omega)}(\,\cdot\,, t)\| \le C\|\boldsymbol{\xi}_m\|', \tag{3.17a}$$

$$\|\tilde{\boldsymbol{w}}_m^{(\mathrm{PML})}(\,\cdot\,, t) - \boldsymbol{w}_m^{(\mathrm{PML})}(\,\cdot\,, t)\| \le C\|\boldsymbol{\xi}_m\|', \tag{3.17b}$$

where $C = \mu(T_1 + T)$ is a constant. Another key advantage of using lacunae is a finite and non-increasing number of summation terms in formula (3.14). Combined with estimate (3.17a), formula (3.14) yields (by the triangle inequality):

$$\|\tilde{\boldsymbol{w}}^{(\Omega)}(\,\cdot\,, t) - \boldsymbol{w}^{(\Omega)}(\,\cdot\,, t)\| \le C_0 \sup_m \|\boldsymbol{\xi}_m\|', \tag{3.18a}$$

where $C_0 = C \cdot (M - M_0 + 1)$ and the norms $\|\boldsymbol{\xi}_m\|'$ are assumed bounded altogether. In contradistinction to (3.13a), estimate (3.18a) implies that even if the PML errors contaminate Ω, *the resulting error on Ω will remain uniformly bounded for all times.* Note that according to (3.11), $\boldsymbol{w}^{(\Omega)}(\,\cdot\,, t)$ can be replaced with $\boldsymbol{w}(\,\cdot\,, t)$ on the left-hand side of (3.18a), which means that we have proved:

Theorem 3.1 *Let $\Omega \subset \mathbb{R}^3$ be a bounded domain, and let problem (3.4) be solved using a PML around Ω combined with the lacunae-based algorithm, see (3.14) and (3.15). Then, assuming that $\sup_m \|\boldsymbol{\xi}_m\|' < \infty$, the error on Ω due to the perturbation (3.16) of the PML will remain uniformly bounded for all times:*

$$\|\tilde{\boldsymbol{w}}^{(\Omega)}(\,\cdot\,, t) - \boldsymbol{w}(\,\cdot\,, t)\|_\Omega \le C_0 \sup_m \|\boldsymbol{\xi}_m\|'. \tag{3.18b}$$

Estimate (3.18b) provides an error bound for the domain Ω. In fact, the error growth inside the PML is also uniformly bounded, i.e., an estimate similar to (3.18b) holds for the complementary domain $\mathbb{R}^3 \setminus \Omega$ as well. It, however, should be written differently:

$$\Big\| \sum_{m=M_0}^{M} \tilde{\boldsymbol{w}}_m^{(\mathrm{PML})}(\,\cdot\,, t) - \sum_{m=M_0}^{M} \boldsymbol{w}_m^{(\mathrm{PML})}(\,\cdot\,, t) \Big\| \le C_0 \sup_m \|\boldsymbol{\xi}_m\|'. \tag{3.18c}$$

The first and second terms on the left-hand side of (3.18c) are solutions in the PML with and without

perturbations, respectively. They are left in the form of the sums because the lossy equations of the PML shall not be expected to be Huygens', and formula (3.14) will not, generally speaking, hold. In other words, since the solution is represented as a finite sum of terms with finite lifespan, the uniform bound (3.18c) is guaranteed. However, unlike on Ω, the solutions obtained in the PML with and without lacunae will not be the same.

3.3 Numerical Experiments

In this section, we demonstrate the performance of the algorithm introduced in Section 3.2.

3.3.1 Computational Setup

For the purpose of relating to prior work, in our numerical experiments we would like to stay as close as possible to the setup of Chapter 2, which was also used in our recent paper [5] and which, in turn, "borrows" certain components from [3]. The two key differences between the simulations in the current chapter and those conducted in Chapter 2 are that here we are using cylindrically symmetric geometry so that to be able to take advantage of the three-dimensional effects (lacunae) in an essentially two-dimensional setting, and also that in Chapter 2 the solution was driven by the initial conditions whereas here it is driven by a continuously operating source term on the right-hand side (described in Section 3.3.2).

Governing Equations and Geometry

Let r, z, and θ denote the cylindrical coordinates; the assumption of axial (cylindrical) symmetry implies that all the derivatives with respect to the polar angle vanish: $\frac{\partial}{\partial\theta} \equiv 0$. Then, the full Maxwell system of equations gets split into two independent subsystems that correspond to the transverse magnetic (TM) and transverse electric (TE) modes. Following Chapter 2, we will be solving the TE Maxwell equations in vacuum (c is the speed of light):

$$\begin{aligned} \frac{1}{c}\frac{\partial E_r}{\partial t} + \frac{\partial H_\theta}{\partial z} &= -\frac{4\pi}{c} j_r, \\ \frac{1}{c}\frac{\partial E_z}{\partial t} - \frac{1}{r}\frac{\partial (r H_\theta)}{\partial r} &= -\frac{4\pi}{c} j_z, \\ \frac{1}{c}\frac{\partial H_\theta}{\partial t} - \left(\frac{\partial E_z}{\partial r} - \frac{\partial E_r}{\partial z}\right) &= 0, \end{aligned} \tag{3.19}$$

where E_r and E_z denote the radial and axial components of the electric field, respectively, and H_θ denotes the angular component of the magnetic field. The first two equations in system (3.19) represent the Ampère law and are driven by the extraneous electric current with the components j_r

and j_z. The third equation in (3.19) represents the Faraday law and is homogeneous (no magnetic currents). The unsteady equations (3.19) are supplemented by the steady-state equation

$$\frac{1}{r}\frac{\partial(rE_r)}{\partial r} + \frac{\partial E_z}{\partial z} = 4\pi\rho, \tag{3.20}$$

where ρ is the electric charge density. Equation (3.20) is the Gauss' law for electricity, it relates the flux of the electric field through a given closed surface to the charge contained inside. A necessary solvability condition for system (3.19)–(3.20) is the continuity equation that represents the conservation of charge:

$$\frac{\partial\rho}{\partial t} + \frac{1}{r}\frac{\partial(rj_r)}{\partial r} + \frac{\partial j_z}{\partial z} = 0. \tag{3.21}$$

As long as condition (3.21) holds for the source terms ρ, j_r, and j_z, the steady-state equation (3.20) can be left out of the consideration when time-marching the unsteady equations (3.19).

At the axis of the cylindrical system, Maxwell's equations require additional attention. Under the natural assumption that all the physical quantities involved must be continuous and bounded, one can easily see that the vector components H_θ, E_r, and j_r can only meet the constraint of axial symmetry if they vanish at $r = 0$:

$$H_\theta(t,r,z)\big|_{r=0} = 0, \quad E_r(t,r,z)\big|_{r=0} = 0, \quad j_r(t,r,z)\big|_{r=0} = 0. \tag{3.22}$$

The axial components E_z and j_z do not have to vanish, although given (3.22), the third equation of system (3.19) reduces to $\frac{\partial E_z}{\partial r}\big|_{r=0} = 0$. The first equation of system (3.19) reduces to the identity $0 = 0$ on the axis, and the only equation that does not degenerate is the second equation. Taking into account the first equality from (3.22), we can use the Taylor formula for $r \ll 1$ and write: $H_\theta(t,r,z) = \frac{\partial H_\theta}{\partial r}\big|_{r=0} \cdot r + \mathcal{O}(r^2)$. Consequently, $\frac{1}{r}\frac{\partial(rH_\theta)}{\partial r} = \frac{1}{r}\frac{\partial H_\theta}{\partial r}\big|_{r=0} \cdot \frac{\partial r^2}{\partial r} + \mathcal{O}(r)$, which yields: $\frac{1}{r}\frac{\partial(rH_\theta)}{\partial r}\big|_{r=0} = 2\frac{\partial H_\theta}{\partial r}\big|_{r=0}$. Therefore, on the axis we have:

$$\frac{1}{c}\frac{\partial E_z}{\partial t} - 2\frac{\partial H_\theta}{\partial r} = -\frac{4\pi}{c}j_z. \tag{3.23}$$

The geometry of the problem is schematically shown in Figure 3.2. The computational domain has a rectangular shape in the (r,z) variables:

$$\Omega = \{(r,z) \mid 0 \le r \le 5,\ -5 \le z \le 5\}.$$

The currents (and charges) that drive the solution, see equations (3.19), (3.20), are assumed to be compactly supported in space on the ball $R \equiv (r^2+z^2)^{1/2} \le R_0$, and we typically choose $R_0 = 3$. The computational domain is terminated by the PML of width $l = 1$ in the axial direction, see

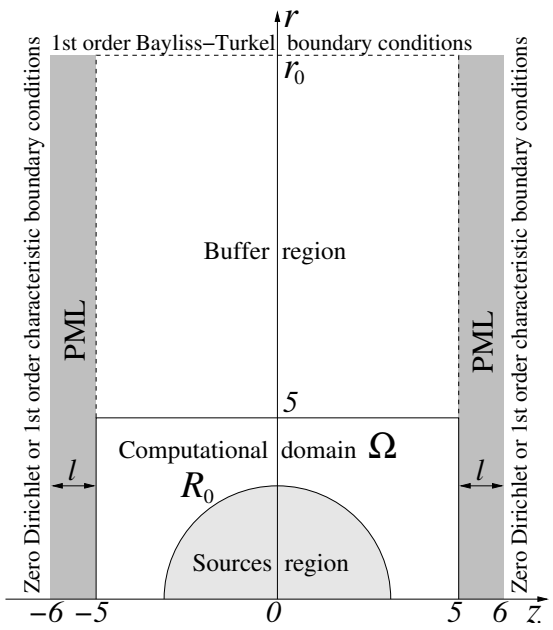

Figure 3.2: Geometric setup in the space.

Figure 3.2. In fact, with the proper choice of damping the width of the layer beyond a certain point no longer affects the quality of the solution on Ω (see Section 3.3.4).

PML

For our computations we take the mathematically derived unsplit PML of [2]. In the experiments of Chapter 2, see also [5], this layer has clearly shown to be prone to the undesirable growth of the solution for long integration times. We note that originally the PML of [2] was constructed for the two-dimensional Cartesian TE Maxwell equations. As, however, the axial coordinate of the cylindrical system is essentially Cartesian, the layer of [2] can be exported to the setup shown in

Figure 3.2 with no change at all:

$$\begin{aligned}
\frac{1}{c}\frac{\partial E_r}{\partial t} + \frac{\partial H_\theta}{\partial z} &= -2\sigma E_r - \sigma P, \\
\frac{1}{c}\frac{\partial E_z}{\partial t} - \frac{1}{r}\frac{\partial (r H_\theta)}{\partial r} &= 0, \\
\frac{1}{c}\frac{\partial H_\theta}{\partial t} - \left(\frac{\partial E_z}{\partial r} - \frac{\partial E_r}{\partial z}\right) &= \sigma' Q, \\
\frac{1}{c}\frac{\partial P}{\partial t} &= \sigma E_r, \\
\frac{1}{c}\frac{\partial Q}{\partial t} &= -\sigma Q - E_r.
\end{aligned} \tag{3.24}$$

Note that the PML (3.24) is built for the homogeneous Maxwell equations, because the right-hand sides of system (3.19), i.e., the currents, may only differ from zero for $R \le R_0$ and hence vanish near the outer boundary of Ω, see Figure 3.2. Compared to (3.19), system (3.24) contains two additional unknown quantities, $P = P(t, r, z)$ and $Q = Q(t, r, z)$. These quantities are identically equal to zero on Ω, and in the layer they are governed by two additional ordinary differential equations. The quantity $\sigma = \sigma(z)$ in (3.24) is the damping coefficient. It is also identically zero on Ω, whereas in the PML a certain degree of flexibility exists in choosing σ. In our computations, we will follow the recommendation of [3] and define:

$$\sigma(z) = \begin{cases} \sigma_0 \left(\frac{5-z}{l}\right)^3, & -5-l \le z \le -5, \\ 0, & -5 < z < 5, \\ \sigma_0 \left(\frac{z-5}{l}\right)^3, & 5 \le z \le 5+l. \end{cases} \tag{3.25}$$

For the PML of width $l = 1$, see Figure 3.2, we normally take $\sigma_0 = 10$ in (3.25).

Boundary Conditions

The PML itself is terminated at $z = 5 + l$ and $z = -5 - l$ either by zero Dirichlet boundary conditions for all field variables or by locally one-dimensional characteristic boundary conditions. Again, as indicated in Section 3.3.4, if the damping inside the layer is sufficiently strong, the boundary conditions at the outer boundaries of the PML make little or no difference as far as the quality of the solution on Ω. The use of characteristic boundary conditions, however, may bring along an additional benefit. With these boundary conditions, if the layer is switched off (i.e., if $\sigma \equiv 0$ everywhere), the boundary still has some non-reflecting properties sufficient for computing the solution with a "non-catastrophic" accuracy over a reasonably long time interval. This computation (see Section 3.3.4) allows us to unambiguously attribute the undesirable long-term growth to the presence of the PML,

because having the PML switched on or off appears the only difference between the two otherwise identical settings. Note that a similar argument was previously used in Chapter 2 for identifying the roots of the long-time growth of the solution.

The quasi-one-dimensional characteristic boundary conditions are set at the outer boundaries of the PML by artificially disregarding the r derivatives in system (3.19) and setting to zero the incoming Riemann variables, see Section 1.2.1. In doing so, we are disregarding the PML (3.24) near the boundary and setting the boundary conditions for the homogeneous version of Maxwell's equations (3.19). In the quasi-one-dimensional z framework, we consider two equations:

$$\frac{1}{c}\frac{\partial E_r}{\partial t} + \frac{\partial H_\theta}{\partial z} = 0 \quad \text{and} \quad \frac{1}{c}\frac{\partial H_\theta}{\partial t} + \frac{\partial E_r}{\partial z} = 0. \tag{3.26}$$

By adding and subtracting equations (3.26) to/from one another, we realize that the Riemann variable $H_\theta - E_r$ is incoming at $z = 5 + l$ and the Riemann variable $H_\theta + E_r$ is incoming at $z = -5 - l$, see Figure 3.2. Consequently, the desired characteristic boundary conditions are:

$$H_\theta - E_r\big|_{z=5+l} = 0 \quad \text{and} \quad H_\theta + E_r\big|_{z=-5-l} = 0. \tag{3.27}$$

The far field treatment that we adopt for the radial direction differs from the one in the axial direction. An unsplit PML similar to (3.24) but built for the genuinely cylindrical setting[3] is not readily available. Therefore, we have decided to introduce a large buffer region and terminate it with the first order Bayliss-Turkel local boundary conditions, see Section 1.2.3 and [12, 14–16]. For the size of the domain Ω in the radial direction equal to 5, we may take, e.g., $r_0 = 15$, see Figure 3.2. The motivation is that as the amplitude of the waves generated by the sources inside Ω decays proportionally to $R^{-1} \equiv (r^2 + z^2)^{-1/2}$, for a sufficiently remote boundary $r = r_0$ the magnitude of the reflections produced by the Bayliss-Turkel boundary conditions will be small. The computations of Section 3.3.4 corroborate that the magnitude of those reflections can indeed be driven down below the truncation error level inside Ω.

The Bayliss-Turkel boundary conditions are standard, but their derivation for system (3.19) requires a little extra care. As for any quasi-one-dimensional treatment, we disregard tangential derivatives (i.e., z derivatives) at the boundary $r = r_0$ and from the homogeneous Maxwell equations

[3]Recall, unlike z, r of the cylindrical system is not a Cartesian variable.

obtain the following independent second order equations for the filed components E_z and H_θ:

$$\frac{1}{c^2}\frac{\partial^2 E_z}{\partial t^2} = \frac{1}{r}\frac{\partial}{\partial r}\left(r\frac{\partial E_z}{\partial r}\right), \tag{3.28a}$$

$$\frac{1}{c^2}\frac{\partial^2 H_\theta}{\partial t^2} = \frac{\partial}{\partial r}\left(\frac{1}{r}\frac{\partial (rH_\theta)}{\partial r}\right). \tag{3.28b}$$

Equation (3.28a) is the standard scalar d'Alembert equation, because E_z is a Cartesian vector component. Equation (3.28b) is a vector d'Alembert equation, because H_θ is a non-Cartesian component. In the frequency space, equations (3.28a), (3.28b) transform into

$$\frac{\partial^2 \hat{E}_z}{\partial r^2} + \frac{1}{r}\frac{\partial \hat{E}_z}{\partial r} + \frac{\omega^2}{c^2}\hat{E}_z = 0, \tag{3.29a}$$

$$\frac{\partial^2 \hat{H}_\theta}{\partial r^2} + \frac{1}{r}\frac{\partial \hat{H}_\theta}{\partial r} - \frac{1}{r^2}\hat{H}_\theta + \frac{\omega^2}{c^2}\hat{H}_\theta = 0. \tag{3.29b}$$

Equation (3.29a) is a Bessel equation of order $\nu = 0$ and equation (3.29b) is a Bessel equation of order $\nu = 1$ because they can both be reduced to the respective standard forms by the change of variable $y = kr$, where $k = \omega/c$. Accordingly, the radiation solutions of these equations are given by the Hankel functions $H_\nu^{(2)}(kr)$, where $\nu = 0$ corresponds to (3.29a) and $\nu = 1$ corresponds to (3.29b). Therefore, the radiation boundary conditions can be obtained by requiring that the desired solution be parallel to $H_\nu^{(2)}(kr)$ in the sense of the corresponding Wronskian (see [116, Section 1.2]):

$$\frac{\partial \hat{E}_z}{\partial r} - \hat{E}_z \frac{\frac{\partial}{\partial r}H_0^{(2)}(kr)}{H_0^{(2)}(kr)} = 0, \tag{3.30a}$$

$$\frac{\partial \hat{H}_\theta}{\partial r} - \hat{H}_\theta \frac{\frac{\partial}{\partial r}H_1^{(2)}(kr)}{H_1^{(2)}(kr)} = 0. \tag{3.30b}$$

For large arguments y, the Hankel functions have the following asymptotic:

$$H_\nu^{(2)}(y) = \sqrt{\frac{2}{\pi y}}e^{-i\left(y - \frac{\pi\nu}{2} - \frac{\pi}{4}\right)} + \mathcal{O}(y^{-\frac{3}{2}})$$

so that for any ν we have:

$$\frac{d}{dy}H_\nu^{(2)}(y) \approx -\frac{1}{2y}H_\nu^{(2)}(y) - iH_\nu^{(2)}(y),$$

and consequently,

$$\frac{d}{dr}H_\nu^{(2)}(kr) \approx \left(-\frac{1}{2r} - ik\right)H_\nu^{(2)}(kr).$$

Therefore, disregarding the residual terms of the asymptotic, we can write instead of (3.30a), (3.30b):

$$\frac{\partial \hat{E}_z}{\partial r} + \frac{1}{2r}\hat{E}_z + ik\hat{E}_z = 0, \tag{3.31a}$$

$$\frac{\partial \hat{H}_\theta}{\partial r} + \frac{1}{2r}\hat{H}_\theta + ik\hat{H}_\theta = 0. \tag{3.31b}$$

Back in the time domain, boundary conditions (3.31a), (3.31b) transform into

$$\frac{1}{c}\frac{\partial E_z}{\partial t} + \frac{\partial E_z}{\partial r} + \frac{1}{2r}E_z = 0, \tag{3.32a}$$

$$\frac{1}{c}\frac{\partial H_\theta}{\partial t} + \frac{\partial H_\theta}{\partial r} + \frac{1}{2r}H_\theta = 0, \tag{3.32b}$$

and we realize that in the end of the day both field variables, E_z and H_θ, satisfy the same boundary condition even though the governing equations (3.28a) and (3.28b) are different. The Bayliss-Turkel boundary conditions (3.32a), (3.32b) are to be set at the far field boundary $r = r_0$, see Figure 3.2.

Discretization

The problem we have described is discretized on the grid with square cells: $h_z = h_r = h$. To demonstrate the convergence, we actually use a sequence of grids in Section 3.3.4 with $h = 0.1,\ 0.05,\ 0.025,$ and 0.0125. The spatial derivatives in system (3.19) (as well as in (3.20)) are approximated by central differences with second order accuracy, and the temporal derivatives are approximated by the conventional fourth order Runge-Kutta method (see, e.g., [111, Section 9.4]). The overall scheme is standard and we therefore do not write it out explicitly except for the approximation of the radial derivative:

$$\frac{1}{r}\frac{\partial (rH_\theta)}{\partial r}\Big|_n = \frac{1}{r_n}\frac{r_{n+1}H_{\theta n+1} - r_{n-1}H_{\theta n-1}}{2h} + \mathcal{O}(h^2),$$

where $r_n = nh$, $n = 0, 1, 2, \ldots$ The same scheme was used in Chapter 2 in the Cartesian case, see equations (2.10), and it led to the growth of the solution inside the PML.

The spatial derivatives in the on-axis equation (3.20) and in the boundary conditions (3.32a), (3.32b) are approximated by one-sided differences with second order accuracy, and all temporal derivatives, including those of P and Q in the PML (3.24) are approximated by the same Runge-Kutta scheme.

The characteristic boundary conditions (3.27) are approximated in the context of Runge-Kutta time marching. Let τ be the time step and assume that the right boundary $z = 5 + l = 6$, see Figure 3.2, corresponds to $m = M$ on the grid. At the first stage of Runge-Kutta, we write for the first equation (3.26):

$$\tilde{E}_{rM} = E_{rM} - \frac{c\tau}{2}\frac{H_{\theta M+1} - H_{\theta M-1}}{2h}$$

and combine it with the second order approximation of the first equation (3.27):

$$E_{r\,M} = \frac{H_{\theta\,M+1} + H_{\theta\,M-1}}{2}.$$

Then, eliminating the ghost variable $H_{\theta\,M+1}$, we obtain:

$$\tilde{E}_{r\,M} = E_{r\,M}\left(1 - \frac{c\tau}{2h}\right) + \frac{c\tau}{2h} H_{\theta\,M-1}, \tag{3.33a}$$

and likewise for the magnetic field with the help of the second equation (3.26):

$$\tilde{H}_{\theta\,M} = H_{\theta\,M}\left(1 - \frac{c\tau}{2h}\right) + \frac{c\tau}{2h} E_{r\,M-1}. \tag{3.33b}$$

Relations (3.33a), (3.33b) are the discrete characteristic boundary conditions. Similar relations can be obtained for other stages of Runge-Kutta and for the opposite boundary $z = -5-l \;\Leftrightarrow\; m = -M$.

3.3.2 Test Solution

To study the performance of the algorithm, we would like to be able to compute the actual numerical error on the grid at different moments of time. As such, we need the exact solution, and we obtain it by "backward engineering."

We begin with the standard scalar retarded potential:

$$\phi = \frac{\chi(t - R/c)}{R} \tag{3.34}$$

that solves the three-dimensional d'Alembert equation driven by the source term $4\pi\delta(\boldsymbol{x})\cdot\chi(t)$, where $R = |\boldsymbol{x}|$. The modulating function $\chi(t)$ is assumed to be sufficiently smooth for $-\infty < t < \infty$ and $\chi(t) \equiv 0$ for $t < 0$.

Along with the cylindrical coordinates (r, θ, z), let us also consider the Cartesian coordinates (x, y, z), so that $x = r\cos\theta$, $y = r\sin\theta$, and $R^2 = r^2 + z^2 = x^2 + y^2 + z^2$. By differentiating the retarded potential ϕ of (3.34), we obtain:

$$\phi'_x = \left[-\frac{\chi(t - R/c)}{R^2} - \frac{1}{c}\frac{\chi'(t - R/c)}{R}\right]\frac{x}{R}, \tag{3.35a}$$

$$\phi'_y = \left[-\frac{\chi(t - R/c)}{R^2} - \frac{1}{c}\frac{\chi'(t - R/c)}{R}\right]\frac{y}{R}. \tag{3.35b}$$

The derivatives $\phi'_x \equiv \frac{\partial\phi}{\partial x}$ and $\phi'_y \equiv \frac{\partial\phi}{\partial y}$ are solutions of the d'Alembert equation driven by the dipoles $4\pi\delta'_x(\boldsymbol{x})\cdot\chi(t)$ and $4\pi\delta'_y(\boldsymbol{x})\cdot\chi(t)$, respectively.

Next, we introduce a new vector field $\boldsymbol{B}$ by defining its Cartesian components:

$$B_x = -\phi'_y, \qquad B_y = \phi'_x, \qquad B_z = 0,$$

where ϕ'_x and ϕ'_y are given by (3.35a) and (3.35b), respectively. For the cylindrical components of $\boldsymbol{B}$ we therefore have:

$$B_\theta = -\sin\theta B_x + \cos\theta B_y = \left[-\frac{\chi(t-R/c)}{R^2} - \frac{1}{c}\frac{\chi'(t-R/c)}{R}\right]\frac{r}{R}, \tag{3.36a}$$

$$B_r = \cos\theta B_x + \sin\theta B_y = 0. \tag{3.36b}$$

By design, the vector field $\boldsymbol{B} = \boldsymbol{B}(\boldsymbol{x}, t)$ is a solution to the three-dimensional vector d'Alembert equation driven by the following dipole at the origin:

$$4\pi(-\delta'_y(\boldsymbol{x}), \delta'_x(\boldsymbol{x}), 0) \cdot \chi(t).$$

This solution is axially symmetric, because $\frac{\partial B_\theta}{\partial \theta} = 0$. This solution is also singular at the origin. Therefore, we introduce a scalar multiplier function $\psi = \psi(R)$ that should have at least p continuous derivatives for $R \geq 0$. We require that $\psi(R) \equiv 1$ for $R \geq R_0$, see Figure 3.2, and $\psi(0) = \psi'(0) = \ldots = \psi^{(p)}(0) = 0$. In practice, we take $p = 6$ and build $\psi(R)$ on $0 \leq R \leq R_0$ as a polynomial of degree 13.

Having constructed $\psi(R)$, we introduce a new vector field $\tilde{\boldsymbol{B}}(\boldsymbol{x}, t) = \boldsymbol{B}(\boldsymbol{x}, t) \cdot \psi(R)$, which no longer has a singularity at the origin. Moreover, it even turns into zero at $R = 0$ along with at least $p - 2$ of its derivatives, see formula (3.36a). Note that for $R > R_0$ the vector field $\tilde{\boldsymbol{B}}(\boldsymbol{x}, t)$ is still an axially symmetric solution to the homogeneous three-dimensional d'Alembert equation. The test solution for Maxwell's equations (3.19) will be obtained by using $\tilde{\boldsymbol{B}}(\boldsymbol{x}, t)$ as a generating function for the vector potential of the electromagnetic field.

It is well known that even though the three-dimensional electromagnetic field consists of two vector quantities, the electric field $\boldsymbol{E}$ and the magnetic field $\boldsymbol{H}$ (six scalar components altogether), there are, in fact, only four independent scalar quantities that determine the field. These four quantities are conveniently represented as the vector potential $\boldsymbol{A}$ and the scalar potential φ. Moreover, the vector and scalar potentials are not defined uniquely either, they may be required to satisfy additional constraints. Each particular form of $\boldsymbol{A}$ and φ under a given set of constraints is known as a gauge, and the independence of $\boldsymbol{E}$ and $\boldsymbol{H}$ on the specific choice of the gauge is known as gauge invariance [91, Chapter 3]. The Coulomb gauge corresponds to $\varphi \equiv 0$, then

$$\boldsymbol{E} = -\frac{1}{c}\frac{\partial \boldsymbol{A}}{\partial t} \quad \text{and} \quad \boldsymbol{H} = \operatorname{curl}\boldsymbol{A}. \tag{3.37}$$

Let us define the vector potential as $\boldsymbol{A} = \mathrm{curl}\tilde{\boldsymbol{B}}$ so that

$$A_r = -\frac{\partial \tilde{B}_\theta}{\partial z}, \quad A_z = \frac{1}{r}\frac{\partial (r\tilde{B}_\theta)}{\partial r}, \quad \text{and} \quad A_\theta = 0. \tag{3.38}$$

The vector potential $\boldsymbol{A} = \boldsymbol{A}(t, r, z)$ is also a solution to the three-dimensional d'Alembert equation; this equation is homogeneous for $R > R_0$ and inhomogeneous for $R \leq R_0$. The specific form of inhomogeneity for $\boldsymbol{A}$ can be derived, but it is of no immediate importance, because what we need is the right-hand sides of the Maxwell equations that drive the fields.

Using the definition of vector potential (3.38) and applying transformation (3.37), we obtain the following components of electromagnetic field:

$$\begin{aligned} E_z(t,r,z) = &-\frac{1}{c^3R^6}\Big(c^2\chi'(t-R/c)\left((r^2-2z^2)R\psi(R) - r^2R^2\psi'(R)\right) \\ &+ R^2\Big(-cr^2R\psi'(R)\chi''(t-R/c) \\ &+ \psi(R)\Big(c(r^2-2z^2)\chi''(t-R/c) + r^2R\chi^{(3)}(t-R/c)\Big)\Big)\Big), \end{aligned} \tag{3.39a}$$

$$\begin{aligned} E_r(t,r,z) = &-\frac{rz}{c^3R^6}\Big(c^2\chi'(t-R/c)\left(-3R\psi(R) + R^2\psi'(R)\right) \\ &- R^2\Big(-cR\psi'(R)\chi''(t-R/c) \\ &+ \psi(R)\Big(3c\chi''(t-R/c) + R\chi^{(3)}(t-R/c)\Big)\Big)\Big), \end{aligned} \tag{3.39b}$$

and

$$\begin{aligned} H_\theta(t,r,z) = &\frac{r}{c^3R^5}\Big(c^3\chi(t-R/c)\left(-2R\psi'(R) + R^2\psi''(R)\right) \\ &- R^2\Big(2cR\psi'(R)\chi''(t-R/c) \\ &+ c^2\chi'(t-R/c)\left(2\psi'(R) - R\psi''(R)\right) \\ &- \psi(R)\Big(c\chi''(t-R/c) + R\chi^{(3)}(t-R/c)\Big)\Big)\Big). \end{aligned} \tag{3.39c}$$

By design, the fields given by (3.39a), (3.39b), (3.39c) solve the Maxwell equations (3.19), and the resulting currents j_r and j_z that we calculate below are non-zero only for $R \leq R_0$. Moreover, as according to (3.37) $\mathrm{div}\boldsymbol{E} = -\frac{1}{c}\frac{\partial \mathrm{div}\boldsymbol{A}}{\partial t}$, and $\boldsymbol{A} = \mathrm{curl}\tilde{\boldsymbol{B}}$, the electric field of (3.39a), (3.39b) is solenoidal, $\mathrm{div}\boldsymbol{E} = 0$, and consequently, the continuity equation (3.21) is satisfied identically.

The currents j_r and j_z are obtained by substituting the fields (3.39a), (3.39b), (3.39c) into the

first two equations of system (3.19):

$$
\begin{aligned}
-\frac{4\pi}{c}j_z(t,r,z) = \frac{1}{c^3R^7}\Big(&- c^3\chi(t-R/c)\big(4(r^2-z^2)R\psi'(R) \\
&- R^2\big((3r^2-2z^2)\psi''(R) - r^2R\psi^{(3)}(R)\big)\big) \\
&- R^2\Big(- 3cr^2R^2\chi''(t-R/c)\psi''(R) + 2\psi'(R) \\
&\times \big(c(r^2-2z^2)R\chi''(t-R/c) + r^2R^2\chi^{(3)}(t-R/c)\big) \\
&+ c^2\chi'(t-R/c)\big(4(r^2-z^2)\psi'(R) \\
&+ R(-3r^2+2z^2)\psi''(R) + r^2R^2\psi^{(3)}(R)\big)\Big)\Big),
\end{aligned}
\tag{3.40a}
$$

$$
\begin{aligned}
-\frac{4\pi}{c}j_r(t,r,z) = \frac{rz}{c^3R^7}\Big(&c^3\chi(t-R/c)\big(8R\psi'(R) \\
&- R^2\big(5\psi''(R) - R\psi^{(3)}(R)\big)\big) \\
&+ R^2\Big(- 3cR^2\chi''(t-R/c)\psi''(R) + 2\psi'(R) \\
&\times \big(3cR\chi''(t-R/c) + R^2\chi^{(3)}(t-R/c)\big) \\
&+ c^2\chi'(t-R/c)\big(8\psi'(R) \\
&- 5R\psi''(R) + R^2\psi^{(3)}(R)\big)\Big)\Big).
\end{aligned}
\tag{3.40b}
$$

By design, the solution of Maxwell's equations (3.19) driven by the currents (3.40a), (3.40b) and subject to the homogeneous initial conditions is given by the fields (3.39a), (3.39b), (3.39c). In Section 3.3.4, we solve system (3.19) with the right-hand sides (3.40a), (3.40b) numerically and evaluate the error by comparing the solution computed on the grid with the exact solution (3.39a), (3.39b), (3.39c).

3.3.3 Implementation Issues

An important consideration to be addressed when implementing the strategy of Section 3.2 in a computational setting is how to preserve the lacunae in the numerical solution. It is clear that a straightforward partition of the continuously operating source according to formula (3.5) may create discontinuities at the splitting points t_m, $m = 0, 1, 2, \ldots$, even if the function $\boldsymbol{f}(\boldsymbol{x}, t)$ itself is smooth. From the standpoint of the original Huygens' principle, having a discontinuous right-hand side presents no problem, and the sharp aft fronts will remain sharp aft fronts. In the discrete context, however, the discontinuities may lead to the deterioration (or loss) of consistency by the scheme, and the aft fronts will then be "smeared out" by numerical artifacts.

Therefore, following our previous work [108, 109, 118, 119], we introduce an alternative approach to partitioning the RHS $\boldsymbol{f}(\boldsymbol{x}, t)$. Consider a smooth partition of unity schematically shown in

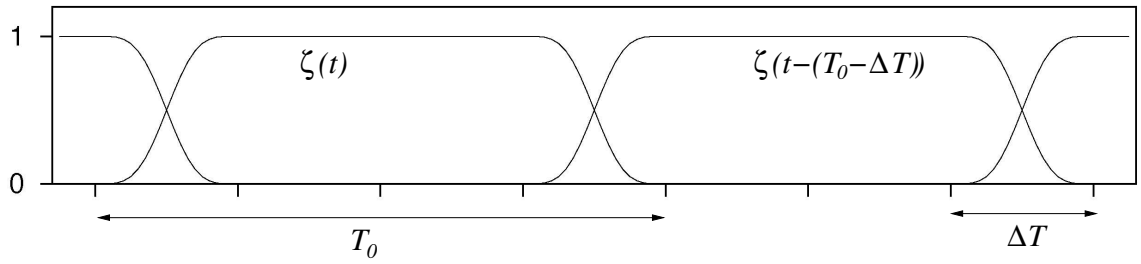

Figure 3.3: Smooth partition of unity.

Figure 3.3. Let T_0 be the size (duration) of each partition element, and ΔT be the width (duration) of the transition zone. Denote by $\zeta(t)$ the smooth compactly supported function that renders the partition so that $\zeta(t) \equiv 1$ for $\Delta T \le t \le T_0 - \Delta T$ and $\zeta(t) + \zeta(t-(T_0-\Delta T)) \equiv 1$ for $T_0 - \Delta T < t < T_0$. Then, the individual partition elements are obtained by a mere translation: $\zeta(t - m(T_0 - \Delta T))$, $m = -1, 0, 1, 2, \ldots$.

Having introduced the partition of unity shown in Figure 3.3, we redefine the partition of the RHS (3.5) as follows. Let $T_1 \stackrel{\text{def}}{=} T_0 - \Delta T$, then

$$\begin{aligned} \boldsymbol{f}(\boldsymbol{x},t) &= \sum_{m=0}^{\infty} \boldsymbol{f}_m(\boldsymbol{x},t), \\ \boldsymbol{f}_m(\boldsymbol{x},t) &= \begin{cases} \boldsymbol{f}(\boldsymbol{x},t) \cdot \zeta(t - mT_1), & t_m \le t < t_{m+1} + \Delta T, \\ \boldsymbol{0}, & \text{otherwise}, \end{cases} \end{aligned} \tag{3.41}$$

where $t_m = mT_1$, $m = 0, 1, 2, \ldots$ Formula (3.41) applies uniformly to all $m = 0, 1, 2, \ldots$ except that no change of the RHS is needed near $t = 0$ and $\boldsymbol{f}_0(\boldsymbol{x},t) \equiv \boldsymbol{f}(\boldsymbol{x},t)$ for $0 \le T \le \Delta T$. The key difference between the new partition (3.41) and the previous partition (3.5) is that as long as $\boldsymbol{f}(\boldsymbol{x},t)$ is smooth, all $\boldsymbol{f}_m(\boldsymbol{x},t)$ defined by formula (3.41) are also smooth. Hence, no loss of consistency shall be expected for any discretization applied to individual subproblems (3.6) or (3.15). Therefore, the corresponding numerical solutions will have the lacunae approximated on the grid with the accuracy that pertains to the specific scheme.

The use of the overlapping partition (3.41) instead of (3.5) causes only minor changes in the algorithm of Section 3.2. In fact, all the formulae stay the same, and only instead of (3.8) we now write:

$$\boldsymbol{w}_m(\boldsymbol{x},t) = \boldsymbol{0}, \quad \boldsymbol{x} \in \Omega, \quad t \ge t_{m+1} + \Delta T + T \equiv t_{m+1} + \Delta T + d/c, \tag{3.42}$$

because the source $\boldsymbol{f}_m(\boldsymbol{x},t)$ ceases to operate at $t = t_{m+1} + \Delta T$ rather than at $t = t_{m+1}$, as in

Section 3.2. Accordingly, in formula (3.9) we need to redefine the lower summation index: $M_0 \stackrel{\text{def}}{=} [(t-\Delta T-T)/T_1]$, where $[\,\cdot\,]$ denotes the integer part, as before. In the computations of Section 3.3.4, the value of T_0 is typically taken much larger than ΔT, see Figure 3.3, and even a few times larger than $T = d/c$. This, in particular, means that we always have $t_m + \Delta T + T < t_{m+1}$. Consequently, the number of terms $M - M_0 + 1$ in the sum (3.9) is equal to either 2 or 1. Namely,

$$M - M_0 + 1 = \begin{cases} 2, & \text{if } \ t_m \le t \le t_m + \Delta T + T, \\ 1, & \text{if } \ t_m + \Delta T + T < t < t_{m+1}. \end{cases} \tag{3.43}$$

It should also be noted that in the context of Maxwell's equations (3.19), the RHS $\boldsymbol{f}(\boldsymbol{x}, t)$ is given by the components of the current j_r and j_z. In the test solution of Section 3.3.2, the current (3.40a), (3.40b) is constructed solenoidal, and the charge density ρ is zero, so that the continuity equation (3.21) is satisfied identically. Obviously, the partition (3.41) will keep the current solenoidal, and hence the necessary solvability condition (3.21) for Maxwell's equations will automatically hold for every individual subproblem (3.6).

3.3.4 Results of Computations

The modulating function $\chi(t)$ that we take for our experiments is

$$\chi(t) = \begin{cases} \sum\limits_{j=1}^{j=4} a_j \sin(\omega_j t), & \text{if } \ t \ge 0, \\ 0, & \text{if } \ t < 0, \end{cases} \tag{3.44}$$

where the frequencies ω_j, $j = 1, \ldots, 4$, are chosen incommensurate:

$$\omega_1 = 1, \quad \omega_2 = \sqrt{3/2}\omega_1, \quad \omega_3 = \sqrt{2}\omega_1, \quad \omega_4 = \sqrt{3}\omega_1,$$

so that to avoid periodicity, and the coefficients a_j, $j = 1, \ldots, 4$, are given by

$$\begin{aligned} a_1 &= -\frac{1}{\omega_1(\omega_1^2-\omega_2^2)(\omega_1^2-\omega_3^2)(\omega_1^2-\omega_4^2)}, \\ a_2 &= -\frac{1}{\omega_2(\omega_2^2-\omega_1^2)(\omega_2^2-\omega_3^2)(\omega_2^2-\omega_4^2)}, \\ a_3 &= -\frac{1}{\omega_3(\omega_3^2-\omega_1^2)(\omega_3^2-\omega_2^2)(\omega_3^2-\omega_4^2)}, \\ a_4 &= -\frac{1}{\omega_4(\omega_4^2-\omega_1^2)(\omega_4^2-\omega_2^2)(\omega_4^2-\omega_3^2)}, \end{aligned}$$

which guarantees that $\chi(t)$ of (3.44) and its derivatives up to order 6 are continuous on the entire line $(-\infty, \infty)$, while $\chi^{(7)}(0+0) = 1$.

Let us first demonstrate the adverse effect that we would subsequently like to counter. The geometry of the computation is shown in Figure 3.2, the width of the PML is set to $l = 1$, and the magnitude of damping $\sigma_0 = 10$, see formula (3.25). The PML is terminated with the characteristic boundary conditions (3.27).

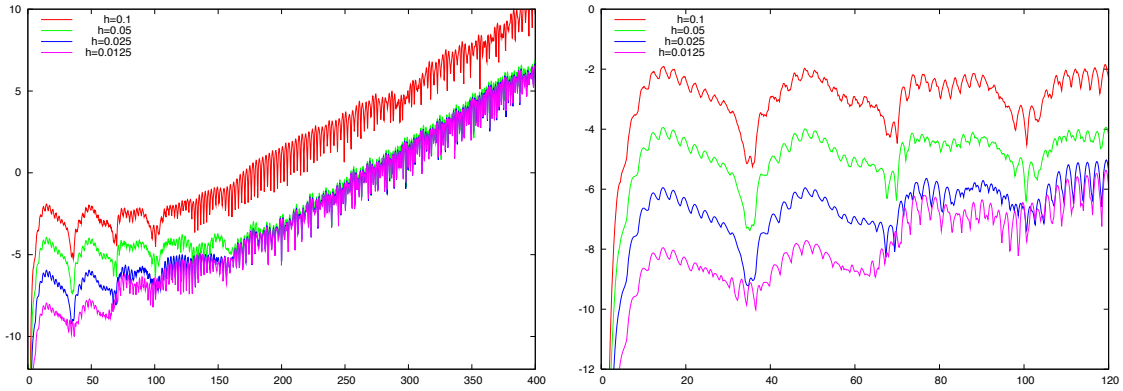

(a) $0 \le t \le 400$ (b) $0 \le t \le 120$

Figure 3.4: Computation with the PML (3.24). Binary logarithm of the maximum norm error for H_θ vs. time.

In Figure 3.4, we are showing the profiles of the error (its binary logarithm) for the magnetic field H_θ evaluated on the domain Ω in the maximum (i.e., L_∞) norm. The solutions are computed on the sequence of four square cell grids with sizes $h = 0.1$, 0.05, 0.025, and 0.0125. The H_θ error at every grid node is defined as the difference between the numerical solution and the exact solution (3.39c). The computations are run until $t = 400$, which is about forty times the time required for the waves to cross the computational domain Ω.

Some immediate observations from Figure 3.4 are as follows. At the initial stage of computation the numerical solution demonstrates the design rate of grid convergence — $\mathcal{O}(h^2)$; this is most clearly seen on the zoomed-in plot of Figure 3.4(b). At later stages, however, the error starts to increase, and the solution deteriorates, see Figure 3.4(a). The rate of deterioration is pretty much the same for all grids, however, the onset occurs somewhat earlier on finer grids.

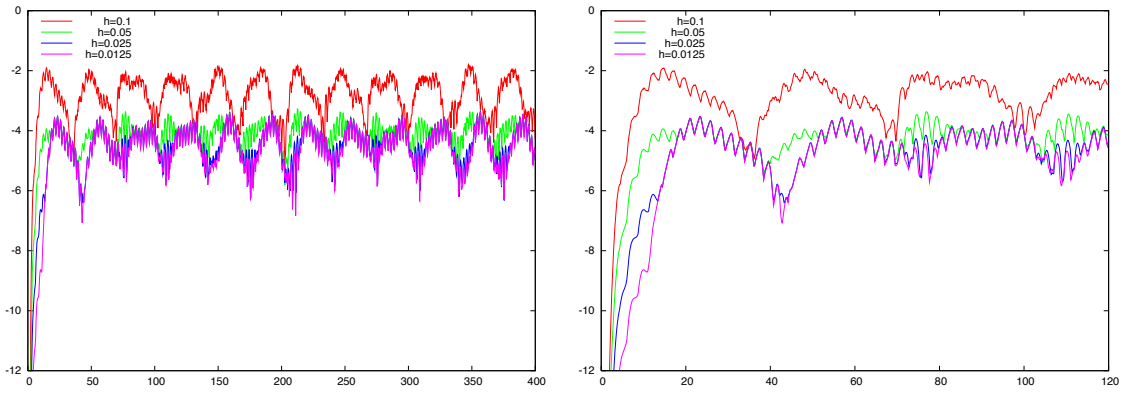

(a) $0 \leq t \leq 400$ (b) $0 \leq t \leq 120$

Figure 3.5: Computation with the the characteristic boundary conditions (3.27) only. Binary logarithm of the maximum norm error for H_θ vs. time.

In Figure 3.5, we are showing two plots similar to those from Figure 3.4. The computational setup that corresponds to Figure 3.5 is identical to that behind Figure 3.4 with one major exception — the PML is switched off, i.e., $\sigma(z) \equiv 0$. We see that the behavior of the error curves shown in Figure 3.5 differs from that of Figure 3.4 in two key aspects. On one hand, the grid convergence gets saturated rather early, there is practically no difference in the absolute value of the error already between $h = 0.05$ and $h = 0.025$. The explanation is straightforward — the error inside Ω is dominated by the reflections from the boundaries $z = 5 + l$ and $z = -5 - l$, see Figure 3.2, and the magnitude of those reflections is not related to the grid size. In other words, the characteristic boundary conditions (3.27) only allow to get so far down in error. On the other hand, we see that in Figure 3.5 there is no long-time error growth of the type Figure 3.4 shows. As the PML is the only difference between the two setups, we conclude that the deterioration of the numerical solution observed in Figure 3.4 should unambiguously be attributed to the presence of the PML.

To avoid any potential inaccuracies in the foregoing comparison, in Figure 3.6 we are showing the same error profiles as in Figures 3.4(a) and 3.5(a), but grouped according to the grid. This allows us to present the PML and no-PML error curves for every grid right next to one another in precisely the same scale. We conclude that on the coarsest grid $h = 0.1$, see Figure 3.6(a), the overall error is dominated by that of the interior discretization, because the two curves coincide in the beginning and at a later stage the PML solution deteriorates. On finer grids, see Figures 3.6(b)–(d), the accuracy of the PML solution at the initial stage improves as the grid size decreases, but then the long-time instability kicks in. At the same time, the error curves for the characteristic boundary

conditions remain "flat" for all t, but the accuracy does not improve as the grid is refined because of the reflections from the outer boundary.

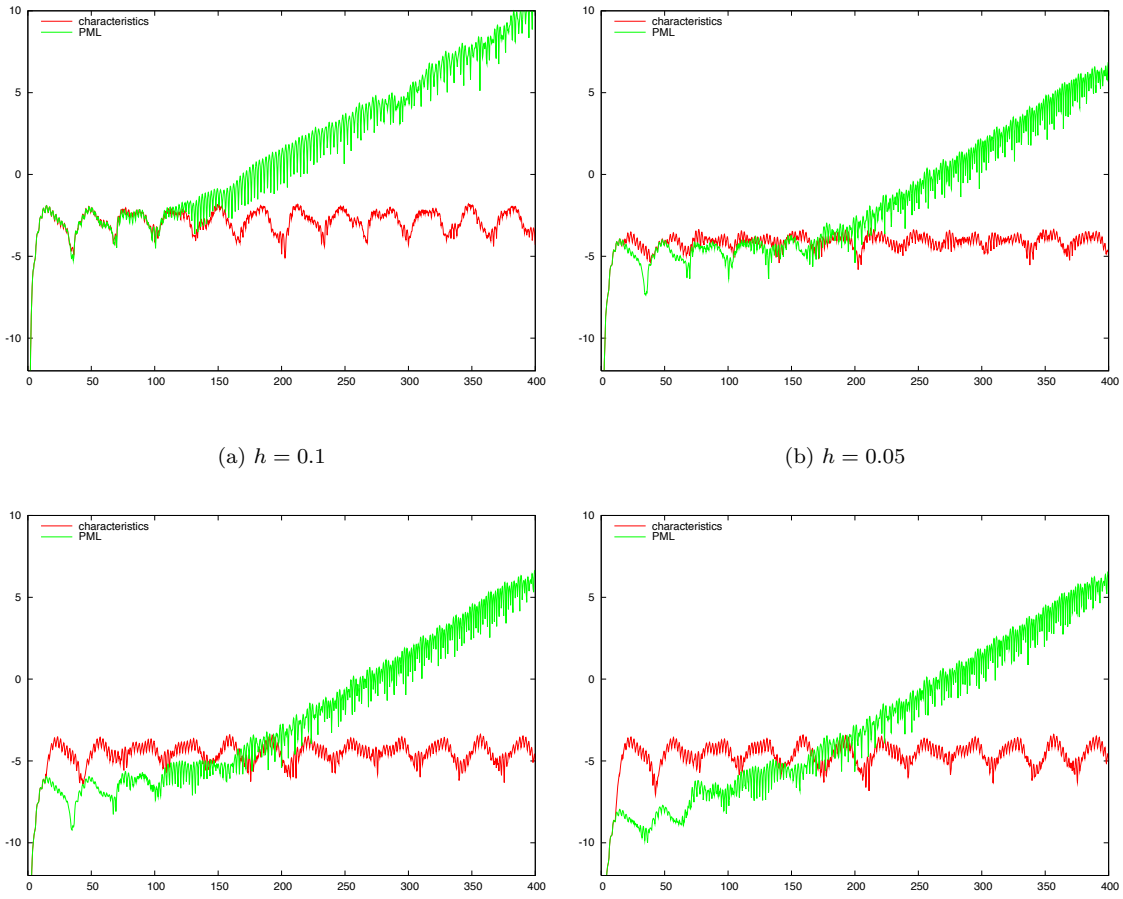

(a) $h = 0.1$ (b) $h = 0.05$

(c) $h = 0.025$ (d) $h = 0.0125$

Figure 3.6: Comparison of the case with the PML against that with no PML on four grids. Binary logarithm of the maximum norm error for H_θ vs. time.

Several comments are in order before we proceed to describing the results of computations with the lacunae-based method of Section 3.2.

- The error profiles for E_r and E_z in all the cases (including those with lacunae) look very much like those for H_θ, and we do not present them hereafter.
- We have repeated the PML computations with the layer twice as thick, $l = 2$, and the results were practically indistinguishable from those shown in Figure 3.4. Hence, we conclude that already with $l = 1$ the layer provides enough damping so that the error on

Ω is dominated by that of the interior discretization. We later corroborate this conclusion by the computations with genuine lacunae-based termination as in [109].

- We have also repeated the PML computations while terminating the layer with the zero Dirichlet boundary conditions rather than the characteristic boundary conditions (3.27). Again, the results were practically indistinguishable from those shown in Figure 3.4. Hence, we conclude that as long as the layer provides enough damping, the outer boundary condition does not make much of a difference.
- The increase of σ_0 does not make any difference in the results either.
- Finally, the log-linear curves shown in Figure 3.4(a) indicate that as the computation advances, the error increases with a slow yet exponential rate. At the same time, the continuous analysis of [3] predicts a polynomial growth. On the one hand, we note in this regard that the problem analyzed in [3] was driven only by the initial conditions and had zero RHS, whereas in this paper the solution is driven by a continuously operating source. On the other hand, the polynomial growth was predicted in [3] for a continuous formulation based on the presence of multiple eigenvalues in the amplification matrix. At the same time, we have seen in Chapter 2 that sometimes a multiple eigenvalue may get split by the discretization yet the growth will stay while in some other cases a multiple continuous eigenvalue will remain multiple for the discretization yet there will be no growth. Consequently, we can say that the reasons for the long-term deterioration of solution in the PML may not be fully understood yet, and there is apparently room for the growth faster than polynomial. (The observed growth is not a numerical instability, because it is not faster on finer grids.) However, as mentioned in Sections 3.1 and 3.2, and as subsequent computations clearly show, the lacunae-based integration allows to correct the long-time growth regardless of its origins and its specific rate (as long as the latter is not catastrophically fast).

Let us now demonstrate how the lacunae-based integration is combined with the PML (3.24). For the parameters of the partition, we take $T_0 = 44$ and $\Delta T = 2$, see Figure 3.3. In Figure 3.7, we are showing the results of computations for exactly the same setup as the one behind Figure 3.4, but with the lacunae-based correction applied (the vertical scale on Figures 3.4(a) and 3.7(a) is not the same). We see that the long-time growth completely disappears due to the lacunae-based correction, and the numerical solution shows the design second order grid convergence for the entire duration of the integration interval.

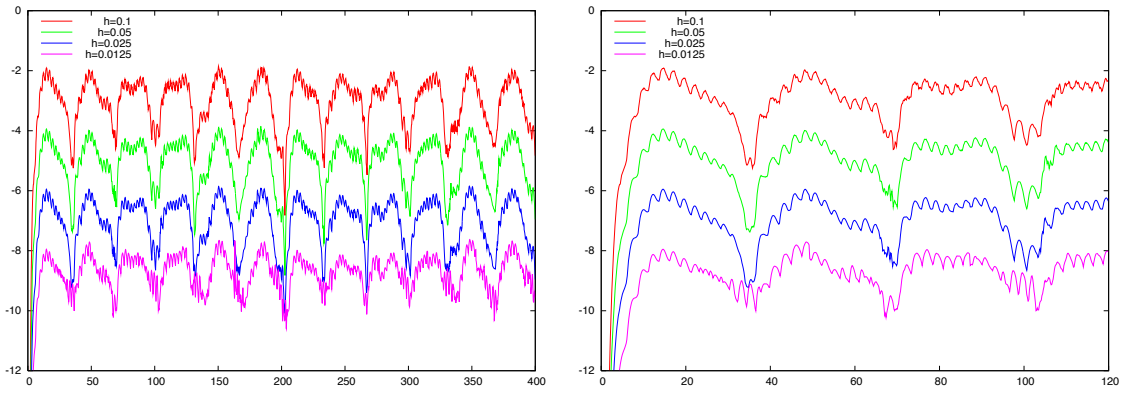

(a) $0 \le t \le 400$ (b) $0 \le t \le 120$

Figure 3.7: Computation with the PML (3.24) and lacunae-based correction. Binary logarithm of the maximum norm error for H_θ vs. time.

As before, to avoid any potential inaccuracies in the foregoing comparison, say, due to different scales on different plots, in Figure 3.8 we are showing the same error profiles as in Figures 3.4(a) and 3.7(a), but grouped according to the grid. This allows us to present the pure PML error profiles and the PML+lacunae profiles for every grid right next to one another in precisely the same scale. We see that at the initial stage the two error curves coincide on every grid, and the actual values of the error are decreasing with the design rate as the grid is refined. Later, the pure PML solutions completely lose their accuracy, whereas the solutions with the lacunae-based correction can maintain it for as long as the computation is run.

We note that the computational overhead associated with the application of lacunae-based algorithm along with the PML is not overwhelming. According to formula (3.43), the fraction of the overall time when we need to compute two solutions is $(T + \Delta T)/(t_{m+1} - t_m)$, and the rest of the time we compute only one solution. For the domain Ω shown in Figure 3.2, we have $T \approx 11$ (recall, $c = 1$), and with $T_0 = 44$ and $\Delta T = 2$ we can write:

$$\frac{T + \Delta T}{t_{m+1} - t_m} \equiv \frac{T + \Delta T}{T_1} \approx 0.31,$$

which puts the overhead at approximately 31%. The same series of computations with the PML and lacunae-based correction was, in fact, repeated for $T_0 = 64$ and $\Delta T = 2$. The results were very similar to those shown in Figures 3.7 and 3.8, with the overhead of about 21%.

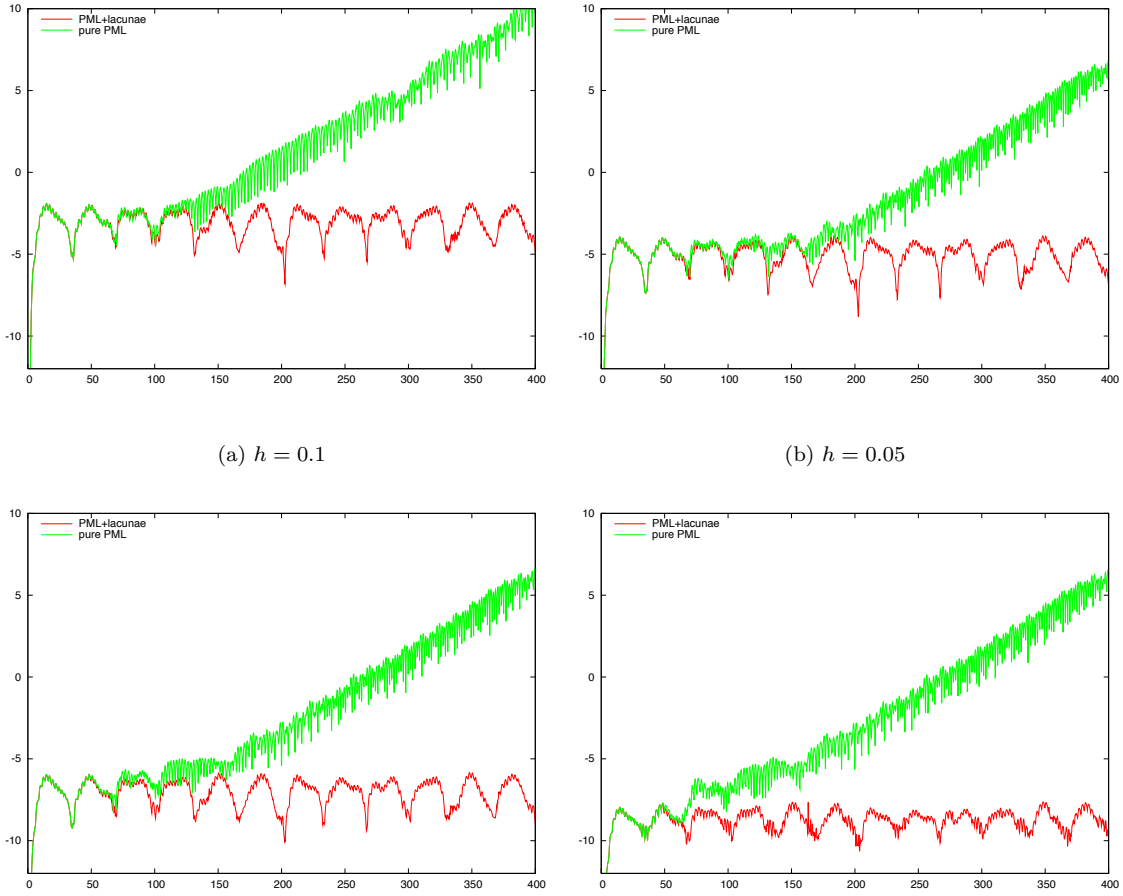

(a) $h = 0.1$

(b) $h = 0.05$

(c) $h = 0.025$

(d) $h = 0.0125$

Figure 3.8: Comparison of the pure PML case against that with the PML and lacunae on four grids. Binary logarithm of the maximum norm error for H_θ vs. time.

The only question that still needs to be addressed is that of the "optimality" of the proposed lacunae+PML treatment of the boundaries. In other words, whether or not a different approach can offer an even better overall accuracy compared to what Figures 3.7 and 3.8 show. To look into this issue, we compare the results obtained using the combination of lacunae and the PML with those obtained using the pure lacunae-based termination of the computational domain [109]. The original method of [109] requires buffer zones to surround Ω wider than the PML, and consequently, the computations are more expensive. However, the method of [109] *provably introduces no error associated with the domain truncation.* Hence, the only source of the error on Ω is the interior

discretization. In Figure 3.9, we compare the error profiles for the pure lacunae case and for the lacunae+PML case on four grids.

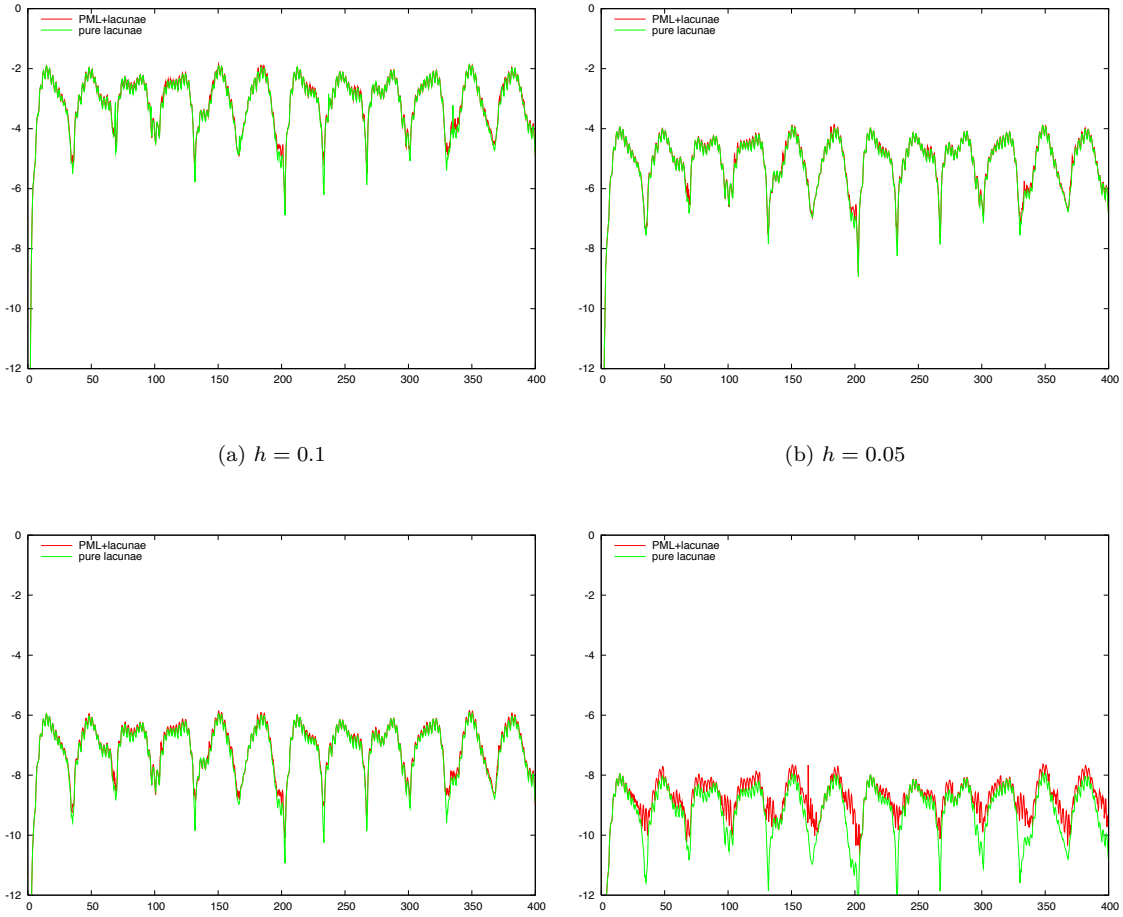

(a) $h = 0.1$

(b) $h = 0.05$

(c) $h = 0.025$

(d) $h = 0.0125$

Figure 3.9: Comparison of the pure lacunae case against that with the PML and lacunae on four grids. Binary logarithm of the maximum norm error for H_θ vs. time.

We see that the two curves basically sit on top of one another for every grid. Hence, the error on Ω obtained using the combined lacunae+PML methodology is the same as that for the pure lacunae-based approach. As the latter is due to the interior discretization only, we conclude that the accuracy of the boundary treatment offered by the combined lacunae+PML methodology exceeds the accuracy of the scheme on Ω and consequently, the overall accuracy cannot be further improved

by changing the boundary procedure.

3.4 Extensions

In this section, we review the application of lacunae-based methods to setting the ABCs [108, 118, 119], and show that the same approach will allow us to extend the applicability of the proposed lacunae-based stabilization of PMLs well beyond the simple problems of radiation of waves by known sources. The following problem formulation that requires unsteady ABCs is typical for many applications.

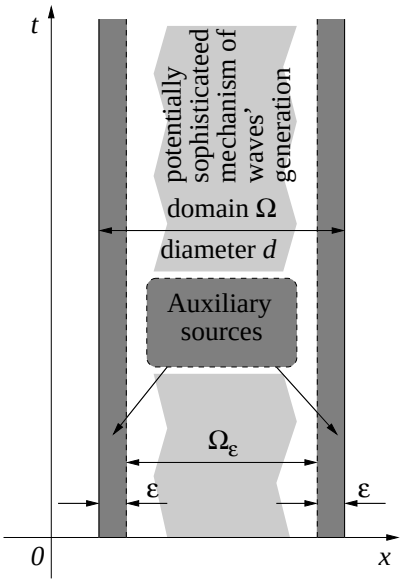

Figure 3.10: Decomposition of the problem.

The wave field of interest is generated inside the bounded domain $\Omega \subset \mathbb{R}^3$ and further propagates outward. We assume that in *the far field,* i.e., on the complementary domain $\mathbb{R}^3 \setminus \Omega$, the propagation of waves is governed by the linear homogeneous system [cf. formula (3.4)]:

$$\frac{\partial \boldsymbol{w}}{\partial t} + \boldsymbol{L}\boldsymbol{w} = \boldsymbol{0}, \quad \boldsymbol{x} \in \mathbb{R}^3 \setminus \Omega, \quad t > 0. \tag{3.45}$$

For our analysis we need to assume that equation (3.45) is Huygens'. The waves' generation mechanism inside Ω can be sophisticated. It can include actual sources (antennas), scatterers, and other objects, there can be damping, the waves can undergo multiple scattering, etc. Moreover, the model

inside Ω does not have to be Huygens'. *Our key assumption, however, is that the overall problem solved both inside and outside* Ω *has a unique solution.*

The goal is to be able to actually solve this problem only in *the near field,* i.e., on Ω, while truncating all of its exterior and replacing it with the appropriate closure procedure at the external boundary $\partial\Omega$, e.g., the ABCs or PML. The assumption on the overall unique solvability will allow us to focus independently on the design of the closure, i.e., on the proper treatment of the outgoing waves.

3.5 Discussion

The first step is the decomposition of the original problem into the interior and auxiliary subproblems. The interior problem is formulated on the bounded domain Ω, it is obtained by truncating the original formulation and as such, it inherits all the features of the latter. It is the interior problem that requires a closure at $\partial\Omega$. The auxiliary problem is formulated on the entire space $\mathbb{R}^3$. This problem is of the type (3.4), with the homogeneous initial conditions: $\boldsymbol{\varphi} = \boldsymbol{0}$. Its solution is driven by the specially constructed auxiliary source terms $\boldsymbol{f}(\boldsymbol{x}, t)$ that are compactly supported in space for all times on a narrow region $\Omega \setminus \Omega_\varepsilon$ next to the boundary $\partial\Omega$, see Figure 3.10. All the sophisticated features of the interior problem (such as scatterers) are supposed to be confined to Ω_ε.

The two problems are connected to one another. The auxiliary sources depend on the interior solution right inside Ω, and the solution of the auxiliary problem right outside Ω can provide the missing data and thus enable a closure for the interior formulation. The construction of the auxiliary sources is described in [108,118,119]. *It guarantees equivalence* between the original problem before the decomposition and the two subproblems after the decomposition considered together. This means, in particular, that the solution of the auxiliary problem on $\mathbb{R}^3 \setminus \Omega$, i.e., the outgoing field, coincides with the solution of the original problem. The key benefit from employing the decomposition is that by design, the auxiliary problem satisfies the Huygens' principle. The unsteady ABCs of [108, 118, 119] are obtained by solving the auxiliary problem with the help of lacunae and supplying the missing boundary data to the interior problem.

We emphasize that although the auxiliary sources depend on the interior solution, it does not imply that the interior problem requires a separate algorithm to be solved. Likewise, the fact that the closure for the interior problem is provided by the exterior solution does not imply that the auxiliary problem has to be solved on the extended region far away from Ω. In fact, both problems are time marched synchronously. Once the interior solution is advanced one time step, the auxiliary sources can also be advanced one time step. Then, the exterior solution can be obtained on the next level; it needs to be known only right outside Ω. This solution provides the missing closure for

the interior problem on the upper time level, after which the interior solution can be advanced yet one more step, and the procedure cyclically repeats itself. We refer the reader to [108, 118, 119] for additional detail on lacunae-based ABCs.

The exact same idea of decomposition can be applied in the framework of stabilizing the PMLs. The PML that surrounds Ω, see Figure 3.1, is designed to absorb all the outgoing waves. The outgoing waves are the same whether they are due to the original radiation/scattering mechanism on Ω_ε or to the auxiliary sources on $\Omega \setminus \Omega_\varepsilon$, see Figure 3.10. Hence, the lacunae-based methodology of Section 3.2 can be applied to the auxiliary problem, which will enable stabilization of the PML without having to put any restrictions on the model inside Ω_ε (besides the requirement of the overall unique solvability).

In Section 3.2, we have proved theoretically, and in Section 3.3 shown experimentally, that lacunae-based integration indeed provides an efficient tool for removing the long-term instabilities induced by PMLs. In doing so, the numerical error becomes uniformly bounded in time.

There is actually no contradiction in obtaining temporally uniform error bounds for the problem that is only weakly well-posed. The explanation is that the lacunae-based algorithm alters the solution of the combined problem inside the PML, and the overall solution coincides with the solution of (3.4) only on the domain Ω, where the Huygens' principle holds. At the same time, unlike in [3], the PML equations never get modified by lacunae-based integration, and for each problem (3.15) the layer remains perfectly matched and absorbing.

It is also clear that even though we have only considered the perturbations of the initial data $\boldsymbol{\xi}$ in Section 3.2, we would have obtained similar temporally uniform estimates if the perturbations of the RHS were included as well. The computations of Section 3.3 corroborate this conclusion experimentally.

The analysis of Section 3.2 imposes *no constraints on the rate of growth* $\mu(t)$, see (3.13), and C_0 in inequality (3.18b) is a constant in any event. The actual value of this constant $C_0 = \mu(T_1 + T) \cdot (M - M_0 + 1)$, however, may or may not be acceptable in a particular context. If $\mu(t)$ is a slowly increasing function, such as a low degree polynomial, then C_0 will not be large. In Section 3.3.4 we saw that the PML-induced growth may, in fact, be nonuniform. At the initial stage, there was no growth at all, and after that it would pick up. Hence, we chose the parameters in such a way so that to keep $T_1 + T$ within the range of no growth and consequently have a low value of $\mu(T_1 + T)$.

It is also important to emphasize that *the source of the growth inside the PML does not matter either.* It can be the mechanism identified in [3], but by no means does it have to be this mechanism only. For example, if *the corner in the PML* leads to long-term instabilities, the lacunae-based methodology will address those as well. In fact, since the idea of the lacunae-based methodology that we have introduced is to represent the solution that evolves over long times as the sum of a

finite number of components that each has a finite fixed "lifespan," the methodology can be used for alleviating any other undesirable long-term phenomenon in computation.

Note, however, that while the proposed procedure alleviates the growth of the field inside the PML, *it does not offer a fix for the numerical instability.* In other words, if the error estimate for the scheme deteriorates as the grid is refined, the deterioration will be inherited by the discretization of every problem (3.15). If, however, the deterioration rate is slow (e.g., linear as in [1]), then the overall algorithm may still be viable.

The computational overhead of the proposed procedure is $\sim (T + \Delta T)/T_1$, which can be kept at acceptable levels by choosing sufficiently large $T_1 = T_0 - \Delta T$. Specific values should be determined by actual numerical experiments.

In Section 3.2, we have only considered a PML of infinite thickness, whereas in real implementations, such as that of Section 3.3, the thickness is always finite. Termination of the PML at a finite distance results in reflections from the outer boundary that propagate back through the layer and then re-enter the computational domain. If, however, the damping inside the PML is sufficiently strong, the magnitude of these reflections is small. Hence, even though the lacunae-based algorithm won't help remove or reduce those reflections, the accuracy of the combined PML+lacunae boundary procedure can still be made sufficiently high so that to have the overall accuracy inside the computational domain dominated by that of the interior discretization (Section 3.3.4).

For Maxwell's equations, there is a necessary solvability condition given by the continuity equation for currents and charges (equation (3.21) in the cylindrically symmetric TE case). Partition of the RHS (3.41) may break the continuity, that's why for the numerical tests of Section 3.3 we have chosen zero charges and solenoidal currents (3.40a), (3.40b) that satisfy the continuity equation identically. As far as the more general framework outlined in Section 3.4, it has been shown in [119] that the auxiliary sources on $\Omega \setminus \Omega_\varepsilon$, see Figure 3.10, can also be obtained in the form of solenoidal currents and zero charges. Hence, they can withstand partition (3.41) with no violation of continuity.

Finally, the original problem (3.4) was formulated for a first order system, and numerical simulations of Section 3.3 have also been conducted using the first order system (3.19) as an example. Instead, we could have had a second order equation or system in (3.4), e.g., the d'Alembert equation itself. Note, there are examples of systems, as opposed to scalar equations, that do not reduce to the d'Alembert equation and yet are Huygens'.[4]

[4]Because systems are not covered by the result of [92].

Chapter 4

Conclusions

The stated objective of this dissertation was the study and stabilization of the PML — a methodology developed for terminating the computational domain in order to obtain a finite dimensional numerical approximation of a problem formulated on an unbounded domain. The methodology was designed to absorb the outgoing waves by first splitting the vector components of the electromagnetic field, and accordingly, it was called the split-field PML. The added degrees of freedom allowed to attenuate the field components without changing the velocity of propagation in the layer as this would immediately cause a reflection from the layer. In the original articles on the PML, see [20, 21], a special emphasis was made on the interface between the computational domain and the layer. In particular, it was shown that the impinging waves generated no reflection from the interface regardless of their frequency and the angle of incidence. However, extensive research and numerical experiments with the split-field PML detected the possibility of a polynomial growth of the solution inside the layer, as well as of instability and contamination of the computational domain [1] due to the weak well posedness of the Cauchy problem, see [90]. This led to an alternative formulation of the PML that is now known as the unsplit PML, see [2, 37, 82, 126]. As the name suggests, the field components are not split in the layer; rather, the damping of the field components is achieved due to the new variables introduced in the layer. The unsplit PML has also been shown to develop instabilities, see [3]; moreover, the contamination of the computational domain by the artifacts from the layer was experimentally demonstrated to be scheme dependent. A variety of approaches to curing the instability of the PML, although experimentally successful, have fallen short of being rigorous as they have relied on changing the governing equations in the layer thus possibly compromising its matching and/or absorption properties, see [3]. Other techniques, e.g., the nonlinear PML of [4], while guaranteeing the strong well posedness of the equations in the layer, have added implementation complications; while the complex frequency-shifted PML of [38, 100] leads to the loss of frequency independent absorption. Albeit the long-time instability of the PML

may have a limited effect on the overall quality and of the computational results, the uncertainties about the nature of the instability and contamination of the solution over the domain of interest prompted a closer consideration of the problem at hand.

As a stepping stone of the study, we have investigated both numerically and analytically the performance of two unsplit PMLs — physical and mathematical, see [3, 5], discretized with the following well known schemes: Lax-Wendroff, leap-frog, Yee and, Runge-Kutta in time with central differences in space, see Chapter 2. The numerical component of the study naturally involved observations of the long-time behavior of the layer; the analytical aspect consists of studying the eigen-structure of the discretizations at the quiescent state. The idea was to extend the results of [3] where the eigen-structure of the *continuous* formulations of the mathematical and physical PML was studied, and the instability was attributed to the missing eigenvectors and multiple eigenvalues. Our analytical study coupled with the numerical experiments has been able to clearly identify which of the combinations "scheme+PML" perform better and which perform worse, but it still could not definitively pinpoint the sources of the growth of the solution in the layer. Overall, the response of the layer seems to be strongly affected not only by the type of the PML but also by the choice of the discretization.

As the sources of growth are not known precisely, we proceeded to develop a stabilizing methodology that would not depend on the particular choice of the PML. The key component of the methodology that we proposed is the lacunae-based integration in time, [108–110, 118, 119]. It applies to hyperbolic partial differential equations and systems that satisfy the Huygens' principle; the equation/system may be driven by a continuously operating RHS compactly supported in space and by compactly supported initial data, see Chapter 3. The essence of the lacunae-based integration is that once the computational domain falls into the lacuna of the solution of the original problem, the integration can be terminated without affecting the solution. The application of lacunae-based integration first requires that the RHS of the original problem be represented as an infinite series with each term being compactly supported in space-time. Then, due to linear superposition the solution itself could be represented as a sum of solutions of the Cauchy problems due to the series representation of the RHS. However, because of the causality and the Huygens' principle (the presence of lacunae) this sum becomes finite with the number of terms that does not depend on time; this number can be determined ahead of time and set at the design stage of the algorithm. Moreover, each term in the sum has a finite and non-icreasing "lifespan" over the computational domain. These two properties translate into temporally uniform stability estimates. They guarantee that there will be no growth of the solution in the layer no matter how long the overall interval of integration may be. We reiterate that the methodology is independent of the structure of the layer and does not hamper its advantageous aspects.

The theoretical findings of Chapter 3 are corroborated by numerical experiments. To maintain the game-plan continuity, our experimental setup closely repeats that of Chapter 2, see also [3] and [5], but with two significant and necessary differences. First, to capture the effects of lacunae (which only occur in odd-dimensional spaces) we use cylindrically symmetric geometry that allows us mimic the three-dimensional behavior in an essentially two-dimensional setting. The mathematical PML (2.1) initially developed for the Cartesian coordinates, [2], lends itself to a smooth translation to the cylindrical coordinate system by observing that the axial coordinate of the latter is essentially Cartesian. Second, to observe the long time response of the PML we solve the problem driven by the sources that operate continuously in time whereas in Chapter 2 the solution was driven by the initial conditions, see Section 2.2. The numerically obtained approximation is compared to the exact solution obtained by backward engineering the test problem, see Section 3.3.2, and additional implementation related issues are successfully resolved in Section 3.3.3. The results of the numerical tests are presented in Section 3.3.4; these are supplanted with numerous figures and extensive commentary and observations. Overall, our numerical results fully corroborate the theoretical design properties of the algorithm.

The dissertation is concluded by a discussion of extending the lacunae-based methodology to solving more complex problems and formulations.

List of References

[1] S. Abarbanel and D. Gottlieb. A mathematical analysis of the PML method. *J. Comput. Phys.*, 134(2):357–363, 1997.

[2] S. Abarbanel and D. Gottlieb. On the construction and analysis of absorbing layers in CEM. *Appl. Numer. Math.*, 27(4):331–340, 1998.

[3] S. Abarbanel, D. Gottlieb, and J. S. Hesthaven. Long time behavior of the perfectly matched layer equations in computational electromagnetics. *J. Sci. Comput.*, 17(1-4):405–422, 2002.

[4] S. Abarbanel, D. Gottlieb, and J. S. Hesthaven. Non-linear PML equations for time dependent electromagnetics in three dimensions. *J. Sci. Comput.*, 28(2-3):125–137, 2006.

[5] Saul Abarbanel, Heydar Qasimov, and Semyon Tsynkov. Long-time performance of unsplit PMLs with explicit second order schemes. *J. of Sci. Comput.*, 2008. Submitted for publication.

[6] V. I. Agoshkov. Poincaré-Steklov's operators and domain decomposition methods in finite-dimensional spaces. In *First International Symposium on Domain Decomposition Methods for Partial Differential Equations (Paris, 1987)*, pages 73–112. SIAM, Philadelphia, PA, 1988.

[7] B. Alpert, L. Greengard, and T. Hagstrom. Rapid evaluation of nonreflecting boundary kernels for time-domain wave propagation. *SIAM J. Numer. Anal.*, 37:1138–1164, 2000.

[8] B. Alpert, L. Greengard, and T. Hagstrom. Nonreflecting boundary conditions for the time-dependent wave equation. *J. Comput. Phys.*, 180(1):270–296, 2002.

[9] M. F. Atiyah, R. Bott, and L. Gårding. Lacunas for hyperbolic differential operators with constant coefficients. I. *Acta Math.*, 124:109–189, 1970.

[10] M. F. Atiyah, R. Bott, and L. Gårding. Lacunas for hyperbolic differential operators with constant coefficients. II. *Acta Math.*, 131:145–206, 1973.

[11] F. V. Atkinson. On Sommerfeld's "radiation condition.". *Philos. Mag. (7)*, 40:645–651, 1949.

[12] Alvin Bayliss, Max Gunzburger, and Eli Turkel. Boundary conditions for the numerical solution of elliptic equations in exterior regions. *SIAM J. Appl. Math.*, 42(2):430–451, 1982.

[13] Alvin Bayliss, Max Gunzburger, and Eli Turkel. Boundary conditions for the numerical solution of elliptic equations in exterior regions. *SIAM J. Appl. Math.*, 42(2):430–451, 1982.

[14] Alvin Bayliss and Eli Turkel. Radiation boundary conditions for wave-like equations. *Comm. Pure Appl. Math.*, 33(6):707–725, 1980.

[15] Alvin Bayliss and Eli Turkel. Far field boundary conditions for compressible flows. *J. Comput. Phys.*, 48(2):182–199, 1982.

[16] Alvin Bayliss and Eli Turkel. Outflow boundary conditions for fluid dynamics. *SIAM J. Sci. Statist. Comput.*, 3(2):250–259, 1982.

[17] E. Bécache and P. Joly. On the analysis of Bérenger's perfectly matched layers for Maxwell's equations. *M2AN Math. Model. Numer. Anal.*, 36(1):87–119, 2002.

[18] Eliane Bécache, Peter G. Petropoulos, and Stephen D. Gedney. On the long-time behavior of unsplit perfectly matched layers. *IEEE Trans. Antennas and Propagation*, 52(5):1335–1342, 2004.

[19] M. Belger, R. Schimming, and V. Wünsch. A survey on Huygens' principle. *Z. Anal. Anwendungen*, 16(1):9–36, 1997. Dedicated to the memory of Paul Günther.

[20] Jean-Pierre Bérenger. A perfectly matched layer for the absorption of electromagnetic waves. *J. Comput. Phys.*, 114(2):185–200, 1994.

[21] Jean-Pierre Bérenger. Three-dimensional perfectly matched layer for the absorption of electromagnetic waves. *J. Comput. Phys.*, 127(2):363–379, 1996.

[22] A. P. Calderon. Boundary-value problems for elliptic equations. In *Proceedings of the Soviet-American Conference on Partial Differential Equations at Novosibirsk*, pages 303–304, Moscow, 1963. Fizmatgiz.

[23] Leonid Chindelevitch, David P. Nicholls, and Nilima Nigam. Error analysis and preconditioning for an enhanced DtN-FE algorithm for exterior scattering problems. *J. Comput. Appl. Math.*, 204(2):493–504, 2007.

[24] R. Courant and K. O. Friedrichs. *Supersonic flow and shock waves*. Springer-Verlag, New York, 1976. Reprinting of the 1948 original, Applied Mathematical Sciences, Vol. 21.

[25] R. Courant and D. Hilbert. *Methods of Mathematical Physics. Volume II.* Wiley, New York, 1962.

[26] S. A. Cummer. A simple, nearly perfectly matched layer for general electromagnetic media. *IEEE Microwave and Wireless Components Letters*, 13(3):128–130, 2003.

[27] Bjorn Engquist and Andrew Majda. Absorbing boundary conditions for the numerical simulation of waves. *Math. Comp.*, 31(139):629–651, 1977.

[28] Björn Engquist and Andrew Majda. Radiation boundary conditions for acoustic and elastic wave calculations. *Comm. Pure Appl. Math.*, 32(3):314–358, 1979.

[29] Björn Engquist and Andrew Majda. Numerical radiation boundary conditions for unsteady transonic flow. *J. Comput. Phys.*, 40(1):91–103, 1981.

[30] L. Ferm and B. Gustafsson. A downstream boundary procedure for the Euler equations. *Computers and Fluids*, 10:261–276, 1982.

[31] Lars Ferm. Open boundary conditions for stationary inviscid flow problems. *J. Comput. Phys.*, 78(1):94–113, 1988.

[32] Lars Ferm. Open boundary conditions for external flow problems. *J. Comput. Phys.*, 91:55–70, 1990.

[33] Lars Ferm. Non-reflecting accurate open boundary conditions for the steady Euler equations. Technical Report 143, Department of Scientific Computing, Uppsala University, Uppsala, Sweden, September 1992.

[34] Lars Ferm. Modified external boundary conditions for the steady Euler equations. Technical Report 153, Department of Scientific Computing, Uppsala University, Uppsala, Sweden, August 1993.

[35] Lars Ferm. Non-reflecting boundary conditions for the steady Euler equations. *J. Comput. Phys.*, 122:307–316, 1995.

[36] P. Garabedian. *Partial Differential Equations.* AMS Chelsea Publishing, Providence, RI, 2007.

[37] S. D. Gedney. An anisotropic perfectly matched layer-absorbing medium for the truncation of FDTD lattices. *IEEE Trans. Antennas Propagat.*, 44(12):1630–1639, 1996.

[38] S. D. Gedney. The perfectly matched layer absorbing medium. In A. Taflove, editor, *Advances in Computational Electrodynamics: The Finite-Difference Time-Domain Method*, pages 263–340. Artech House, Boston, MA, 1998.

[39] D. Givoli. Non-reflecting boundary conditions. *J. Comput. Phys.*, 94:1–29, 1991.

[40] Dan Givoli. *Numerical methods for problems in infinite domains*, volume 33 of *Studies in Applied Mechanics*. Elsevier Scientific Publishing Co., Amsterdam, 1992.

[41] Dan Givoli. A spatially exact nonreflecting boundary condition for time dependent problems. *Comput. Methods Appl. Mech. Engrg.*, 95(1):97–113, 1992.

[42] Dan Givoli. High-order nonreflecting boundary conditions without high-order derivatives. *J. Comput. Phys.*, 170(2):849–870, 2001.

[43] Dan Givoli. High-order local non-reflecting boundary conditions: A review. *Wave Motion*, 39(4):319–326, 2004. New computational methods for wave propagation.

[44] Dan Givoli. Non-reflecting boundaries: high-order treatment. In *A celebration of mathematical modeling*, pages 53–72. Kluwer Acad. Publ., Dordrecht, 2004.

[45] Dan Givoli, Thomas Hagstrom, and Igor Patlashenko. Finite element formulation with high-order absorbing boundary conditions for time-dependent waves. *Comput. Methods Appl. Mech. Engrg.*, 195(29-32):3666–3690, 2006.

[46] Dan Givoli and Joseph B. Keller. A finite element method for large domains. *Comput. Methods Appl. Mech. Engrg.*, 76(1):41–66, 1989.

[47] Dan Givoli and Joseph B. Keller. Nonreflecting boundary conditions for elastic waves. *Wave Motion*, 12(3):261–279, 1990.

[48] Dan Givoli and Joseph B. Keller. Special finite elements for use with high-order boundary conditions. *Comput. Methods Appl. Mech. Engrg.*, 119(3-4):199–213, 1994.

[49] Dan Givoli and Beny Neta. High-order non-reflecting boundary conditions for dispersive waves. *Wave Motion*, 37(3):257–271, 2003.

[50] Dan Givoli and Beny Neta. High-order non-reflecting boundary scheme for time-dependent waves. *J. Comput. Phys.*, 186(1):24–46, 2003.

[51] Dan Givoli and Beny Neta. High-order nonreflecting boundary conditions for the dispersive shallow water equations. *J. Comput. Appl. Math.*, 158(1):49–60, 2003. Selected papers from

the Conference on Computational and Mathematical Methods for Science and Engineering (Alicante, 2002).

[52] Dan Givoli and Igor Patlashenko. Optimal local artificial boundary conditions. In Thomas L. Geers, editor, *IUTAM Symposium on Computational Methods for Unbounded Domains (Boulder, CO, 1997)*, volume 49 of *Fluid Mech. Appl.*, pages 151–158. Kluwer Acad. Publ., Dordrecht, 1998.

[53] Dan Givoli, Igor Patlashenko, and Joseph B. Keller. High-order boundary conditions and finite elements for infinite domains. *Comput. Methods Appl. Mech. Engrg.*, 143(1-2):13–39, 1997.

[54] Dan Givoli and Shmuel Vigdergauz. Artificial boundary conditions for 2D problems in geophysics. *Comput. Methods Appl. Mech. Engrg.*, 110(1-2):87–101, 1993.

[55] M. J. Grote and J. B. Keller. On nonreflecting boundary conditions. *J. Comput. Phys.*, 122:231–243, 1995.

[56] Marcus J. Grote and Joseph B. Keller. Exact nonreflecting boundary conditions for the time dependent wave equation. *SIAM J. Appl. Math.*, 55(2):280–297, 1995. Perturbation methods in physical mathematics (Troy, NY, 1993).

[57] Marcus J. Grote and Joseph B. Keller. Nonreflecting boundary conditions for time-dependent scattering. *J. Comput. Phys.*, 127(1):52–65, 1996.

[58] Marcus J. Grote and Joseph B. Keller. Nonreflecting boundary conditions for Maxwell's equations. *J. Comput. Phys.*, 139(2):327–342, 1998.

[59] Marcus J. Grote and Joseph B. Keller. Exact nonreflecting boundary condition for elastic waves. *SIAM J. Appl. Math.*, 60(3):803–819 (electronic), 2000.

[60] Murthy N. Guddati and John L. Tassoulas. Continued-fraction absorbing boundary conditions for the wave equation. *J. Comput. Acoust.*, 8(1):139–156, 2000. Finite elements for wave problems (Trieste, 1999).

[61] Paul Günther. *Huygens' principle and hyperbolic equations*, volume 5 of *Perspectives in Mathematics*. Academic Press Inc., Boston, MA, 1988. With appendices by V. Wünsch.

[62] Bertil Gustafsson. Far-field boundary conditions for time-dependent hyperbolic systems. *SIAM J. Sci. Statist. Comput.*, 9(5):812–828, 1988.

[63] Bertil Gustafsson and Lars Ferm. Far field boundary conditions for steady state solutions to hyperbolic systems. In *Nonlinear hyperbolic problems (St. Etienne, 1986)*, volume 1270 of *Lecture Notes in Math.*, pages 238–252. Springer, Berlin, 1987.

[64] J. Hadamard. *Lectures on Cauchy's Problem in Linear Partial Differential Equations*. Yale University Press, New Haven, 1923.

[65] J. Hadamard. *Problème de Cauchy*. Hermann et cie, Paris, 1932. [French].

[66] J. Hadamard. The problem of diffusion of waves. *Ann. of Math. (2)*, 43:510–522, 1942.

[67] T. Hagstrom. Radiation boundary conditions for the numerical simulation of waves. In A. Iserlis, editor, *Acta Numerica*, volume 8, pages 47–106, Cambridge, 1999. Cambridge University Press.

[68] T. Hagstrom and J. Lorenz. Boundary conditions and the simulation of low mach number flows. In D. Lee and M. H. Schultz, editors, *Theoretical and Computational Acoustics, Proceedings of the First International Conference on Theoretical and Computational Acoustics, July 5–9, 1993, Mystic, Connecticut, USA*, volume 2, pages 657–668, Singapore, 1994. World Scientific Publishing Co.

[69] T. M. Hagstrom. Exact and high-order boundary conditions in time domain. In Thomas L. Geers, editor, *IUTAM Symposium on Computational Methods for Unbounded Domains (Boulder, CO, 1997)*, volume 49 of *Fluid Mech. Appl.*, pages 179–186. Kluwer Acad. Publ., Dordrecht, 1998.

[70] T. M. Hagstrom and S. I. Hariharan. Progressive wave expansions and open boundary problems. In B. Engquist and G. A. Kriegsmann, editors, *Computational Wave Propagation*, volume 86 of *IMA Volumes in Mathematics and its Applications*, pages 23–43. Springer-Verlag, Berlin, 1996.

[71] T. M. Hagstrom and H. B. Keller. Asymptotic boundary conditions and numerical methods for nonlinear elliptic problems on unbounded domains. *Math. Comp.*, 48(178):449–470, 1987.

[72] Thomas Hagstrom. Asymptotic boundary conditions for dissipative waves: general theory. *Math. Comp.*, 56(194):589–606, 1991.

[73] Thomas Hagstrom. Conditions at the downstream boundary for simulations of viscous, incompressible flow. *SIAM J. Sci. Statist. Comput.*, 12(4):843–858, 1991.

[74] Thomas Hagstrom and S. I. Hariharan. Accurate boundary conditions for exterior problems in gas dynamics. *Math. Comp.*, 51(184):581–597, 1988.

[75] Thomas Hagstrom, S. I. Hariharan, and David Thompson. High-order radiation boundary conditions for the convective wave equation in exterior domains. *SIAM J. Sci. Comput.*, 25(3):1088–1101 (electronic), 2003.

[76] Thomas Hagstrom and H. B. Keller. Exact boundary conditions at an artificial boundary for partial differential equations in cylinders. *SIAM J. Math. Anal.*, 17(2):322–341, 1986.

[77] Thomas Hagstrom and Timothy Warburton. A new auxiliary variable formulation of high-order local radiation boundary conditions: corner compatibility conditions and extensions to first-order systems. *Wave Motion*, 39(4):327–338, 2004. New computational methods for wave propagation.

[78] Thomas M. Hagstrom. Asymptotic expansions and boundary conditions for time-dependent problems. *SIAM J. Numer. Anal.*, 23(5):948–958, 1986.

[79] Thomas M. Hagstrom. Boundary conditions at outflow for a problem with transport and diffusion. *J. Comput. Phys.*, 69(1):69–80, 1987.

[80] S. I. Hariharan and T. M. Hagstrom. A systematic approach for constructing asymptotic boundary conditions for wave-like equations. In Thomas L. Geers, editor, *IUTAM Symposium on Computational Methods for Unbounded Domains (Boulder, CO, 1997)*, volume 49 of *Fluid Mech. Appl.*, pages 197–206. Kluwer Acad. Publ., Dordrecht, 1998.

[81] G. W. Hedstrom. Nonreflecting boundary conditions for nonlinear hyperbolic systems. *J. Comput. Phys.*, 30(2):222–237, 1979.

[82] J. S. Hesthaven. On the analysis and construction of perfectly matched layers for the linearized Euler equations. *J. Comput. Phys.*, 142(1):129–147, 1998.

[83] R. L. Higdon. Absorbing boundary conditions for dispersive waves. In Thomas L. Geers, editor, *IUTAM Symposium on Computational Methods for Unbounded Domains (Boulder, CO, 1997)*, volume 49 of *Fluid Mech. Appl.*, pages 217–220. Kluwer Acad. Publ., Dordrecht, 1998.

[84] Robert L. Higdon. Absorbing boundary conditions for difference approximations to the multidimensional wave equation. *Math. Comp.*, 47(176):437–459, 1986.

[85] Robert L. Higdon. Numerical absorbing boundary conditions for the wave equation. *Math. Comp.*, 49(179):65–90, 1987.

[86] Robert L. Higdon. Radiation boundary conditions for elastic wave propagation. *SIAM J. Numer. Anal.*, 27(4):831–869, 1990.

[87] Robert L. Higdon. Absorbing boundary conditions for acoustic and elastic waves in stratified media. *J. Comput. Phys.*, 101(2):386–418, 1992.

[88] Robert L. Higdon. Radiation boundary conditions for dispersive waves. *SIAM J. Numer. Anal.*, 31(1):64–100, 1994.

[89] Joseph B. Keller and Dan Givoli. Exact nonreflecting boundary conditions. *J. Comput. Phys.*, 82(1):172–192, 1989.

[90] Heinz-Otto Kreiss and Jens Lorenz. *Initial-Boundary Value Problems and the Navier-Stokes Equations*, volume 136 of *Pure and Applied Mathematics*. Academic Press Inc., Boston, MA, 1989.

[91] L. D. Landau and E. M. Lifshitz. *Course of Theoretical Physics, Vol. 2, The Classical Theory of Fields*. Pergamon Press, Oxford, fourth edition, 1975. Translated from the Russian by Morton Hamermesh.

[92] M. Matthisson. Le probléme de Hadamard relatif á la diffusion des ondes. *Acta Math.*, 71:249–282, 1939. [French].

[93] David P. Nicholls and Nilima Nigam. Exact non-reflecting boundary conditions on general domains. *J. Comput. Phys.*, 194(1):278–303, 2004.

[94] David P. Nicholls and Nilima Nigam. Error analysis of an enhanced DtN-FE method for exterior scattering problems. *Numer. Math.*, 105(2):267–298, 2006.

[95] Louis Nirenberg. *Lectures on linear partial differential equations*. American Mathematical Society, Providence, R.I., 1973. Expository Lectures from the CBMS Regional Conference held at the Texas Technological University, Lubbock, Tex., May 22–26, 1972, Conference Board of the Mathematical Sciences Regional Conference Series in Mathematics, No. 17.

[96] I. Patlashenko and D. Givoli. Local non-reflecting finite-element schemes for acoustic wave guides. In J.-A. Desideri, P. Le Tallec, E. O nate, J. Périaux, and E. Stain, editors, *Numerical Methods in Engineering. Proceedings of the Second ECCOMAS Conference on Numerical Methods in Engineering September 9–13, 1996, Paris, France*, pages 337–343, Chichester, 1996. John Wiley & Sons.

[97] Peter G. Petropoulos. Reflectionless sponge layers as absorbing boundary conditions for the numerical solution of Maxwell equations in rectangular, cylindrical, and spherical coordinates. *SIAM J. Appl. Math.*, 60(3):1037–1058 (electronic), 2000.

[98] I. Petrowsky. On the diffusion of waves and the lacunas for hyperbolic equations. *Matematicheskii Sbornik (Recueil Mathématique)*, 17 (59)(3):289–370, 1945.

[99] H. Qasimov and S. Tsynkov. Lacunae based stabilization of PMLs. *J. Comput. Phys.*, 227:7322–7345, 2008.

[100] J. A. Roden and S. D. Gedney. Convolution PML(CPML): An efficient FDTD implementation of the CFS-PML for arbitrary media. *Microwave and Optical Technology Letters*, 27(5):334–339, 2000.

[101] David H. Rudy and John C. Strikwerda. A nonreflecting outflow boundary condition for subsonic Navier-Stokes calculations. *J. Comput. Phys.*, 36(1):55–70, 1980.

[102] David H. Rudy and John C. Strikwerda. Boundary conditions for subsonic compressible Navier-Stokes calculations. *Computers and Fluids*, 9:327–338, 1981.

[103] V. S. Ryaben'kii. Boundary equations with projections. *Russian Math. Surveys*, 40:147–183, 1985.

[104] V. S. Ryaben'kii. *Difference Potentials Method for Some Problems of Continuous Media Mechanics*. Nauka, Moscow, 1987. (In Russian).

[105] V. S. Ryaben'kii. Exact transfer of difference boundary conditions. *Functional Anal. Appl.*, 24(3):251–253, 1990.

[106] V. S. Ryaben'kii. *Method of Difference Potentials and Its Applications*, volume 30 of *Springer Series in Computational Mathematics*. Springer-Verlag, Berlin, 2002.

[107] V. S. Ryaben'kii and S. V. Tsynkov. Artificial boundary conditions for the numerical solution of external viscous flow problems. *SIAM J. Numer. Anal.*, 32:1355–1389, 1995.

[108] V. S. Ryaben'kii, S. V. Tsynkov, and V. I. Turchaninov. Global discrete artificial boundary conditions for time-dependent wave propagation. *J. Comput. Phys.*, 174(2):712–758, 2001.

[109] V. S. Ryaben'kii, S. V. Tsynkov, and V. I. Turchaninov. Long-time numerical computation of wave-type solutions driven by moving sources. *Appl. Numer. Math.*, 38:187–222, 2001.

[110] V. S. Ryaben'kii and V. I. Turchaninov. The use of lacunae of hyperbolic equations and the method of difference potentials for computing wave diffraction in a bounded neighborhood of a scatterer at large time values. *Comput. Math. Math. Phys.*, 45(8):1385–1399, 2005. [Translated from the Russian: Zh. Vychisl. Mat. Mat. Fiz., 45, No. 8 (2005) pp. 1435–1449.].

[111] Victor S. Ryaben'kii and Semyon V. Tsynkov. *A Theoretical Introduction to Numerical Analysis*. Chapman & Hall/CRC, Boca Raton, FL, 2007.

[112] R. T. Seeley. Singular integrals and boundary value problems. *Amer. J. Math.*, 88:781–809, 1966.

[113] F. L. Teixeira and W. C. Chew. PML-FDTD in cylindrical and spherical grids. *IEEE Microwave and Guided Wave Letters*, 7(9):285–287, 1997.

[114] Fernando L. Teixeira and Weng Cho Chew. Finite-difference computation of transient electromagnetic waves for cylindrical geometries in complex media. *IEEE Transaction on Geoscience and Remote Sensing*, 38(4):1530–1543, July 2000.

[115] S. V. Tsynkov. An application of nonlocal external conditions to viscous flow computations. *J. Comput. Phys.*, 116:212–225, 1995.

[116] S. V. Tsynkov. Numerical solution of problems on unbounded domains. A review. *Appl. Numer. Math.*, 27:465–532, 1998.

[117] S. V. Tsynkov. External boundary conditions for three-dimensional problems of computational aerodynamics. *SIAM J. Sci. Comp.*, 21:166–206, 1999.

[118] S. V. Tsynkov. Artificial boundary conditions for the numerical simulation of unsteady acoustic waves. *J. Comput. Phys.*, 189(2):626–650, August 2003.

[119] S. V. Tsynkov. On the application of lacunae-based methods to Maxwell's equations. *J. Comput. Phys.*, 199(1):126–149, September 2004.

[120] S. V. Tsynkov, S. Abarbanel, J. Nordström, V. S. Ryaben'kii, and V. N. Vatsa. Global artificial boundary conditions for computation of external flows with jets. *AIAA Journal*, 38:2014–2022, 2000.

[121] S. V. Tsynkov and V. N. Vatsa. An improved treatment of external boundary for three-dimensional flow computations. *AIAA Journal*, 36:1998–2004, 1998.

[122] V. van Joolen, B. Neta, and D. Givoli. A stratified dispersive wave model with high-order nonreflecting boundary conditions. *Comput. Math. Appl.*, 48(7-8):1167–1180, 2004.

[123] Vince J. van Joolen, Beny Neta, and Dan Givoli. High-order boundary conditions for linearized shallow water equations with stratification, dispersion and advection. *Internat. J. Numer. Methods Fluids*, 46(4):361–381, 2004.

[124] Vince J. van Joolen, Beny Neta, and Dan Givoli. High-order Higdon-like boundary conditions for exterior transient wave problems. *Internat. J. Numer. Methods Engrg.*, 63(7):1041–1068, 2005.

[125] K. S. Yee. Numerical solution of initial boundary value problem involving Maxwell's equations in isotropic media. *IEEE Trans. Antennas Propagat.*, 14:302–307, 1966.

[126] R. W. Ziolkowski. Time-derivative Lorenz material model based absorbing boundary conditions. *IEEE Trans. Antennas Propagat.*, 45(10):1530–1535, 1997.

Appendices

4.A Well-Posedness of the Cauchy Problem for Hyperbolic Systems

4.A.1 Introduction

As we have mentioned in Section 1.5.2, transition from the original Maxwell's equations to PML affects the well-posedness of the system. This result was established in [1], and the corresponding analysis is based on the definitions of hyperbolicity and well-posedness given in [90]. In what follows we present an adaptation of Chapter 2 from [90] where the concepts of well-posedness and hyperbolicity for the Cauchy problem are transparently and succinctly developed. The main results below are given without proofs but the interested reader will find them in the original monograph.

4.A.2 Well-Posedness of the Cauchy Problem

We will consider problems in a d-dimensional space; therefore, $\mathbf{x} = (x_1, \ldots, x_d) \in \mathbb{R}^d$. The multi-index vector of nonnegative integers $\nu = (\nu_1, \ldots, \nu_d)$ is defined to have order $|\nu| = \sum_{j=1}^{d} \nu_j$. The differential operator

$$D^\nu = \frac{\partial^{|\nu|}}{\partial x_x^{\nu_1} \ldots \partial x_s^{\nu_s}}$$

The Euclidean norm $\|u\|_2 \equiv \sqrt{(u,u)_2}$ is used unless otherwise stated; for $A \in \mathbb{C}^{n,n}$ $\|A\| = max\{\|Au\|, \|u\| = 1\}$. We will consider the following Cauchy problem

$$u_t = P(\partial/\partial x)u \equiv \sum_{|\nu| \le m} A_\nu D^\nu u, \mathbf{x} \in \mathbb{R}^d,\ t \ge 0 \tag{A-1a}$$

with the initial condition

$$u(\mathbf{x}, 0) = f(\mathbf{x}) \tag{A-1b}$$

and $A_\nu \in \mathbb{C}^{n,n}$ are constant matrices and the solution, if one exists, is complex-valued and has the form

$$u(\mathbf{x}, t) \quad = \quad \begin{pmatrix} u_1(\mathbf{x}, t) \\ \vdots \\ u_n(\mathbf{x}, t) \end{pmatrix}$$

The observation $\frac{\partial}{\partial x_j} \to i\omega_j$ leads to the definition of the *symbol* of the differential operator $P(\partial/\partial x)$ by

$$P(i\omega) \equiv \sum_{|\nu| \le m} A_\nu (i\omega_1)^{\nu_1} \ldots (i\omega_d)^{\nu_d}$$

Definition 4.1 *The Cauchy problem (A-1) is* well-posed *if* $\exists$ *constants* α, K *such that*

$$\|e^{P(i\omega)t}\| \leq Ke^{\alpha t} \ \forall \ t \geq 0, \ \omega \in \ \mathbb{R}^d \tag{A-2}$$

The well-posedness of the Cauchy problem is particularly attractive, because an L_2 estimate of the solution at any time $t \geq 0$ in terms of the L_2 norm of the initial data is then available. One can show that the Definition 4.1 is equivalent to the following more intuitive definition of well-posedness:

1. for all initial data f in a certain class there is a unique solution in a certain class;

2. the solution depends continuously on the initial data with respect to certain norms;

Definition 4.2 *The Cauchy problem (A-1) is* weakly well-posed *if* $\exists$ *constants* α, K *and* q *such that*

$$\|e^{P(i\omega)t}\| \leq K(1+|\omega|^q)e^{\alpha t} \ \forall \ t \geq 0, \ \omega \in \ \mathbb{R}^d \tag{A-3}$$

For a weakly well-posed Cauchy problem the L_2 norm of the estimate of the solution at time $t \geq 0$ will in general include the derivative terms of the initial data as well. However, weakly well posed problems can become ill-posed if the operator $P(\partial/\partial x)$ is perturbed by lower-order terms leading to an exponential growth.

The solution of the problem (A-1) is obtained by Fourier transforming the initial data

$$f(\mathbf{x}) = \frac{1}{(2\pi)^{d/2}} \int_{\mathbb{R}^d} e^{i(\omega,\mathbf{x})} \hat{f}(\omega) d\omega, \ \mathbf{x} \in \ \mathbb{R}^d$$

where

$$\hat{f}(\omega) = \frac{1}{(2\pi)^{d/2}} \int_{\mathbb{R}^d} e^{-i(\omega,\mathbf{x})} f(\mathbf{x}) dx, \ \omega \in \ \mathbb{R}^d$$

In particular, consider the space $\mathbf{M}_0$ of functions $f = f(\mathbf{x})$ such that their Fourier transform is a C_0^∞, i.e., compactly supported with derivatives of any order. The solution of the Cauchy problem (A-1) with the initial data $f(\mathbf{x}) \in \mathbf{M}_0$ and consequently $\hat{f} \in C_0^\infty$ is given by

$$u(\mathbf{x},t) = \frac{1}{(2\pi)^{d/2}} \int_{\mathbb{R}^d} e^{i(\omega,x)} e^{P(i\omega)t} \hat{f}(\omega) d\omega \tag{A-4}$$

which can be differentiated under the integral sign since $\hat{f} \in C_0^\infty$.

Definition 4.3 *The* $\mathbf{M}_0$ *solution of the Cauchy problem (A-1) is such that*

1. $u(\star,t) \in \mathbf{M}_0 \ \forall \ t \geq 0$

2. *the function* $\hat{u}(\omega, t)$ *is continuous and* $\exists\ K$ *independent of* t *such that* $\forall\ |\omega| > K\ \hat{u}(\omega, t) = 0$

3. *u is a classical solution of the Cauchy problem (A-1)*

We state without proving that any Cauchy problem with an $\mathbf{M}_0$ initial data has a unique $\mathbf{M}_0$ solution; this solution is given by the formula (A-4) and $\hat{u}(x,t) = e^{P(i\omega)t}\hat{f}(\omega)$.

Stability of physical phenomena with respect to the initial conditions is a reasonable expectation; coupling this with the linearity of the Cauchy problem (A-1) one can expect to obtain an estimate for the solution at a future time in terms of the initial data. In order to obtain such an estimate we will need *Parceval's relation*

$$(f,g) = (\hat{f},\hat{g}),\ \|f\| = \|\hat{f}\|$$

where $(f,g) = \int_{\mathbb{R}^d} f(\mathbf{x})g(\mathbf{x})dx$ and $\|f\| = \sqrt{(f,f)},\ f,\ g\ \in L_2$. Then, the estimate in Definition 4.1 coupled with Parceval's relation yields

$$\|u(\star,t)\| = \|e^{P(i\omega)t}\hat{f}(\omega)\| \leq Ke^{\alpha t}\|\hat{f}\| = Ke^{\alpha t}\|f\|$$

One can show the following

Theorem 4.1 *If* $P(\partial/\partial x)$ *is a constant-coefficient operator, then for any* real $K,\ \alpha$ *the following are equivalent:*

1. *The symbols satisfy the estimate in Definition 4.1*

2. *for all initial date* $f\ \in\ \mathbf{M}_0$ *the estimate* $\|u(\star,t)\| \leq Ke^{\alpha t}\|f\|, t \geq 0$

Next, we provide a characterization of weak well-posedness by allowing derivative terms of the initial data to factor in obtaining the estimate of the solution at later times. First, define

$$\|f\|^2_{H^q} = \sum_{\|\nu\|\leq q} \|D^\nu f\|^2,\ f\ \in \mathbf{M}_0$$

Parceval's relation yields $\|D^\nu\| = \|\omega_1^{\nu_1}\dots\omega_d^{\nu_d}\hat{f}(\omega)\|$ so that

$$\|f\|^2_{H^q} = \frac{1}{(2\pi)^{2/d}}\int_{\mathbb{R}^d}\sum_{|\nu|\leq q}\left\{\omega_1^{2\nu_1}\dots\omega_d^{2\nu_d}\right\}|\hat{f}(\omega)|^2 d\omega$$

Then, the inequality

$$\frac{1}{c}(1+|\omega|^q)^2 \leq \sum_{|\nu|\leq q}\omega_1^{2\nu_1}\dots\omega_d^{2\nu_d} \leq c(1+|\omega|^q)^2$$

holds, $c = c_q$ is independent of ω and one can show that for a constant coefficient $P(\partial/\partial x)$, $q \in \{1,2,\dots\}$ and $\alpha \in \mathbb{R}$ the following are equivalent:

1. $\exists\ K_1$ with $|e^{P(i\omega)t}| \leq K_1(1+|\omega|^q)e^{\alpha t},\ \omega \in \mathbb{R}^d,\ t \leq 0$

2. $\exists\ K_2$ *such that* $\|u(\star,t)\| \leq K_2 e^{\alpha t}\|f\|_{H^q},\ t \geq 0$

In contradistinction to the well-posed and the weakly well-posed problems stand the *ill-posed in any sense* formulations where the symbol $|e^{P(i\omega)t}|$ grows faster than any polynomial in ω, i.e., an *exponential explosion* occurs.

The well-posed and the weakly well-posed formulations can be solved numerically; weakly well-posed problems require more care in obtaining their approximations. Ill-posed problems will in general require additional restrictions to regularize the solution before they can be approached. Weak well-posedness causes serious difficulties for variable coefficient formulations.

4.A.3 Hyperbolicity of the Cauchy Problem

Next we will describe the notions of hyperbolicity for the constant coefficient Cauchy problems. Consider the first order system

$$u_t = P(\partial/\partial x)u \equiv \sum_{j=1}^{d} A_j \frac{\partial u}{\partial x_j},\ x \in\ \mathbb{R}^d,\ A_j\ \in \mathbb{C}^{n,n} \tag{A-5}$$

The symbol $P(i\omega) = i\sum_{j=1}^{d}\omega_j A_j = |\omega|P(i\omega')$ where $\omega' = \omega/|\omega|$ and $\omega\ \in \mathbb{R}^d$. The characterization of the first order constant coefficient well posed systems is given by

Theorem 4.2 *The first order system (A-5) is well posed if and only if the following two conditions are satisfied:*

1. $\forall\ \omega'\ \in \mathbb{R}^d,\ |\omega'| = 1$, *all eigenvalues of* $P(i\omega')$ *are pure imaginary.*

2. $\exists$ *a constant* K_{31} *and for each* $\omega' \in \mathbb{R}^d$ *there is a transformation* $S(\omega')$ *with* $|S(\omega')|+|S^{-1}(\omega')| \leq K_{31}$ *such that the transformation* $S(\omega')P(i\omega')S^{-1}(i\omega')$ *is diagonal*

The proof of Theorem 4.2 can be found in [90].

Definition 4.4 *The first order system (A-5) is*

1. strongly hyperbolic *if Theorem 4.2 holds*

2. weakly hyperbolic *if* $\forall\ \omega \in \mathbb{R}^d$ *the eigenvalues of* $P(i\omega)$ *are pure imaginary*

3. symmetric hyperbolic *if* $A_j = A_j^{\star},\ j = \{1,\ldots,d\}$

4. strictly hyperbolic *if* $\forall\omega \in \mathbb{R}^d, \omega \neq \boldsymbol{0}$, *the eigenvalues of* $P(i\omega)$*are pure imaginary and distinct*

The relationship between the well-posedness and the hyperbolicity of the Cauchy problem is summarized by the following:

- the Cauchy problem for a weakly hyperbolic system is generally not well posed.
- the Cauchy problem for strongly hyperbolic, symmetric hyperbolic and strictly hyperbolic systems is well-posed.